NOVA SCHOOL OF SCIENCE & TECHNOLOGY

DEPARTMENT OF PHYSICS

ANA MARGARIDA PINGO DUARTE

Bachelor of Science in Biomedical Engineering

NONINVASIVE INTRACRANIAL ARTERIAL FLOW ANALYSIS

A REPRODUCIBILITY STUDY OF 4D FLOW MRI IN INTRACRANIAL VESSELS

MASTER IN BIOMEDICAL ENGINEERING

NOVA University Lisbon
September, 2022

NOVA SCHOOL OF SCIENCE & TECHNOLOGY

DEPARTMENT OF PHYSICS

NONINVASIVE INTRACRANIAL ARTERIAL FLOW ANALYSIS

A REPRODUCIBILITY STUDY OF 4D FLOW MRI IN INTRACRANIAL VESSELS

ANA MARGARIDA PINGO DUARTE

Bachelor of Science in Biomedical Engineering

Adviser: Ricardo Vigário
Associate Professor, NOVA University Lisbon

Co-adviser: Pedro Vilela
Neuroradiologist, Hospital da Luz

Examination Committee

Chair: Susana Isabel dos Santos Silva Sério Venceslau
Assistant Professor, NOVA University Lisbon

Rapporteur: Rita Homem de Gouveia Constanzo Nunes
Assistant Professor, University of Lisbon

Adviser: Ricardo Nuno Pereira Verga e Afonso Vigário
Associate Professor, NOVA University Lisbon

MASTER IN BIOMEDICAL ENGINEERING

NOVA University Lisbon
September, 2022

Noninvasive intracranial arterial flow analysis

This document was created with the (pdf/Xe/Lua)LaTeX processor and the NOVAthesis template (v6.9.15) [1].

To my family.

Acknowledgements

The development of this study would not have been possible without the contribution and assistance of several people who have supported me throughout this journey.

First, I would like to express my sincere gratitude to Professor Ricardo Vigário, for the unconditional support and availability provided throughout these months and for the perseverance and serenity that he always transmitted. Thank you for the encouraging words and for always believing in the potential of this work. Professor Ricardo was essential in the choice and development of this thesis, since he always demonstrated his enormous interest in MRI and its potential, which I now share. I would like to thank Dr. Pedro Vilela, for the enormous knowledge transmitted. With him, I have learned to always see further and to be more ambitious. I am also grateful for the opportunity to work at Hospital da Luz with all the equipment available and to be able to be part of this project that I enjoyed so much.

I would also like to acknowledge the medical imaging technicians at Hospital da Luz, especially Cristina, for their assistance during image acquisition and collection. I would like to thank Pablo Garcia-Polo, for all the help regarding the MRI sequence and for the availability to answer all my doubts.

My grattitude goes to Eric Schrauben, since without his tool and help, this work would not be possible. I would like to thank Professor Miguel Fonseca, for the assistance in the statistical analysis.

I would also like to express my appreciation for the availability of the volunteers present in this study, since without them, this research would not be possible.

To my friends, Catarina, Pedro, André, Marta and Pedro, thank you so much for all the support and for the tranquility that you transmitted in the most anxious moments. Without you, the last months would have not been the same. To my dear Adriana and Maria Inês, I could not have asked for a better "family" throughout this journey. Thank you for never leaving my side and for the unconditional support.

To Tiago, without you, this would not be possible. The immense love, patience, dedication and support you provided during all these years were fundamental. I am so grateful to have you by my side.

Lastly, a heartfelt thank you to my family, for always believing in me and motivating me. To Hugo, Tânia and my nephew and niece, for all the great moments of happiness. To my grandparents, who I am lucky enough to still be present to accompany me through this journey. And to my parents, to whom I couldn't be more grateful to, for always being my support, for allowing me to have this opportunity, and for motivating me throughout this journey.

"Out of clutter, find simplicity. From discord, find harmony. In the middle of difficulty lies opportunity."

Albert Einstein

Abstract

4D flow magnetic resonance imaging allows for quantitative measurements of blood flow and velocities that may be useful for early diagnosis and treatment monitoring of neurovascular pathologies. To validate the potential of this technique in clinical applications, its accuracy and reproducibility need to be investigated.

Hence, the goal of this thesis was to assess the test-retest reproducibility of 4D flow results in intracranial arteries. On two occasions, 24 hours apart, and on a population of 10 healthy volunteers, the pulsatility index, flow volume pulsatility, cross-sectional area, and minimum, mean, and maximum blood flow velocities were measured in the internal carotid artery, of both the left and right sides, the middle cerebral artery, of both hemispheres, and basilar artery.

To evaluate the accuracy of the results, a series of analyses were performed, which included the calculation of intraclass correlation coefficients, Wilcoxon signed-rank tests, Bland-Altman plots, and Pearson correlations, between data collected at both time stamps. A correlation analysis was also employed to evaluate heart rate and blood pressure associations with the obtained vascular function recordings.

In general, good test-retest reproducibility was observed for all arteries. Higher reliability was verified for the internal carotid arteries and the basilar artery than for the middle cerebral arteries. Worse results were found for the pulsatility index and flow volume pulsatility, when compared to flow velocities and cross-sectional area. Several correlations were found between neurovascular data and physiological parameters, especially for the middle cerebral arteries.

Keywords: 4D Flow MRI, Cerebral Vessels, Reproducibility, Cerebral Blood Flow, Cerebral Hemodynamics, Cerebrovascular Diseases

Resumo

A ressonância magnética de fluxo 4D permite medições quantitativas de fluxo sanguíneo e velocidades que podem ser úteis para o diagnóstico precoce e monitorização do tratamento de patologias neurovasculares. Para validar o potencial desta técnica para aplicações clínicas é necessário analisar a sua exatidão e reprodutibilidade.

Assim, o objetivo desta tese é avaliar a reprodutibilidade das medições de ressonância magnética de fluxo 4D em artérias intracranianas. O índice de pulsatilidade, pulsatilidade do volume de fluxo, área da secção transversal, e velocidades mínimas, médias e máximas de fluxo sanguíneo foram medidas nas artérias carótidas internas, artérias cerebrais médias e artéria basilar em duas ocasiões espaçadas 24 horas numa população de 10 voluntários saudáveis.

Para a avaliação da precisão, foi calculado o índice de correlação intraclasse e realizados um teste de Wilcoxon, uma análise de Bland-Altman e , por fim, uma análise de correlação de Pearson. Foi também realizada uma análise de correlação para avaliar as associações de frequência cardíaca e pressão arterial com os valores obtidos.

Em geral, observou-se uma boa reprodutibilidade entre as duas medidas para todas as artérias. Foi verificada uma maior fiabilidade para as artérias carótidas internas e artéria basilar do que para as artérias cerebrais médias. Foram encontrados piores resultados para o indíce de pulsatilididade e pulsatilidade de volume de fluxo quando comparados com as velocidades de fluxo e a área da secção transversal. Por fim, verificaram-se várias correlações entre os resultados e os parâmetros fisiológicos, especialmente para as artérias cerebrais médias.

Palavras-chave: Ressonância Magnética de Fluxo 4D, Vasos Cerebrais, Reprodutibilidade, Fluxo Sanguíneo Cerebral, Hemodinâmica Cerebral, Doenças Cerebrovasculares

Contents

List of Figures

List of Tables

Abbreviations

2D	two-dimensional
4D	four-dimensional
ACA	anterior cerebral artery
ACS	autocalibration signals
AP	anterior-posterior
BA	basilar artery
BP	blood pressure
CBF	cerebral blood flow
CD	complex difference
CI	confidence interval
CPP	cerebral perfusion pressure
CSVD	cerebral small vessel disease
CT	computed tomography
CVR	cerebrovascular resistance
DBP	diastolic blood pressure
DSA	digital subtraction angiography
ECG	electrocardiogram
FID	free induction decay
FLAIR	fluid attenuated inversion recovery
FOV	field of view
FVP	flow volume pulsatility
HR	heart rate

ICA internal carotid artery
ICC intraclass correlation coefficient
ICP intracranial pressure

LoA limits of agreement
LR left-right

MAP mean arterial pressure
MBP mean blood pressure
MCA middle cerebral artery
MRA magnetic resonance angiography
MRI magnetic resonance imaging

PC-MRI phase-contrast magnetic resonance imaging
PCA posterior cerebral artery
PCC Pearson correlation coefficient
PI pulsatility index

RF radiofrequency
ROI region of interest

SBP systolic blood pressure
SI superior-inferior

TCD transcranial doppler

VDR variable density random

WMH white matter hyperintensities

1 Introduction

1.1 Context and Motivation

Blood flow provides the brain tissue with oxygen and glucose, thus being a crucial factor in brain health and overall function [2]. Increasing age, hypertension and other vascular risk factors [3] contribute to structural changes to the vessel wall, and the development of atherosclerosis. This phenomenon is associated with several cerebrovascular diseases [4], such as ischaemic stroke [5], [6], vascular dementia [7], and even Alzheimer's disease [8] and cerebral small vessel disease (CSVD) [9].

CSVD is a term used to refer to a variety of pathological, clinical or radiological conditions that are thought to be caused by disease affecting the small perforating arteries and arterioles that supply the deep brain areas [10]. About 25% of strokes and the majority of hemorrhagic strokes are caused by CSVD. It also frequently causes mild cognitive impairment and vascular dementia [11], therefore contributing to roughly 50% of dementia cases and a significant cost on worldwide health [12]. The implications of understanding CSVD extend beyond the disease itself, since it contributes to dementia and even Alzheimer's disease and other neurovascular pathologies [13].

Vascular function imaging techniques allow for quantitative measurements of blood flow and blood flow velocities that can be used for not only diagnosis and treatment monitoring of these pathologies but also to understand and possibly detect early disease indicators [4], [14]. Together with morphological information, vascular function imaging will aid in determining specific blood vessel and blood flow abnormalities at the earliest stages of neurovascular disease and contribute with innovative information to support new diagnostic techniques and therapies [9], [15].

Early physiological studies of hemodynamic parameters in the intracerebral arteries included mainly transcranial doppler (TCD) ultrasound and digital subtraction angiography (DSA). Although TCD is low cost and highly portable [14], this technique presents disadvantages, since it is typically limited to large intracranial vessels, it has large operator dependence and in some instances, it is not possible to acquire sufficient bone window [8], which are skull regions that allow for ultrasound propagation. The DSA technique also

presents several disadvantages, such as thromboembolic risks, its invasive nature, the required exposure to radiation, and the need to use contrasting agents [16].

In recent years, two-dimensional (2D) phase-contrast magnetic resonance imaging (PC-MRI), as a non-invasive technique, has become widely used for the assessment of flow and velocity related neurovascular information in a clinical setting [15], [17]. However, the magnetic resonance imaging (MRI) technician needs to manually define a cross-sectional plane that intersects the vessel of interest, and the concomitant blood flow, perpendicularly. Therefore, this technique is extremely dependent on the operator, and since the process needs to be repeated for each artery, the acquisition is highly time-consuming. In addition, only the vessel sections that were targeted during the scan can be analysed to retrieve information.

More recently, four-dimensional (4D) flow emerged as a PC-MRI technique, which acquires one reference anatomical image and velocity-encoded images along the three orthogonal directions, creating a three dimensional dataset, collected over the cardiac cycle [4]. Due to the large quantity of data required, the acquisition time constitutes a major drawback of this technique in a clinical setting. However, over time, several acceleration techniques have been developed, allowing for whole brain coverage in a 10 minute scan. 4D PC-MRI has been gaining notoriety because it is capable of measuring blood flow velocity in cerebral arteries and veins in the same scan. Additionally, data can be analysed post-hoc to assess flow, velocity and several other hemodynamic parameters without needing to plan the cross-sectional position during the scan.

To validate the potential of 4D flow for both clinical and research applications, several studies have been carried out to assess the accuracy, reproducibility, and observer dependence of the sequence and post-processing schemes. The accuracy of 4D flow has been demonstrated when compared with TCD [18] and 2D PC-MRI [17], [19]. Additionally, good test-retest reproducibility has already been reported for the aorta [20], [21], the mid portion of the pulmonary trunk [21], intraheart applications [22] and arterial and portal venous liver hemodynamics [23]. However, there is still a need to evaluate the validity of this technique for intracranial applications, considering that the spatial resolution is limited compared to the small size of these vessels.

Although some studies reported good reproducibility for cerebral arteries [14], [24], only basic flow parameters were evaluated therein.

Thus, this thesis aims to evaluate the test-retest accuracy and normal ranges for 4D flow results in intracranial arteries. For this purpose, a pilot study, involving 10 healthy individuals, was conducted, to quantify the pulsatility index (PI), flow volume pulsatility (FVP), lumen area, and minimum, mean, and maximum velocities in the internal carotid arteries, middle cerebral arteries and basilar artery (BA). In addition, the relationship between the results found for neurovascular characteristics and physiological variables, such as heart rate (HR) and blood pressure (BP) is assessed.

1.2 Specific objectives

The goal of this thesis is to assess the test-retest reproducibility of 4D PC-MRI measurements of pulsatility-related indexes, flow, velocity, and anatomical parameters of the main intracranial arteries (internal carotid artery (ICA), middle cerebral artery (MCA) and BA). Also, it is important to develop a normative base of healthy volunteer's results, to which this study will also contribute. To accomplish the aforementioned goals it is necessary:

- to measure PI, FVP, minimum, maximum and mean velocities, and vessel areas of intracranial arteries, in an exploratory pilot study with 10 healthy volunteers, contributing to the construction of a normative database of healthy subjects;
- to validate the 4D flow MRI sequence, developed by GE, and a concomitant post-processing tool, by performing test and retest for each healthy subject in two consecutive days;
- to analyse, statistically, the test-retest results, as well as to study the influence of heart rate and arterial blood pressure on the stability of measurement results found from 4D PC-MRI.

1.3 Thesis overview

This dissertation is composed of the following chapters:

- Chapter 1 - Introduction: Thesis contextualization and motivation, followed by the definition of the study goals.
- Chapter 2 - Theoretical Considerations: Description of the theoretical foundations and basic concepts of 4D flow MRI and cerebral blood flow, which are necessary for a better understanding of the methodology and the analysis performed in this dissertation.
- Chapter 3 - State of The Art: Definition of what has already been accomplished and the main conclusions found by other 4D PC-MRI reproducibility studies. Additionally, studies related to CSVD, performed with 4D flow MRI are presented.
- Chapter 4 - Methodology: Description of the methods applied throughout this project, including the data acquisition, the software utilized, with the changes performed, and the conducted statistical analysis.
- Chapter 5 - Results: Presentation of the results found.
- Chapter 6 - Discussion: Analysis and interpretation of this study's findings.

- Chapter 7 - Conclusion: Presentation of the main conclusions of the project and identification of its limitations. Suggestions to overcome such limitations and future perspectives for research conclude the chapter.

2

Theoretical Considerations

This chapter presents the main concepts necessary for the understanding of this thesis.

Initially, the basic principles of MRI are described in Section 2.1. These are necessary to comprehend the magnetic resonance angiography (MRA) techniques, especially 2D and 4D PC-MRI and acceleration techniques currently used to decrease the acquisition time, which are explained in Section 2.2. Furthermore, cerebral blood vessels anatomy, as well as blood flow physiology and autoregulation fundamentals are explored in Section 2.3.

Since this thesis is integrated in a project in which the goal is to investigate the relationship between CSVD and hemodynamic biomarkers assessed with 4D flow, a more thorough understanding of the disease and its relevance is required, hence these are clarified in Section 2.4.

2.1 Magnetic resonance

MRI is a non-invasive technique that produces detailed anatomical images of the organs and tissues. In addition to regular structural MRI, other unique contrast mechanisms, such as diffusion-weighted imaging [25], perfusion-weighted imaging [26], functional MRI [27] and MRA [28] have shown great relevance for disease detection, diagnosis, and treatment monitoring.

2.1.1 Magnetic resonance imaging fundamentals

Magnetic resonance is based on the interaction between an applied magnetic field and a nucleus that possesses spin. The ^1H nucleus, containing one proton, is frequently used for MRI techniques due to being the most abundant isotope for hydrogen. Additionally, hydrogen is a part of water and lipids, making up 75–80% of the human body [29].

A single positively charged proton that spins around its axis [30] constitutes the nucleus of the hydrogen atom. The proton possesses a magnetic property called nuclear spin. These spins are randomly oriented in the absence of a magnetic field, producing no net magnetization [31]. However, when a constant magnetic field B_0 is applied, the spins of the hydrogen nuclei tend to align in the direction of the field and start to precess around

B_0 at a constant rate called Larmor frequency. The vector sum of the spins creates a net magnetization, M_z, parallel with B_0 [29].

The Larmor Frequency, ω_0, is proportional to magnetic field intensity B_0, and to the proportional constant, γ, called gyromagnetic constant, which is characteristic of each nucleus, according to the Larmor Equation [29]:

$$\omega_0 = \gamma B_0 \tag{2.1}$$

To create a measurable magnetic resonance signal, the spins must be set to precess in a coherent manner (in phase) in the xy plane (transverse plane). This is achieved with radiofrequency (RF) pulses, B_1, applied perpendicular to the main magnetic field. If B_1 matches the Larmor frequency, there is rotation of the net magnetization of all spins in the sample, M_z, around B_1. The flip angle is the angle of rotation of the initial magnetization M_z, from the longitudinal axis to the transverse plane, and is proportional to the RF pulse duration and intensity. A flip angle of 90° implies that M_z is flipped completely onto the transverse plane and the global net magnetization can be detected in the receiver coil. Once the B_1 pulse is turned off, the only field affecting the magnetization is B_0 and the spins return to the equilibrium state, through a process known as relaxation, emitting electromagnetic energy. The signal, measured in the transverse plane, originated from this process is called free induction decay (FID).

Two types of relaxation times characterize the relaxation process. The spin-lattice (longitudinal) relaxation time, T1, results from the reestablishment of the initial magnetization along the z-axis [30]. The spin-spin (transversal) relaxation time, T2, characterizes the decay in the transverse component of the magnetization, M_{xy}, due to the interaction between neighboring spins, resulting in a randomization of the phase of the precessing spins.

The formation of a magnetic resonance image is performed through spatial encoding with gradient fields (variations in B_0 field strength). A two-dimensional image is created by applying a slice selection gradient (G_z) simultaneously to the RF excitation pulse.

After, phase and frequency encoding gradients (G_y and G_x, respectively) are used for in-plane localization. The magnetic resonance signal is then used to form the image in the spatial frequency domain, also know as k-space. To produce an anatomical image, k-space data is transformed using the inverse Fourier transform.

2.2 Magnetic resonance flow analysis

MRA encompasses several imaging techniques (time-of-flight methods [32], phase-contrast, contrast-enhanced MRA [33] and several others [34]) based on MRI to depict blood vessels. Unlike x-ray based angiography, MRA is completely non-invasive.

2.2.1 2D Phase-contrast magnetic resonance imaging

When a spin is moving along a magnetic field gradient, $G1$, as represented in Fig. 2.1, its resonance frequency changes because the location along the gradient is constantly altered. On the other hand, on a static spin, the resonance frequency remains constant. Thus, if an equal, but opposite gradient, $G2$, is applied afterward, the phase shift caused by $G1$ upon the stationary spins will be canceled. However, for moving spins, the faster and slower frequencies will not cancel, which results in a phase shift ($\Delta\phi$) in the acquired signal that is directly proportional to velocity and the intensity of the gradient [35], [36]. The phase shift can be obtained by:

$$\Delta\phi = \gamma v \Delta M_1 \tag{2.2}$$

where γ is the gyromagnetic constant, v is the proton velocity, and ΔM_1 is the change in the magnetic moment, that is directly proportionate to the gradient strength. Hence, the phase shift is directly proportionate to the gradient strength [37].

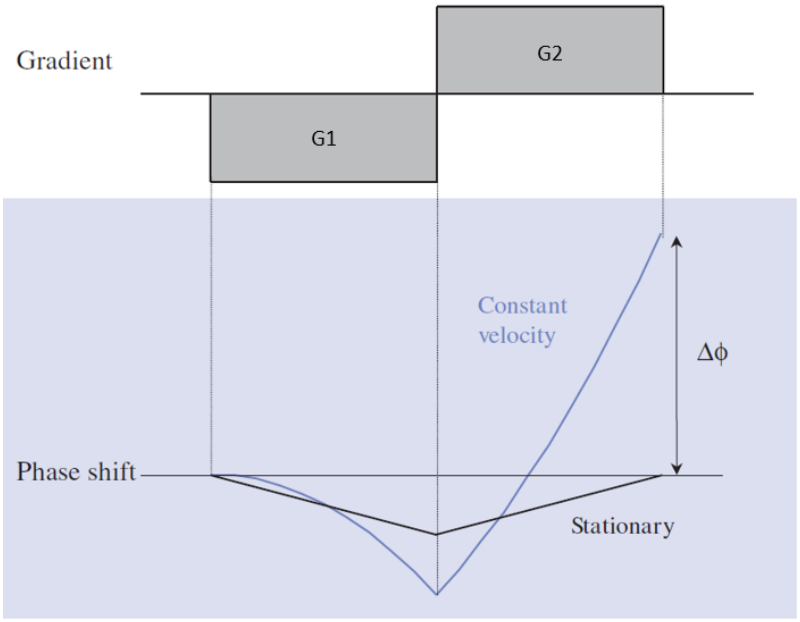

Figure 2.1: A phase shift $\Delta\phi$ is induced in the moving spins (blue line) by the application of opposing gradients $G1$ and $G2$, collectively referred to as a bipolar gradient. Adapted from [29].

The signal intensities in the resulting phase-difference images are directly related to the blood flow velocity and can be used to visualize and quantify blood flow [38]. Since both the forward and backward directions are important, phase changes that range from $-180°$ ($-\pi$ radians) to $180°$ (π radians) are chosen. Any angle measurements that exceed $180°$ in the positive or negative direction will demonstrate aliasing and not be displayed accurately. Therefore, for a given gradient, there is a maximum velocity that can be measured before aliasing occurs [35]. This velocity is called the encoding velocity, v_{enc},

and can be selected by the operator so that the maximum velocity selected corresponds to a 180° phase shift. By adapting the amplitude and duration of the bipolar gradients, it is possible to adjust the v_{enc}, which determines the degree of sensitivity to slow or fast flows. A v_{enc} too high compared to the expected maximum velocity should be avoided since the noise in velocity images increases with larger v_{enc} values [39].

The velocity is encoded within a single slice plane, defined by the MRI technician, so that it perpendicularly intersects the vessel and, consequently, the expected velocity direction [40]. An acquisition must be conducted for each vessel of interest, allowing the v_{enc} and the plane direction to be optimized every time, which constitutes an advantage of this technique. However, the plane needs to be placed perfectly perpendicular to the direction of flow, and since the intracranial vessels are tortuous, in the majority of times, it is not an easy task. Additionally, since the plane is manually positioned by the technician, an error in this placement can lead to complications in velocity and flow estimation, which means that the values obtained are highly dependent of the MRI operator. Thus, these factors represent major disadvantages of the technique.

This process requires the application of the bipolar gradient previously mentioned, before the phase-encoding, G_y, and frequency encoding, G_x, gradients, as represented in Fig. 2.2.

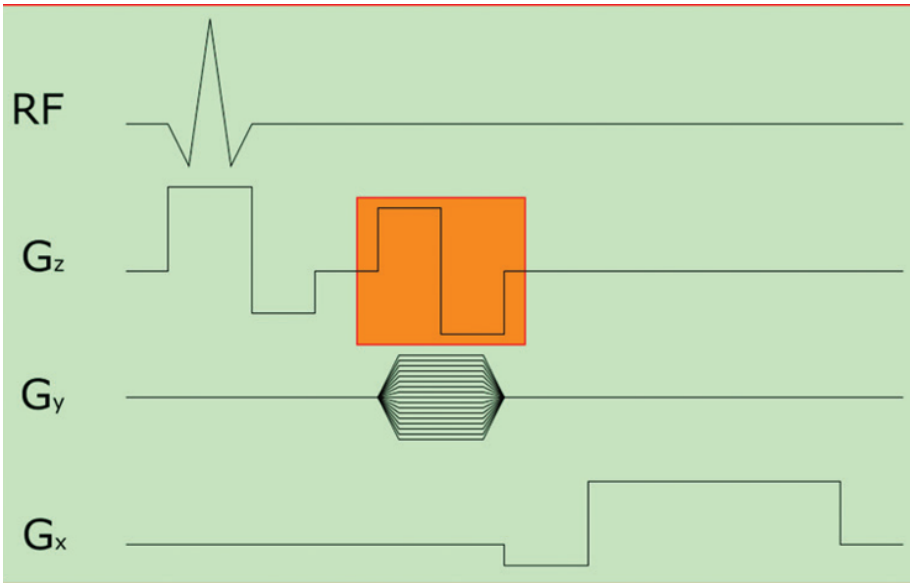

Figure 2.2: During signal acquisition, a bipolar gradient (orange box) is applied along the direction of flow (in this case the z direction). G_z is the image plane selection gradient; G_y and G_x are the phase-encoding and frequency-encoding gradients, respectively. From [35]

MRI associated to blood flow is typically acquired with two spatial dimensions and one temporal dimension representing the cardiac phase (often triggered using an electrocardiogram (ECG) signal) [5]. The synchronization of the MRI data with the cardiac cycle, is achieved by prospective or retrospective gating. Prospective gating is triggered by the R-wave of the ECG signal, to start the data acquisition. To compensate for physiologic

variations in the R-R interval, 10–15% [29] of the end of each cardiac cycle is not sampled. As a consequence, the flow of late diastole may not be measured correctly [39]. In retrospective gating, data is continuously collected throughout the cardiac cycle, with the R-wave causing a real-time update of the phase-encoding gradient. During image reconstruction, the recorded trigger signals are retrospectively sorted to create time-resolved images of the complete cardiac cycle. To account for physiologic variations in the length of the cardiac cycle, the data has to be interpolated to represent a mean cardiac cycle [29], [39].

After image reconstruction, 2D PC-MRI yields a series of anatomic and flow velocity images that represent the temporal changes in morphology and blood flow [38].

2.2.2 4D Phase-contrast magnetic resonance imaging

In 4D flow MRI, as represented in Fig. 2.3, velocity is encoded along all three spatial dimensions, hence, a time-resolved 3D velocity field is provided throughout the cardiac cycle.

After conclusion of the 4D flow acquisition, three-directional velocity measurements (v_x, v_y and v_z) can be efficiently achieved by using interleaved four-point velocity encoding, which acquires one reference anatomical image and three velocity-encoded images along the three orthogonal directions [38].

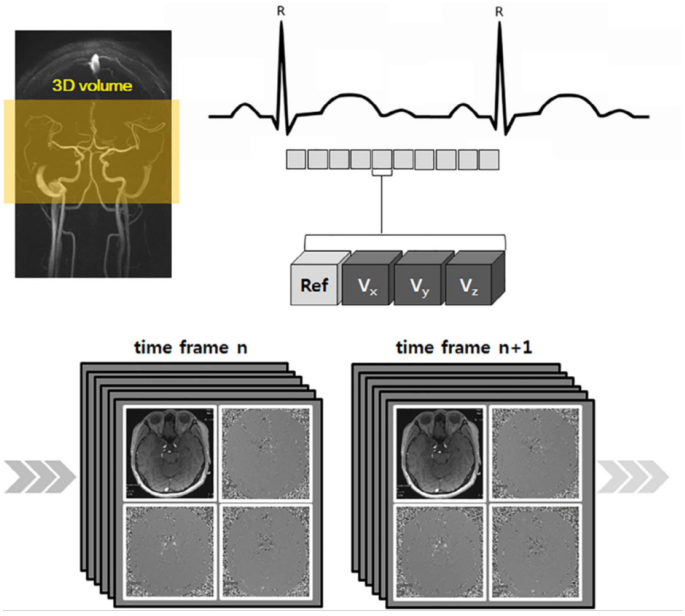

.

Figure 2.3: 4D flow data is obtained by synchronization of data acquisition with the cardiac cycle, and registered over multiple R-R intervals. For each timeframe (n, n + 1, etc.) of the cardiac phase, four 3D raw datasets are collected, consisting of a magnitude and three velocity-encoded scans that comprise a 4D flow dataset, allowing three-directional velocity measurements (v_x, v_y and v_z). From [41]

The subtraction of these two types of images is called complex difference (CD) and suppresses signal from stationary tissues, highlighting vasculature [42]. The CD is

obtained based on velocity in the three orthogonal directions (v_x, v_y and v_z), the used velocity for encoding (v_{enc}), and magnitude (m) data, using the relationship:

$$CD = m * sin(\theta) \tag{2.3}$$

$$\theta = \pi\sqrt{v_x^2 + v_y^2 + v_z^2}/v_{enc} \tag{2.4}$$

Due to the large amount of data that needs to be collected, 4D flow imaging takes a significant amount of time, which is one of the major limitations of the technique [35]. For intracranial applications, typically 10–20 cardiac phases are acquired [36], resulting in scan times ranging between 5 and 15 minutes [38].

However, 4D PC-MRI is more time efficient, compared to 2D PC-MRI, where each artery requires one separate MRI scan, that has to be planned in advance and positioned during the scan [4]. The 4D flow MRI technique has the advantage that data can be processed post-hoc at any time, to analyse the vessels captured [5].

The initial step in flow analysis is the segmentation of the vascular structures from the imaging volume, i.e., the separation of the vessels from the background. The resulting vascular and flow data are subsequently analysed using a 4D flow processing tool. The flow field can be transected by 2D planes at the desired location and angle [36].

4D flow MRI currently has several clinical applications, namely in studies dealing with cardiac and vascular regions in the human circulatory system. Studies investigating arterial and venous blood flow in intracranial vessels are essential, not only to characterize the advanced stages of some diseases, but also to find early indicators of emerging cerebrovascular dysfunction [4]. Several studies have been conducted with 4D flow, for better understanding of arterial stenosis [43]–[45], arterial stiffening and atherosclerotic disease [3], [46], [47], aneurysms [48], [49], vascular malformations [50], dural sinus pathology [24], Alzheimer's disease [8], [51], small vessel disease [42] and multiple sclerosis [52]. Nevertheless, for a successful clinical implementation and acceptance of 4D flow, further research is still needed, namely in the creation of normative bases for parameters measured with this technique. Additionally, it is of great importance to further study the reproducibility and the accuracy of both the technique and the processing methods [41].

2.2.3 Acceleration techniques

In order to decrease the acquisition time and increase spatial and temporal resolutions, acceleration techniques have been implemented.

Parallel imaging techniques such as SENSE (Sensitivity encoding) or GRAPPA (GeneRalized Autocalibrating Partially Parallel Acquisition) take advantage of multichannel receiver coils, reducing the number of phase encoding steps required [5]. With SENSE, aliased images are reconstructed from each coil and then combined using the coil sensitivities (calculated before or during the scan) to cancel or unwrap the aliasing [53]. With

GRAPPA the aliasing correction is made in the k-space before the Fourier transformation [54].

The acceleration technique applied for this research is a k-t acceleration method (kat-ARC) [55], with a variable density random (VDR) [56] k-t sampling scheme, to improve the reconstruction accuracy and reduce artifacts. In this scheme multiple coils are used and, although undersampling is performed in the center and outer k-space, low acceleration is used in the k-space center (called autocalibration signals (ACS) region) for accurate reconstruction. On the other hand, high acceleration is applied to fill the outer k-space. The accelerations are applied using a time-interleaved scheme, as represented in Fig 2.4.

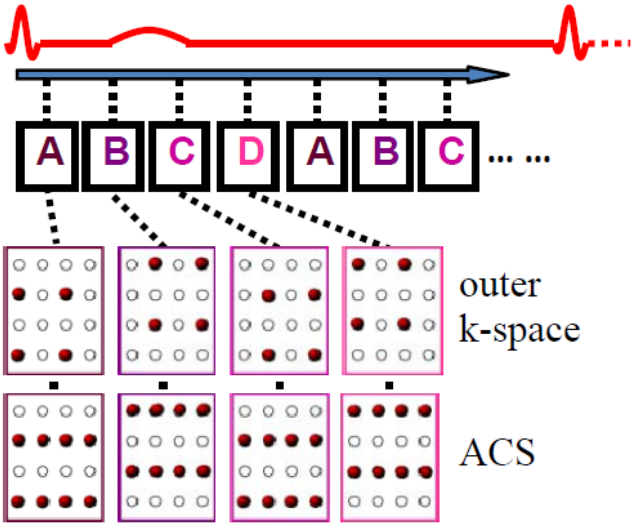

Figure 2.4: Time-interleaved sampling scheme for 4D flow data acquisition. In this case, 4× acceleration is used to sample the outer k-space, while 2× acceleration is used for the center of the k-space (ACS). The letters represent the different cardiac phases. Adapted from [55].

This sampling pattern is optimized by maximizing spatiotemporal correlation between sampled and unsampled data. The data from the ACS region is used to calculate weighting factors for each coil and then estimate the missing points that are undersampled. Unlike conventional ARC, k-t ARC utilizes data from adjacent time frames as well, to interpolate missing data [57].

When all the lines are filled, Fourier transformation is performed to create individual images from each coil, which are combined, using a sum of squares method, into the final magnitude image.

2.3 Cerebral blood flow

Anatomy

The blood is delivered to the brain by two pairs of large arteries, the right and left internal carotid, and the right and left vertebral arteries. The anterior circulation is formed

by branches of the ICA, while the vertebral arteries join to form the BA to originate the vertebrobasilar arterial system that composes the posterior circulation. The ICA divides into the MCA and the anterior cerebral artery (ACA), while the BA bifurcates into the left and right posterior cerebral arterys (PCAs). These divide into progressively smaller arteries and arterioles that supply oxygen and nutrients to the various regions of the cerebral cortex. At the central cranial base, the vertebrobasilar circulation is connected by communicating arteries to the two ICAs, forming an anastomotic ring called "circle/polygon of Willis", represented in Fig. 2.5.

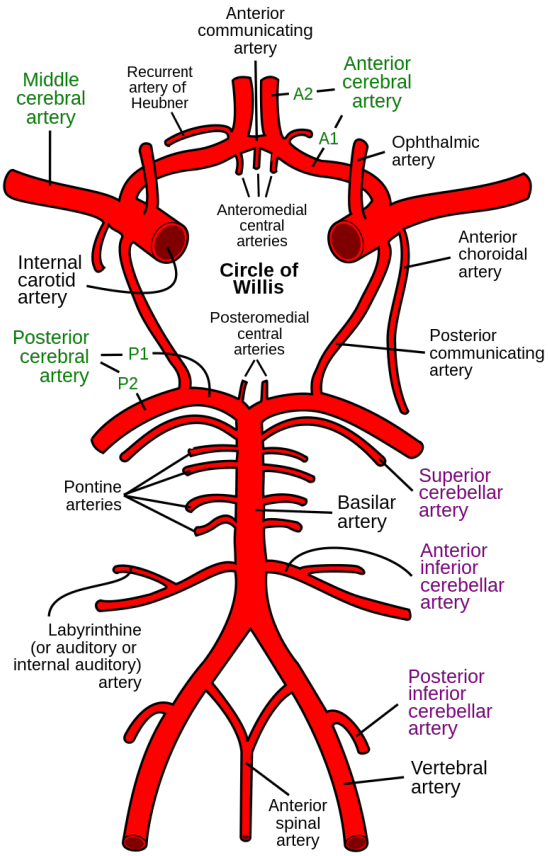

Figure 2.5: Circle of Willis diagram representation. From file freely available through public domain (the Wikimedia Commons).

Physiology and autoregulation

Although the brain only accounts for 2% of adult body mass, it is one of the most highly perfused organs in the body, receiving approximately between 15-20% of the resting cardiac output [58]. Due to the brain's constant high metabolic demand, the cerebral blood flow (CBF) must be strictly controlled through a process known as autoregulation [2].

The pressure gradient responsible for driving the blood flow to cerebral tissue is known as cerebral perfusion pressure (CPP) [59]. The CPP is given by the difference between the mean arterial pressure (MAP) and the intracranial pressure (ICP), while CBF is given by

CPP divided by cerebrovascular resistance (CVR). Thus, cerebral autoregulation consists of the process of maintaining CBF in response to changes in CPP, by altering CVR. Small arteries and arterioles are the primary contributors to CVR, since their radius can be altered by vasodilation and vasoconstriction.

An increase in MAP would result in increased CPP if the cerebral autoregulation was not present. However, in healthy individuals, the vascular resistance is increased by vasoconstriction of the vessels, maintaining CBF. Likewise, if the MAP decreases, cerebral autoregulation causes vasodilation, reducing CVR and rebalancing CBF.

In healthy individuals, the cerebral autoregulation process occurs as long as MAP is within the range of 50 to 150 mmHg [2]. However, in certain pathologies, such as CSVD, the autoregulation process is impaired and CBF is highly affected by MAP alterations [59].

Under normal circumstances, blood flow moves through the arteries in a series of concentric layers with a pattern referred to as laminar flow, as represented in Fig. 2.6 - center. The thin layer of blood flow adjacent to the vessel wall is considered to have null velocity [60]. The flow velocities gradually increase until the center of the lumen, where maximum velocity is found. This phenomenon occurs in long, straight blood vessels, under steady flow conditions [61].

However, in the majority of vessels, the velocity profile is typically more blunted, as observed in Fig. 2.6 - left, due to elasticity, pulsatility effects and short vessel length. The velocity presents a more homogeneous distribution, also known as plug flow, with nearly the same velocity throughout the lumen.

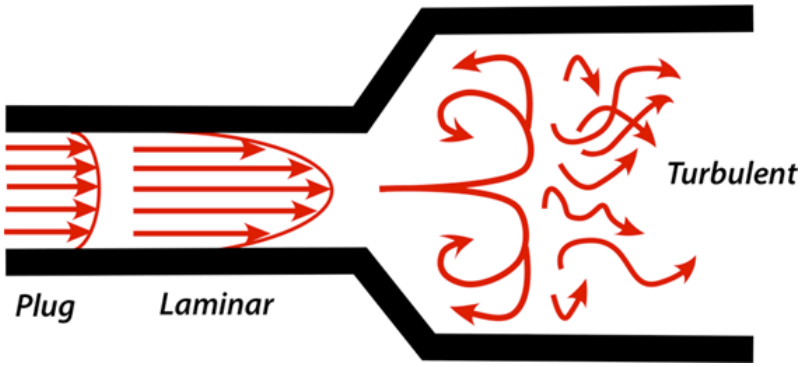

Figure 2.6: **Left**. The flow usually presents a more blunted pattern, known as plug flow, in the majority of the arteries. **Center**. Under normal circumstances, and in straight long vessels, the blood presents a parabolic shape. **Right**. In branching points or curved sections, the blood flow may present a turbulent behaviour. Adapted from [61].

The mentioned laminar or plug flow patterns are not observed in branching points or curved sections frequently present in intracerebral arteries, where the blood flow is turbulent [59], as shown in Fig 2.6 - right, and may form swirls referred to as eddy currents [62].

The flow measured with the techniques mentioned, including 4D flow, represents the average velocity of the entire vessel cross-section.

Arterial pulsatility, resistance and compliance

The role of the arterial system is to not only conduct an adequate blood supply to peripheral tissues, but also to cushion the pulsations generated by the heart, ensuring an almost steady flow to the peripheral tissues and organs [63], [64].

In order to dampen the arterial pressure (Windkessel function), about half of stroke volume is momentarily stored in the aorta and large elastic arteries, while the remaining blood volume is forwarded directly to the peripheral tissues [63]. This phenomenon is only possible because large arteries branching from the aorta are highly elastic, while distal arteries gradually become more muscular and less elastic, offering peripheral resistance to flow.

During the systole, the aorta, as a compliant artery, that is, with the capacity to distend and store blood in response to an increase in pressure [62], stretches to accommodate the blood ejected by the left ventricle, thereby dampening an increase in systolic blood pressure (SBP). During the diastole, the drop in SBP is limited due to the aortic wall's elastic recoil, resulting in the delivery of the remaining blood to the peripheral circulation, enabling continued aortic blood flow [63], [65]. As a consequence, an increased aortic stiffening, often related to increased age [64], causes the loss of Windkessel function and the entire stroke volume will flow through the arterial system and peripheral tissues only during the systole. Undamped pulsatile pressure extends to the vulnerable microcirculation of unprotected organs with low vascular resistance.

As mentioned in Section 2.3, the brain is one of the most highly perfused organs in the body, however it has low vascular resistance. As such, the loss of arterial elasticity has been associated with CSVD [66], stroke [67], and impaired cognitive function in the elderly [68]–[70] as well as in young to middle-aged adults [71].

In order to investigate the propagation of pulsations or what locally remains of pulsations in cerebral arteries, several studies have been conducted using arterial pulsatile volume load (ΔV) or FVP [72]–[74] and PI [75], [76]. Whilst the PI reflects the vascular resistance [77], [78], FVP corresponds to the cyclic distention of downstream arteries, required to convert the pulsatile arterial flow to a nonpulsatile capillary, assuming a stationary downstream capillary flow.

Measurements of PI can be obtained and expressed as:

$$PI = \frac{Q_{syst} - Q_{diast}}{Q_{mean}} \tag{2.5}$$

where Q_{syst}, Q_{diast} and Q_{mean} are the systolic, diastolic and mean flow, respectively [42]. FVP can be obtained by:

$$FVP = \int_{systole} (Q(t) - Q_{mean})dt \tag{2.6}$$

where $Q(t)$ is the flow at a given time t [17], [42], [79].

Processing of 4D PC-MRI data enables the estimation of mean flow rates and velocities, flow amplitudes, or arterial volume changes that can be derived from local arterial waveforms for quantification of cerebral arterial pulsations. Velocity and flow rate, defined as the product of the velocity and the cross sectional area of the vessel, can be measured from a 2D plane that is perpendicular to the target vessel [36]. These parameters can be helpful to understand the pathophysiological processes behind not only aging, but also cerebrovascular pathologies.

2.4 Small vessel disease

Cerebral small vessel disease is a widely used term to refer to intracranial vascular diseases based on various pathological and neurological processes, as well as a condition referring to various clinical indications and neuroimaging characteristics induced by structural changes of vascular and brain parenchyma [80]. This condition arises from disease affecting the cerebral microcirculation (small arteries, arterioles, venules, and capillaries) [72] and primarily impacts the tissue and blood supply of the deep white and grey matter of the brain [73].

CSVD is responsible for a diverse range of clinical problems, accounting for up to 25% of all ischemic strokes [74], vascular and mixed dementias, intracerebral hemorrhages, gait, balance and bladder dysfunctions [9], [73]. Still, when it comes to prevention, treatment options are limited, since no therapeutics are currently available [81].

CSVD, as an umbrella term, describes pathology of the small vessels on the brain, regardless of its underlying pathogenesis. In consequence, many pathophysiological processes may be at its origin. It becomes a highly complex process to unravel, since most of these pathophysiological processes can coexist with mutual interactions. Additionally, since CSVD affects the smallest vessels in the brain, the currently available in vivo medical imaging equipments do not have sufficient spatial resolution to visualize them [75].

The risk factors associated with CSVD are age, hypertension, diabetes and smoking [76]. These cardiovascular risk factors contribute to structural and functional changes of the arterial wall, resulting in increased stiffness of the arteries. The central elastic arteries (e.g., aorta and the carotid artery) are compliant arteries, which provides a Windkessel effect [65] to dampen cardiac-driven hemodynamic pulsatility and facilitates a continuous blood flow in the capillaries. The stiffened vessel walls may lead to less effective Windkessel effect [82], gradually increasing pulsations reaching the distal cerebral arteries and microvasculature, resulting in damage [83].

CSVD is usually assessed using computed tomography (CT) and MRI. Signs of CSVD on conventional MRI include recent small subcortical infarcts, white matter hyperintensities (WMH), lacunes, prominent perivascular spaces, cerebral microbleeds, and atrophy [84]. These lesions are commonly assessed through structural MRI, including sequences such fluid attenuated inversion recovery (FLAIR), T2-weighted, T1-weighted and gradient echo/T2*/susceptibility-weighted.

The main goal of 4D flow and CSVD related studies is to assess the relationship between the flow related alterations measured with 4D flow MRI and WMH severity scored with the Fazekas scale [85]. If this connection is proved, a better understanding of the pathophysiology behind the origin of CSVD is achieved. Thus, this technique may play an important role in the process of early detection of the disease, preferably before significant lesions occur. Furthermore, it would also be important for monitoring the evolution of patient condition, in order to track the effect of therapeutic options.

3

State of The art

This chapter initially presents the techniques clinically used to assess the vascular function in Section 3.1. The studies with the purpose of validating 4D flow MRI are mentioned in Section 3.2, comparing the results obtained with reference techniques, such as TCD ultrasound and 2D PC-MRI. The same section also contains a number of articles testing the reproducibility of 4D PC-MRI. Section 3.3 highlights studies relating CSVD and hemodynamic parameters measured with PC-MRI, for a better understanding of the parameters chosen within this thesis.

3.1 Vascular function imaging techniques

Until recently, TCD ultrasound and DSA [16] have been used to assess hemodynamic parameters of intracerebral vessels. However, DSA presents several disadvantages, such its invasive nature due to the necessity to insert a small catheter into an artery, exposure to radiation, since it is an x-ray based technique, and the need to use contrast and, in some cases, general anesthesia. On the other hand, although TCD is a non-invasive and non-ionizing technique, it is typically restrained to large intracranial vessels and suffers limitations [86], since the doppler signal is only obtain through acoustic windows, which in some individuals do not have enough quality or are non existent. Additionally it is significantly operator dependent, since an extensive knowledge of cerebrovascular anatomy is necessary for the performance of this technique [3], [81].

In recent years, 2D PC-MRI, as a non-invasive technique, has been widely used for the assessment of flow and velocity related information in a clinical setting [15], [17]. However, as mentioned in Section 2.2.1, this technique requires the operator to plan the cross-section position of the images, so it perpendicularly intersects the vessel of interest, resulting in a time-consuming process. In addition, only the vessel sections that were targeted during the scan can be analysed to retrieve information.

4D PC-MRI has been gaining notoriety because it allows for whole brain coverage in one scan and the data can be analysed post-hoc to assess blood flow, velocity and several other hemodynamic parameters.

In order to validate the potential of 4D flow for clinical applications, several studies have been carried out, and discussed in the following section, to assess the accuracy, reproducibility, and observer dependence of the sequence and post-processing schemes.

3.2 Validation studies

To validate the 4D flow technique, several studies compared the technique's results with reference ones, such as TCD and 2D PC-MRI. Harloff et al. [18] compared velocities provided by 4D flow with TCD measures in the carotid bifurcation of healthy volunteers, and found a high concordance between the PI and resistivity index of TCD and MRI measurements (13-16% difference). However, velocities were systematically underestimated by 4D flow, when compared to TCD, with a difference of 31-39%. These differences were related to lower spatial and temporal resolutions of MRI, which results in spatial averaging and temporal low-pass filtering. Additionally, these findings may also be due to errors in angle corrections in TCD, or the fact that hemodynamic data is averaged within a period of a few seconds for TCD, in contrast to a period of up to 15 min in 4D PC-MRI.

Wåhlin et al. [17] applied a radially undersampled 4D flow approach to assess the volume of arterial pulsatility in major cerebral vessels, with the main objective to evaluate the agreement with conventional 2D PC-MRI acquisitions. According to their research, there were no significant statistical differences between 4D and 2D PC-MRI-derived ΔV or mean flow when considering the entire ensemble of vessels analysed, supporting the idea of using a single 4D flow acquisition to effectively assess pulsatility in many intracranial arteries.

More recently, Holmgren et al. [19] investigated the feasibility of pulsatility assessments with 4D flow MRI in cerebral arteries of an elderly population and compared the results with reference 2D PC-MRI measurements of flow waveform amplitudes, ΔV and PI. An excellent agreement with 2D PC-MRI was found for flow waveform amplitudes and ΔV. However, multiple plane averages and lowpass filtering were required to attain such results.

To further investigate the feasibility of the 4D flow technique it is necessary to assess the reproducibility of the technique, comparing two measurements on the same subject in equal conditions, but in two different instances.

Good reproducibility has been demonstrated for 4D flow MRI measures in the aorta [20], [21], the mid portion of the pulmonary trunk [21], intraheart [22] and arterial and portal venous liver hemodynamics [23]. Nonetheless, it is important to assess the reproducibility in cerebral vessels, and such investigation is still limited. Wen et al. [14] studied the test–retest reliability of blood flow and peak velocity in the left and right ICAs, left and right MCAs and in the sagittal sinus. Good test-retest reliability was observed in this study. However, as one of the limitations, the authors mentioned that only the blood flow and peak velocity were investigated.

3.3 Hemodynamic biomarkers for cerebral small vessel disease

This thesis is part of a project that aims to investigate the relationship between hemodynamic alterations and CSVD with 4D PC-MRI. Hence, it is of extreme importance to understand what has already been found regarding this topic.

As mentioned before, increasing pulsations reaching the distal cerebral arteries and microvasculature caused by arterial stiffness are hypothesized to reflect and possibly even be a contributing mechanism to CSVD.

Although there is not yet much research using 4D PC-MRI to assess pulsatility and CBF in patients with CSVD, some conclusions can be drawn from existing studies.

Birnefeld et al. [42] used 4D PC-MRI with the aim of investigating the cross-sectional relationship between arterial pulsatility and CSVD in patients with ischemic stroke and transient ischemic attack. Cerebral arterial pulsatility was measured in the ICAs and in the MCAs. It was found that ICA pulsatitily is associated with increased white matter lesion volume. Additionally, increased PI and FVP in the M1 segment of the MCA was also associated with decreased cognitive function. Furthermore, ICA-FVP was associated with WMH volume, and both ICA-FVP and M1-FVP were associated with decreasing total brain volume in patients with CSVD. This research suggests that FVP may be a useful biomarker for CSVD, as it proved to possess strong associations with the disease.

Shi et. al. [87] concluded, in a review article assessing intracranial pulsatility in patients with CSVD, that most data supports a cross-sectional association between CSVD and higher pulsatility in large intracranial arteries such as MCA and ICA, although it is still not known if high pulsatility leads to more WMH or the opposite.

Thus far, the available data is conflicting regarding the roles of both CBF and pulsatility in CSVD. The current study provides the first step to evaluate the clinical feasibility of utilizing 4D flow MRI to asess pulsatility and blood flow related measures. Additionally, it contributes to validate this promising technique, that presents several advantages when compared to previously used methods and with useful potential in breakthrough research, not only to study CSVD, but other cerebrovascular diseases as well.

4

Methodology

This chapter comprises the information about the volunteers present in the pilot study in Section 4.1. The sequence used for image acquisition, and an explanation of the obtained data are exhibited in Section 4.2. The software used for data processing and the methodology employed to obtain the parameters are described in Section 4.3, followed by the statistical analysis exhibited in Section 4.4.

4.1 Study population

Between June and July 2022, ten healthy volunteers (four females, age range 18-28, mean 22.5 years with standard deviation 2.8) with no history of neurological disease and no contraindications to MRI participated in the experiment. The study protocol was approved by the Medical Ethics Committee of Hospital da Luz and written informed consent was obtained from all subjects.

4.2 Magnetic resonance imaging acquisitions

The experiments were conducted on a 3T MR system (Signa Premier, GE Healthcare, Waukesha) equipped with a 48 channel receiver head AIR^{TM} coil. 4D flow acquisition was performed using a k-t acceleration method, kat-ARC, with a VDR k-t sampling scheme, leading to an overall undersampling factor of 8. The scan parameters were: echo time/repetition time (TE/TR) = 2.792/4.736 msec, flip angle = 10°, field of view (FOV) = 220 × 220 mm^2, acquisition matrix size = 220 × 220, reconstruction matrix size = 256 × 256, bandwidth = 62.5 kHz, spatial resolution = 0.9 × 0.9 × 0.5 mm^3, velocity encoding sensitivity along all three directions = 80 cm/s. The number of excitations (NEX), which defines the number of signal averages used for image reconstruction, was equal to 4. A total of 180 axial slices were acquired to cover the whole brain with a slice thickness of 1 mm, and was then interpolated to 0.5 mm using zero filling interpolation. The cardiac synchronization was ECG triggered. The acquisition was retrospectively triggered with

10 timeframes acquired within the R-R interval, and 30 frames were reconstructed. The total scan time was about 6–10 minutes, depending on the subject's heart rate.

To assess the reproducibility of the measurements, all subjects were scanned in two consecutive days (test scan and retest scan) at approximately the same time of the day.

Although the sequence was implemented by a GE Healthcare Engineer, I assisted the process by processing datasets with different sequence parameters to achieve the best results and also helped find the best moment to trigger the ECG in order to visualize the waveforms with the intended shape (first the systole and then the dyastole).

Each 4D flow dataset comprised a total of 21600 scans. For each of the 30 cardiac frames, 180 planes were acquired, which gives a total of 5400 images for the magnitude (anatomy) and flow in each of the three orthogonal directions. An anatomy scan example can be observed in Fig. 4.1A. The combination of the anatomy images alongside the anterior-posterior (AP) (Figure 4.1B), left-right (LR) (Figure 4.1C) and superior-inferior (SI) (Figure 4.1D) flow images is then used to obtain information about the velocities in the x (v_x), y (v_y) and z (v_z) directions, respectively.

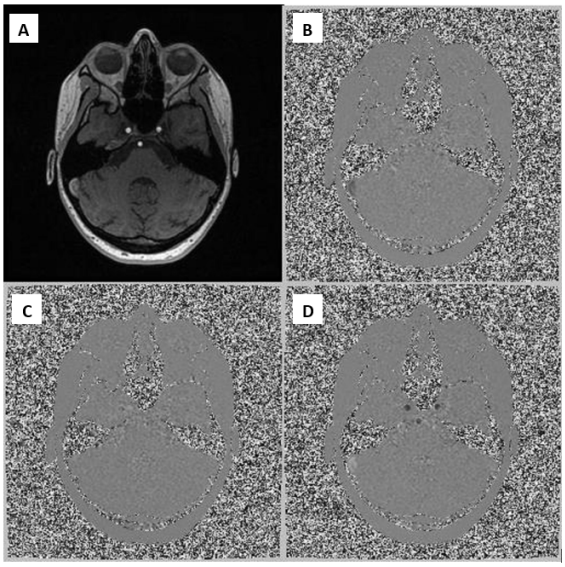

Figure 4.1: Example Images of the 4D flow dataset. (**A**) Anatomy image. (**B**) Anterior-Posterior flow image. (**C**) Left-Right flow image. (**D**) Superior-Inferior flow image.

4.3 Data processing and analysis

To analyse the 4D flow data, The 4D Flow PWV Tool, created by Eric Schrauben [88], was used.

The first step is the creation of a 4D flow MRI-derived CD volume that suppresses stationary tissue and highlights blood vessels. They are separated from the background through automatic thresholding [88], resulting in a binarized volume. The volume can be cropped on the axial, sagittal and coronal projections of the CD to only include the

region of interest (ROI), which can then be visualized on a three-dimensional model of the vasculature, as represented in Fig. 4.2 - right.

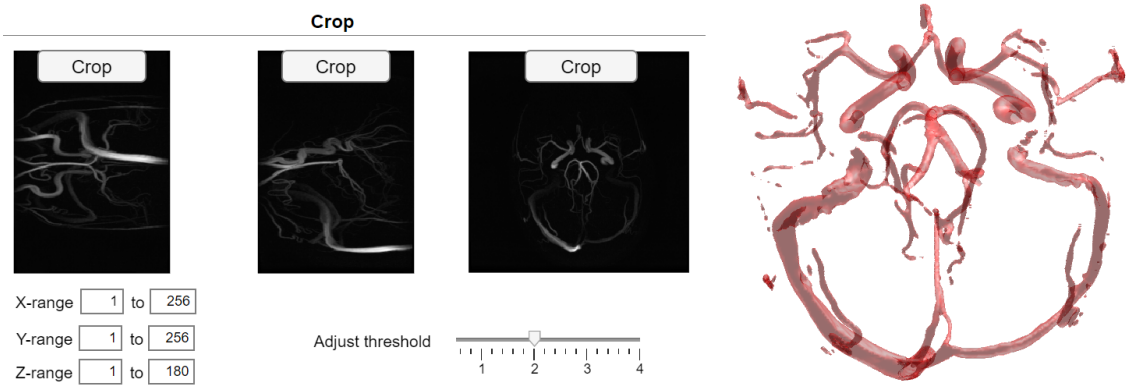

Figure 4.2: **Left**. Complex difference images from the coronal, sagittal, and axial projections (respectively from left to right) can be viewed and cropped to only include the regions of interest. Cropping can be performed by manually choosing an area of interest in each of the projections or by entering the range of each of the three dimensions (x, y, and z). In addition, the threshold can be manually adjusted with a slider bar. With increasing threshold, less vasculature is included in the volume. **Right**. A 3D model of the vessels is constructed and visualized.

Skeletonization is then performed via a thinning algorithm [56], resulting in a one-voxel wide vessel centerline representation, present in Fig. 4.3. Each vessel is labeled with a number, allowing for the software user to choose which vessel to further analyse.

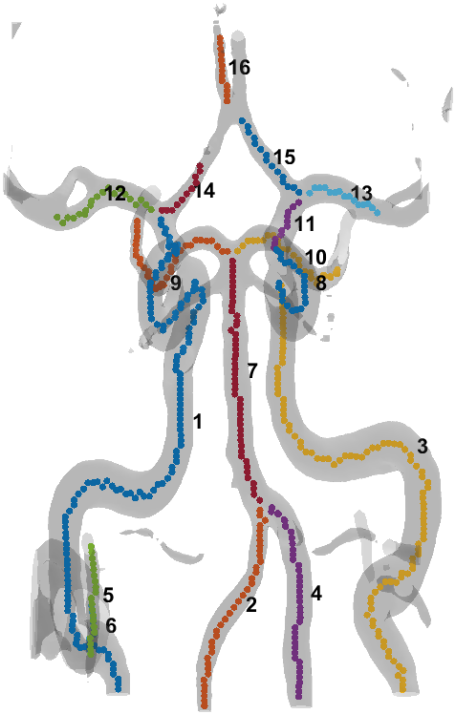

Figure 4.3: Each vessel of the centerline representation is identified with a unique number that the user can choose to select the vessel of interest for analysis.

The direction of flow propagation within the vessel is estimated based on the analysis of two points before and after the current centerline voxel along the chosen vessel length. Orthogonal cutplanes are automatically placed in each one of the centerline points throughout the entire vessel. The cutplanes are squares with 11-pixel sides and an interpolation is then performed to increase the resolution by a factor of 4.

Originally the software separated the vessel from the background with a k-means clustering algorithm, combining the CD and velocity information. However, according to [89], in a comparison between three different segmentation methods (k-means clustering, local thresholding and global thresholding), k-means clustering produced a flow underestimation when compared directly to the reference method (2D flow MRI), probably due to underestimation of the lumen area. Since the flow estimation results from the multiplication of the velocity by the cross-sectional area, an area underestimation causes a flow underestimation. Hence it was considered that the local threshold produced the best flow results. Several threshold values were tested and, a local threshold of 20% was considered to be independent from vessel size and non biased, indicating the best outcome. For that reason, a local threshold of 20% of the maximum intensity of the CD cutplane (referred as angio images by the software) was used to develop the segmentation of the vessels. An example of a vessel segmentation can be visualized in Fig. 4.4. The vessel cross-sections presented in the angio images (Figure 4.4 - left) are separated from the background with a threshold of 20% of the maximum intensity of each section, resulting in a binarized segmentation (Figure 4.4 - right).

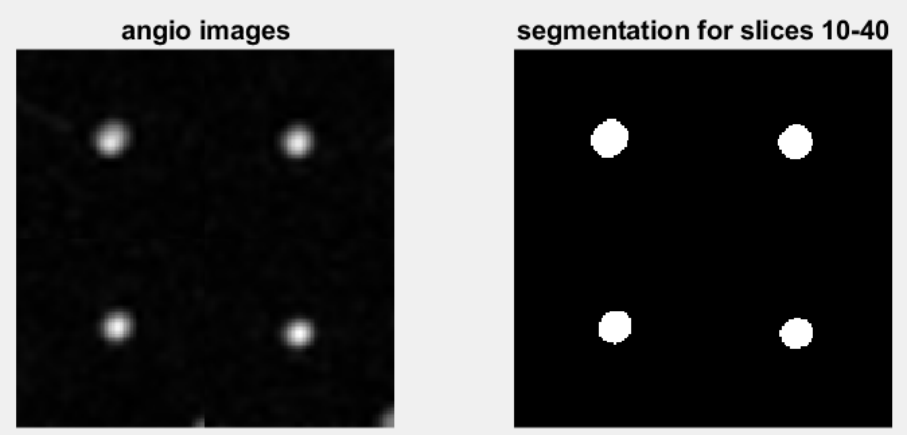

Figure 4.4: **Left**. Complex difference (angio) images of the vessel cross-sections.**Right**. Respective segmentation using a local threshold of 20% of the maximum intensity.

The average x, y and z velocities were then estimated, and the final velocity estimate was calculated as the dot product of the velocity vector obtained and the vessel direction [3]. The vessel cross-sectional area was estimated by considering the sum of the areas of included pixels in the segmentation process. The blood flow was determined by multiplying the vessel area by blood velocity. A blood flow waveform can then be reconstructed by extracting the blood flow for the 30 cardiac frames, considering the same vessel area for

the entire cardiac cycle. The process is then repeated for every cutplane along the vessel, allowing for the observation of all the waveforms contained in the vessel. Each line in Fig. 4.5 depicts a different centerline point location in the blood vessel.

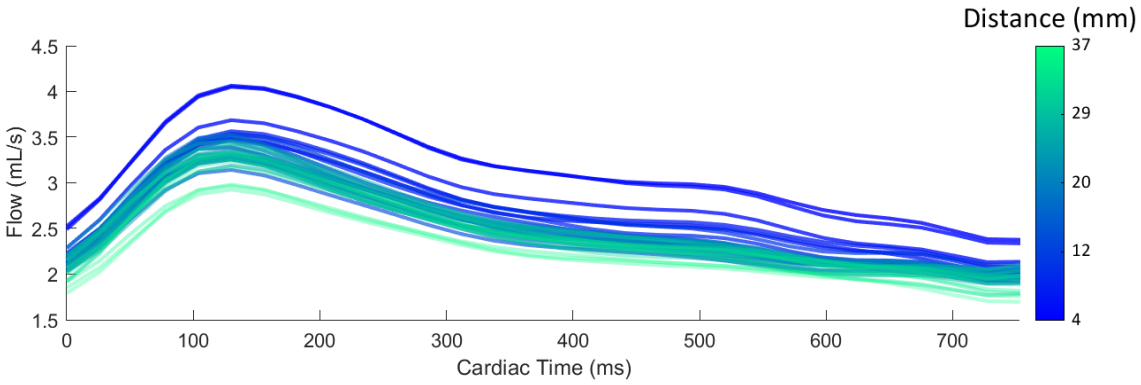

Figure 4.5: Blood flow waveforms for each one of the cross-sectional planes along a vessel. The vertical axis represents the blood flow in ml/s, while the horizontal axis stands for the time of the cardiac cycle in ms. The colormap denotes the different distances along the vessel. In this figure, the systole is represented by an increasing flow, around the 150 ms mark. After, the diastole is depicted by the decreasing amplitude of the waveforms.

Extra to the 4D flow PWV Tool, that only outputed the pulse wave velocity, the pulsatility index and flow volume pulsatility were also computed, using waveform information. PI was calculated as expressed in Equation 2.5, by dividing the difference between the maximum flow (Q_{max}) and the minimum flow (Q_{min}) by the mean flow (Q_{mean}), as represented in Fig. 4.6 - left.

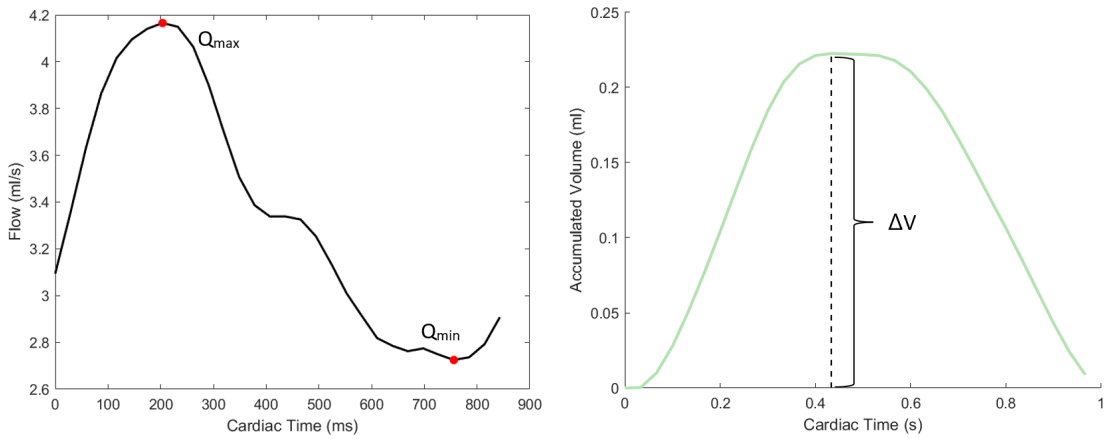

Figure 4.6: **Left**. The pulsatility index is calculated by dividing the difference between Q_{max} and Q_{min} by the Q_{mean}. **Right**.The flow volume pulsatility (ΔV) is considered the difference between the maximum and minimum volumes.

To calculate the flow volume pulsatility (also known as arterial volume load), the mean flow was subtracted from the flow waveform and the cumulative integral of the remaining waveform was obtained. The curve was then shifted vertically, so that minimum volume

corresponds to zero. FVP is considered the difference between the maximum and the minimum of the shifted curve (Figure 4.6 - right). This is equivalent to Equation 2.6.

As mentioned in [42], the FVP was standardized by R–R interval, otherwise this measurement would be highly dependent on heart rate, since it is calculated by an integration over time that depends on the length of the cardiac cycle. This process consists on standardizing all R-R intervals to one second.

Additionally, the vessel area, minimum, maximum and mean velocities were also outputed for reproducibility analysis.

All data processing was performed in MATLAB version 2022a [90]. For each acquisition, the PI, FVP, vessel cross-sectional area and maximum, minimum and mean velocities were measured. Similarly to [17], [42], the considered ROIs were the M1 segment of the right and left MCAs (Figure 4.7 - numbers 1 and 2), the cavernous segment of the right and left ICAs (Figure 4.7 - numbers 3 and 4) and the middle of the BA (Figure 4.7 - numbers 5).

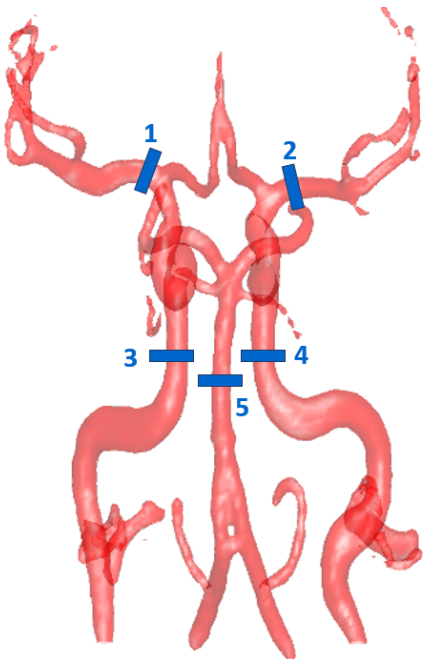

Figure 4.7: Regions of interest identified in the 3D volume reconstructed by the software. Measurements were executed in the M1 segment of the right and left middle cerebral arteries (1 and 2), in the cavernous segment of the right and left internal carotid arteries (3 and 4) and in the basilar artery (5).

In order to achieve a result that represents a region of interest, measurements were considered as an average of the values obtained from six consecutive centerline voxels, following the methodology described in [42].

Additional functionalities were added to the software, such as the possibility to save the waveforms and respective cardiac series in '.mat' files, together with the results of PI, FVP, minimum, maximum and mean velocities and vessel area, on an excel spreadsheet.

4.4 Statistical analysis

All results of the measurements and calculations are reported as mean ± standard deviation.

In order to assess the reproducibility and accuracy of 4D flow measurements and to validate the software used for scan processing, intraclass correlation coefficient (ICC), Wilcoxon signed-rank test, Bland-Altman and Pearson correlation analyses were conducted. The Wilcoxon tests and Bland-Altman plots analyse the agreement between measurements, whereas the Pearson correlation coefficients (PCCs) are used to evaluate correlation [91]. The ICCs reflect not only the degree of correlation, but also the agreement between the results.

The ICC estimates and their 95% confidence interval (CI) were calculated based on a single rating, absolute-agreement, 2-way mixed-effects model (ICC(2,1)). According to [91], the ICC values are interpreted as poor reliability for values inferior to 0.5; moderate reliability for values between 0.5 and 0.75; good reliability for values between 0.75 and 0.9 and excellent reliability for values higher than 0.9.

The differences between the test and retest scan were tested for normality with the Shapiro-Wilk test [92]. Since not all differences presented a normal distribution, a Wilcoxon signed-rank [93] test was employed, instead, to analyse the agreement between the two measurements. This test is a non-parametric alternative to the paired samples t-test, in which the null hypothesis states that the median of differences between pairs of measurements (Day 1 and Day 2, in this case) equals 0. A p-value ≤ 0.05 was considered statistically significant and indicates that the median difference is statistically different from 0.

The mean differences and limits of agreement (LoA) were displayed in Bland-Altman plots for agreement estimation between the two measurements. In these plots, the relative difference, calculated as the difference between the two measurements divided by the mean of the two measurements, are plotted against the mean of the two measurements, similarly to the methodology presented in [15]. Relative differences were chosen rather than absolute differences, since they allow for easier interpretation of the results and comparison between parameters. The LoA were calculated as the mean ± 1.96 times the relative standard deviation (given as a percentage of the mean). It is important to clarify the maximum acceptable values for mean difference and LoA. In a 2D PC-MRI study, with repeated flow and ΔV measurements [94], intrasubject standard deviations of 0.067 - 0.070 ml for the ΔV, were reported in the ICAs, which is about 13% of the mean value observed for that measurement. Therefore, a standard deviation lower than 13% (meaning LoA inferior to 25.5%) was considered the goal for FVP and PI parameters. Since these are not direct measurements, but rather the result of operations made from them, the associated variability may be higher than the observed for the parameters that result from direct estimations.

In the same article, the standard deviation observed for the mean flow was slightly

lower. Hence, for the remaining parameters, a 10% standard deviation (LoA = 19.6%) was defined as the limit for acceptable accuracy. Additionally, in line with what was mentioned in [14], a mean relative difference inferior to 5% was also considered a good result.

Additionally, a Pearson correlation analysis was held in order to evaluate the linear correlation between the two measurements. Since the minimum acceptable value for the Pearson correlation coefficient highly depends on the research nature [95], the result of 0.75 was chosen as the goal for minimum correlation, similarly to [14], since it already indicates good correlation [96]. A p-value ≤ 0.05 was considered statistically significant. The same correlation measure was also used to assess HR and BP associations with the obtained values.

All statistical analyses were conducted using the SPSS software, version 26 (IBM, Armonk, NY).

5

Results

In this chapter the results of the study are presented and analysed. Initially, the reproducibility analysis for accuracy detection of the 4D flow technique and the use of the 4D Flow PWV Tool is presented. The results concerning the correlation analysis between the measurements, HR and BP are then reported. Lastly, a comparison of the results with previously reported data is performed, in order to further validate the findings from this research.

5.1 Reproducibility analysis

The test and retest (Day 1 and Day 2) mean values and standard deviations for all parameters and arteries examined are presented in Tables 5.1 and 5.2.

Table 5.1: Mean and standard deviation for the pulsatility index (PI), flow volume pulsatility (FVP) and vessel cross-sectional area (Area) for all arteries analysed in both days.

	PI		**FVP (ml)**		**Area (mm^2)**	
Vessel	Day 1	Day 2	Day 1	Day 2	Day 1	Day 2
BA[1]	0.49 ± 0.06	0.49 ± 0.08	0.18 ± 0.02	0.17 ± 0.02	8 ± 1	8 ± 1
ICA L[1]	0.46 ± 0.07	0.47 ± 0.09	0.30 ± 0.09	0.29 ± 0.06	15 ± 3	15 ± 4
ICA R[1]	0.47 ± 0.07	0.46 ± 0.09	0.29 ± 0.06	0.27 ± 0.06	14 ± 3	15 ± 2
MCA L[1]	0.45 ± 0.04	0.45 ± 0.05	0.22 ± 0.06	0.21 ± 0.05	9 ± 1	9 ± 1
MCA R[1]	0.42 ± 0.04	0.43 ± 0.07	0.22 ± 0.05	0.23 ± 0.08	9 ± 1	10 ± 2

[1] **BA** = basilar artery; **ICA L** = left internal carotid artery; **ICA R** = right internal carotid artery; **MCA L** = left middle cerebral artery; **MCA R** = right middle cerebral artery.

5.1.1 Intraclass correlation coefficient analysis

The ICC and 95% CI results for all the researched parameters of all arteries are provided in Tables 5.3 and 5.4.

Regarding the BA, the PI and FVP measures revealed a moderate reliability (ICC equal to 0.74 and 0.71) between both measures. The vessel area, V_{min}, V_{mean} and V_{max} presented

an excellent reliability (ICC equal to 0.95, 0.97, 0.98 and 0.96, respectively).

Table 5.2: Mean and standard deviation for the minimum velocity (V_{min}), mean velocity (V_{mean}) and maximum velocity (V_{max}) of all arteries analysed in both days.

	V_{min} (cm/s)		**V_{mean} (cm/s)**		**V_{max} (cm/s)**	
Vessel	Day 1	Day 2	Day 1	Day 2	Day 1	Day 2
BA[1]	24 ± 5	24 ± 6	31 ± 6	31 ± 6	39 ± 7	40 ± 7
ICA L[1]	23 ± 4	23 ± 4	29 ± 4	29 ± 5	37 ± 5	36 ± 5
ICA R[1]	23 ± 5	22 ± 1	30 ± 5	28 ± 2	37 ± 5	35 ± 3
MCA L[1]	30 ± 2	31 ± 3	38 ± 3	39 ± 4	47 ± 4	48 ± 5
MCA R[1]	31 ± 4	30 ± 5	39 ± 5	38 ± 5	48 ± 6	46 ± 6

[1] **BA** = basilar artery; **ICA L** = left internal carotid artery; **ICA R** = right internal carotid artery; **MCA L** = left middle cerebral artery; **MCA R** = right middle cerebral artery.

Table 5.3: Intraclass correlation coefficient (ICC) and 95% confidence intervals (CI) for the pulsatility index (PI), flow volume pulsatility (FVP) and vessel cross-sectional area (Area).

	PI		**FVP**		**Area**	
Vessel	ICC	95% CI	ICC	95% CI	ICC	95% CI
BA[1]	0.74	(0.238 - 0.929)	0.71	(0.17 - 0.92)	0.95	(0.82 - 0.99)
ICA L[1]	0.76	(0.27 - 0.933)	0.80	(0.40 - 0.95)	0.97	(0.90 - 0.99)
ICA R[1]	0.77	(0.33 - 0.94)	0.77	(0.34 - 0.94)	0.86	(0.56 - 0.96)
MCA L[1]	0.55	(-0.128 - 0.866)	0.89	(0.618 - 0.972)	0.83	(0.45 - 0.95)
MCA R[1]	0.77	(0.32 - 0.94)	0.69	(0.129 - 0.912)	0.31	(-0.34 - 0.77)

[1] **BA** = basilar artery; **ICA L** = left internal carotid artery; **ICA R** = right internal carotid artery; **MCA L** = left middle cerebral artery; **MCA R** = right middle cerebral artery.

The left ICA exhibited good reliability for the PI, FVP and V_{max} (ICC equal to 0.76, 0.80 and 0.84), and excellent reliability for for the minimum and mean velocities (V_{min} and V_{mean}) (ICC = 0.91 for both) and vessel area (ICC = 0.97).

In the case of the right ICA, although it presented good reliability for the PI and FVP (ICC = 0.77 for both) and for the cross-sectional vessel area (ICC = 0.86), poor reliability for all the velocity parameters was obtained (ICC equal to 0.40, 0.38 and 0.34).

Concerning the MCAs, the left artery presented moderate results for the PI (ICC = 0.55) and for the minimum, mean and maximum velocities (ICC equal to 0.57, 0.74 and 0.56, respectively), whereas the FVP and area exhibited good reliability (ICC = 0.89 and 0.83). On the other hand, the right MCA revealed good reliability (ICC = 0.77) for the PI, moderate reliability (ICC = 0.69) for the FVP and all the velocity parameters (ICC = 0.57, 0.62 and 0.54, respectively). However, poor reliability was exhibited regarding the vessel area (ICC = 0.31).

To present an overview measure of the results, a mean ICC over all values obtained within each artery was calculated. Additionally, the parameter with the highest ICC result

was also identified for each vessel. The results are represented in Table 5.5.

Table 5.4: Intraclass correlation coefficient (ICC) and 95% confidence intervals (CI) for the minimum velocity (V_{min}), mean velocity (V_{mean}) and maximum velocity (V_{max}).

	$\mathbf{V_{min}}$		$\mathbf{V_{mean}}$		$\mathbf{V_{max}}$	
Vessel	ICC	95% CI	ICC	95% CI	ICC	95% CI
BA[1]	0.97	(0.88 - 0.99)	0.98	(0.92 - 0.99)	0.96	(0.86 - 0.99)
ICA L[1]	0.91	(0.70 - 0.98)	0.91	(0.68 - 0.98)	0.84	(0.48 - 0.96)
ICA R[1]	0.40	(-0.23 - 0.80)	0.38	(-0.20 - 0.79)	0.34	(-0.23 - 0.77)
MCA L[1]	0.57	(0.01 - 0.87)	0.74	(0.28 - 0.93)	0.56	(-0.03 - 0.87)
MCA R[1]	0.57	(-0.00 - 0.87)	0.62	(0.20 - 0.89)	0.54	(-0.09 - 0.86)

[1] **BA** = basilar artery; **ICA L** = left internal carotid artery; **ICA R** = right internal carotid artery; **MCA L** = left middle cerebral artery; **MCA R** = right middle cerebral artery.

Table 5.5: Mean intraclass correlation coefficient (ICC) for all arteries and the identification of the parameter with the highest ICC result and respective value for each vessel.

	BA[1]	**ICA L**[1]	**ICA R**[1]	**MCA L**[1]	**MCA R**[1]
Mean ICC	0.88	0.86	0.59	0.69	0.58
Best result	0.98	0.97	0.86	0.89	0.77
Best parameter	V_{mean}	Area	Area	FVP	PI

[1] **BA** = basilar artery; **ICA L** = left internal carotid artery; **ICA R** = right internal carotid artery; **MCA L** = left middle cerebral artery; **MCA R** = right middle cerebral artery.

The BA exhibited the best average ICC of 0.88, which indicates good reliability. Moreover, the mean velocity was the parameter in the BA that achieved the highest ICC, with an excellent reliability of 0.98.

Regarding the left ICA, the mean ICC observed was 0.86, while the cross-sectional area showed the best ICC = 0.97. On the other hand, the right ICA presented a mean ICC = 0.59 and, similarly to the left ICA, the best result for this artery was found for the cross-sectional area (ICC = 0.86).

Concerning the left MCA, the average ICC was 0.69, whereas the best result on this vessel was obtained for the FVP (ICC = 0.89). Finally, the right MCA displayed the worst results, with an average ICC of 0.58 and the best ICC = 0.77 for the PI.

Similarly to the methodology previously reported for the arteries, the mean ICC values for each parameter were calculated and the artery with the highest ICC found for each one was also identified. The results are presented in Table 5.6.

As far as the analysed parameters are concerned, the vessel cross-sectional area presented the highest mean ICC (0.78) and the best result of 0.97 for the left ICA. Moreover, the FVP exhibited a similar mean ICC = 0.77, while the best result was found for the left

Table 5.6: Mean intraclass correlation coefficient (ICC) for all parameters and the identification of the artery with the highest ICC result and respective value for each parameter.

	PI	**FVP**	**Area**	$\mathbf{V_{min}}$	$\mathbf{V_{mean}}$	$\mathbf{V_{max}}$
Mean ICC	0.72	0.77	0.78	0.68	0.72	0.65
Best result	0.77	0.89	0.97	0.97	0.98	0.96
Best artery	MCA R[1]	MCA L[1]	ICA L[1]	BA[1]	BA[1]	BA[1]

[1] **BA** = basilar artery; **ICA L** = left internal carotid artery; **MCA L** = left middle cerebral artery; **MCA R** = right middle cerebral artery.

MCA (ICC = 0.89). Regarding the PI, the average ICC was 0.72, while the highest value was 0.77 for the right MCA.

The V_{min}, V_{mean} and V_{max} presented a mean ICC of 0.68, 0.72 and 0.65, respectively. The best velocity results were all found for the BA, with an ICC of 0.97 for the minimum velocity, 0.98 for the mean velocity and 0.96 for the maximum velocity.

The ICC differences between the left and right ICAs are due to observed deviations between the measurements of a single volunteer, probably related to movement or physiological alterations. A similar situation occurred for the left and right MCAs, with another volunteer. Since there were only ten volunteers in this study, a significant discrepancy in the measurements of one of the samples causes a substantial difference in the resulting ICC.

The results present in Tables 5.7 and 5.8 were achieved by excluding the data related to the two outlier volunteers, only for the respective artery where the significant difference occurred. Additionally, the mean ICC values and the respective parameter and artery with the best result after the exclusion are represented in Tables 5.9 and 5.10

Table 5.7: Intraclass correlation coefficient (ICC) and 95% confidence intervals (CI) for the pulsatility index (PI), flow volume pulsatility (FVP) and vessel cross-sectional area (Area) for the remaining 9 volunteers.

	PI		**FVP**		**Area**	
Vessel	ICC	95% CI	ICC	95% CI	ICC	95% CI
ICA R[1]	0.64	(0.03 - 0.91)	0.76	(0.29 - 0.94)	0.99	(0.96 - 0.99)
MCA R[1]	0.76	(0.22 - 0.94)	0.68	(0.05 - 0.92)	0.77	(0.23 - 0.942)

[1] **ICA R** = right internal carotid artery; **MCA R** = right middle cerebral artery.

After the exclusion of outliers, the mean general ICC result for the right ICA raised to 0.78, which is significantly closer to the value obtained for the left ICA (0.86). Similarly, after this process, the average ICC for the right MCA is 0.72, more consistent with the previously reported result for the left MCA of 0.69. Additionally, the cross-sectional area showed a mean ICC of 0.9, which is considered excellent. The FVP and the minimum, mean and maximum velocities presented a good average reliability (ICC = 0.77, 0.75, 0.84 and 0.77). PI had, once again, the worst mean ICC observed (0.69).

Table 5.8: Intraclass correlation coefficient (ICC) and 95% confidence intervals (CI) for the minimum velocity (V_{min}), mean velocity (V_{mean}) and maximum velocity (V_{max}) for the remaining 9 volunteers.

	$\mathbf{V_{min}}$		$\mathbf{V_{mean}}$		$\mathbf{V_{max}}$	
Vessel	ICC	95% CI	ICC	95% CI	ICC	95% CI
ICA R[1]	0.57	(-0.11 - 0.89)	0.86	(0.46 - 0.97)	0.84	(0.46 - 0.96)
MCA R[1]	0.72	(0.16 - 0.93)	0.72	(0.13 - 0.93)	0.65	(-0.00 - 0.91)

[1] **ICA R** = right internal carotid artery; **MCA R** = right middle cerebral artery.

Table 5.9: Mean intraclass correlation coefficient (ICC) for the right internal carotid artery and middle cerebral artery and the identification of the parameter with the highest ICC result and respective value for each vessel, for the remaining 9 volunteers.

	ICA R[1]	**MCA R**[1]
Mean ICC	0.78	0.72
Best result	0.99	0.77
Best parameter	Area	Area

[1] **ICA R** = right internal carotid artery; **MCA R** = right middle cerebral artery.

Table 5.10: Mean intraclass correlation coefficient (ICC) for all the parameters and the identification of the artery with the highest ICC result and respective value for each parameter, for the remaining 9 volunteers.

	PI	**FVP**	**Area**	$\mathbf{V_{min}}$	$\mathbf{V_{mean}}$	$\mathbf{V_{max}}$
Mean ICC	0.69	0.77	0.90	0.75	0.84	0.77
Best result	0.76	0.89	0.99	0.97	0.98	0.96
Best artery	MCA R[1]	MCA L[1]	ICA R[1]	BA[1]	BA[1]	BA[1]

[1] **BA** = basilar artery; **ICA R** = right internal carotid artery; **MCA L** = left middle cerebral artery; **MCA R** = right middle cerebral artery.

5.1.2 Wilcoxon signed-rank test

To further statistically analyse the test-retest reliability of the 4D PC-MRI technique and subsequent post-processing, the difference between the measurements in each vessel was tested for normality with a Shapiro-Wilks test. The *p*-values obtained are presented in Table 5.11.

Since a p-value ≤ 0.05 is considered significant, it is possible to conclude that not all variations observed have a normal distribution. Therefore, a statistical test that assumes such a distribution is discarded, and a Wilcoxon matched-pairs signed-rank test was used instead. It is a non-parametric alternative to the paired samples *t*-test.

As mentioned before, the Wilcoxon signed-rank test evaluates if the median of differences between the measurements of the two consecutive days equals 0. If the resulting

p-value is lower than 0.05, the median of differences is statistically different from zero, which, in the case of a test-retest comparison, would indicate a negative outcome. The results obtained are presented in Table 5.12.

Table 5.11: *p*-value results for the Shapiro-Wilks test for the pulsatility index (PI), flow volume pulsatility (FVP) and vessel cross-sectional area (Area), minimum velocity (V_{min}), mean velocity (V_{mean}) and maximum velocity (V_{max}).

Vessel	PI	FVP	Area	V_{min}	V_{mean}	V_{max}
BA[1]	0.361	0.895	0.017	0.449	0.424	0.413
ICA L[1]	0.539	0.213	0.030	0.185	0.572	0.109
ICA R[1]	0.506	0.648	0.000	0.001	0.000	0.010
MCA L[1]	0.048	0.170	0.018	0.254	0.975	0.789
MCA R[1]	0.002	0.627	0.002	0.108	0.043	0.029

[1] **BA** = basilar artery; **ICA L** = left internal carotid artery; **ICA R** = right internal carotid artery; **MCA L** = left middle cerebral artery; **MCA R** = right middle cerebral artery.

Table 5.12: Wilcoxon signed-rank test results for the pulsatility index (PI), flow volume pulsatility (FVP) and vessel cross-sectional area (Area), minimum velocity (V_{min}), mean velocity (V_{mean}) and maximum velocity (V_{max}).

Vessel	PI	FVP	Area	V_{min}	V_{mean}	V_{max}
BA[1]	0.799	0.878	0.575	0.878	0.721	0.508
ICA L[1]	0.878	0.508	0.721	0.386	0.445	0.959
ICA R[1]	0.386	0.203	0.203	0.285	0.037	0.445
MCA L[1]	0.721	0.721	0.445	0.203	0.285	0.333
MCA R[1]	0.721	0.799	0.953	0.445	0.878	0.799

[1] **BA** = basilar artery; **ICA L** = left internal carotid artery; **ICA R** = right internal carotid artery; **MCA L** = left middle cerebral artery; **MCA R** = right middle cerebral artery.

As visible in Table 5.12, the *p*-values for all parameters analysed in all arteries are higher than 0.05, except for the mean velocity of the right ICA. These results indicate that the median of differences between the measurements is not statistically different from zero. This test demonstrates the agreement between measures, reassuring the generally good results presented by the ICC.

In this case, the best results were encountered for the right MCA, followed by the BA. The other arteries analysed exhibited similar *p*-value results, except for the right ICA, that presented the worst values of the test, indicating that the median differences between measurements observed in this artery are more statistically different from zero.

The parameter with the highest average *p*-value for all arteries was the PI, followed by the area and FVP, and the maximum velocity. The minimum and mean velocities presented similar average *p*-value results for all arteries.

As mentioned before, significant differences where found in the right ICA and right

MCA for one of the volunteers (a different subject for each artery). Therefore, following the process referred to ICC, and excluding data related to the two outlier volunteers, only for the respective artery where the significant difference occurred, the results presented in Table 5.13 were obtained for the Wilcoxon signed-rank test.

A significant improvement is observed for *p*-values associated with the right ICA, namely the cross-sectional area and the three velocities, where the differences between the two measurements where substantial. The mean velocity result is now higher than 0.05, which indicates that the median difference is not statistically different from 0. The *p*-values concerning the PI and FVP decreased in the case of the right ICA because there where no significant differences between the test-retest measures when comparing with the results of the remaining volunteers, as observed for the other parameters.

However, because the *p*-values after the outlier exclusion were all higher than 0.05, the results were considered satisfactory.

Table 5.13: Wilcoxon signed-rank test results for the pulsatility index (PI), flow volume pulsatility (FVP), vessel cross-sectional area (Area), minimum velocity (V_{min}), mean velocity (V_{mean}) and maximum velocity (V_{max}) for the remaining 9 volunteers.

Vessel	PI	FVP	Area	V_{min}	V_{mean}	V_{max}
ICA R[1]	0.260	0.086	0.401	0.515	0.066	0.767
MCA R[1]	0.374	0.767	0.779	0.767	0.678	0.767

[1] **ICA R** = right internal carotid artery; **MCA R** = right middle cerebral artery.

5.1.3 Bland-Altman plots and analysis

Bland-Altman plots were used to visualize the agreement between test and retest (Figures 5.1-5.6). A mean difference inferior to 5% was set to consider the results as acceptable. In these graphs, the relative LoA (presented with dashed lines) and mean relative diferrence (presented with continuous lines) are depicted separately for each artery and parameter analysed. Results for the ICAs and BA are plotted on the left, while the MCAs are plotted on the right, to improve visualization of all points. Additionally, the mean relative differences and relative LoA are summarized in Tables 5.14 and 5.15.

By examining Fig. 5.1 and Table 5.14 it is possible to observe that there are no significant differences between PI results in all the arteries presented. All mean differences are similar and close to zero, clearly shown by the continuous lines for each artery. The LoA (represented by the dashed lines in Figure 5.1) are also similar for the BA and left and right ICAs. The MCAs presented narrower LoA. Additionally, no bias is present in the measurements of PI, since the differences are evenly distributed.

In the case of the FVP, presented in Fig. 5.2, the right ICA exhibited a mean relative difference of 6.25%, which is higher than 5%, revealing worse agreement than the other arteries, and a possible bias. This higher mean difference is due to an outlier present

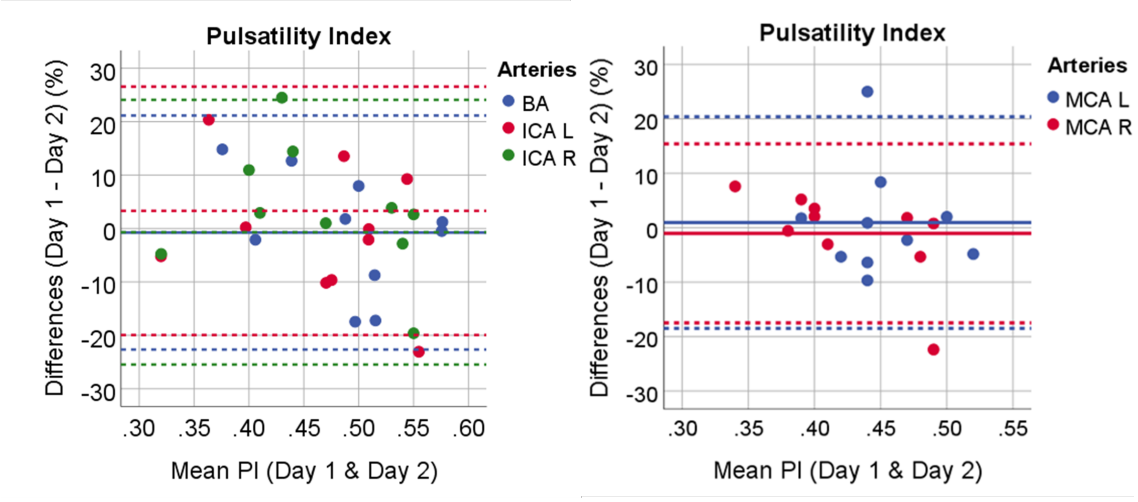

Figure 5.1: Bland-Altman plot for pulsatility index in the basilar artery and left and right internal carotid arteries (left) and left and right middle cerebral arteries (right). The relative difference between the measurements of the two days is plotted against the mean between the two measurements. The relative LoA are presented with dashed lines, and mean relative differences presented with continuous lines.

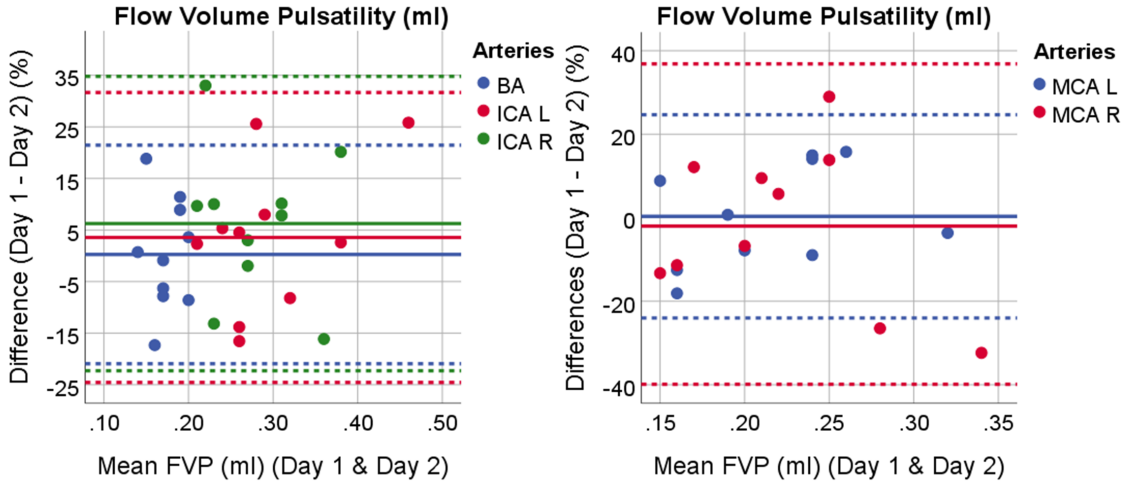

Figure 5.2: Bland-Altman plot for flow volume pulsatility in the basilar artery and left and right internal carotid arteries (left) and left and right middle cerebral arteries (right). The relative difference between the measurements of the two days is plotted against the mean between the two measurements. The relative LoA are presented with dashed lines, and mean relative differences presented with continuous lines.

that is responsible for a difference of 33% between the measurements of the two days. However, since this significant difference is only observed in the measurements of this specific volunteer for the FVP, it was chosen not to exclude it. The LoA are narrower for the left MCA when compared to right MCA. Significant but symmetrical differences where observed for the right MCA. No significant bias is present for the FVP measurements.

In the Bland-Altaman plots related to the cross-sectional area, present in Fig. 5.3, the

LoA are in general narrower than previously observed for the PI and FVP, except for the right MCA.

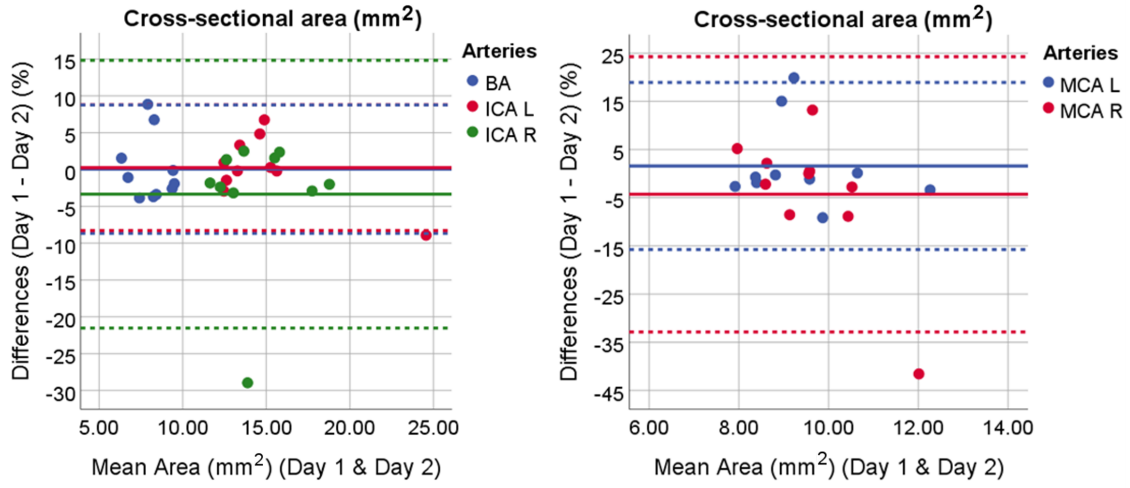

Figure 5.3: Bland-Altman plot for cross-sectional area (mm^2) in the basilar artery and left and right internal carotid arteries (left) and left and right middle cerebral arteries (right). The relative difference between the measurements of the two days is plotted against the mean between the two measurements. The relative LoA are presented with dashed lines, and mean relative differences presented with continuous lines.

However, the significant differences previously mentioned for the right ICA and MCA, in two of the volunteers, are clearly present in the Bland-Altman plots. Therefore, the mean relative differences for this arteries are affected by this outliers. Additionally, the LoA are wider for the same reason.

Similarly to the previous parameters, there is no significant bias present in these results.

When analyzing the Bland-Altman plots related to the velocity parameters, shown in Figs. 5.4, 5.5 and 5.6, similar conclusions are drawn.

Once again, an outlier is present for both the right ICA and MCA in every parameter, causing an increase in the mean relative difference and wider LoA.

The BA presented narrower LoA and mean relative differences closer to zero when compared with the other arteries. Moreover, albeit low, mean differences higher than 5% (5.46% and 5.90%) were found for the mean and maximum velocity, respectively, in the right ICA. These results are in agreement with the previous ICC and Wilcoxon-test results.

Similarly to what occurred for the majority of the PI, FVP and area results, there is no significant bias observed for the velocity measurements.

In general, the LoA for the area and velocity parameters (Figures 5.3, 5.4, 5.5 and 5.6) were narrower than the ones observed for the PI and FVP (Figures 5.1 and 5.2).

In order to assess the effect of the significant differences encountered for the right ICA and right MCA in the mean relative differences and LoA, those cases were excluded and the analysis was repeated. The results of this analysis are presented in Tables 5.16

and 5.17.

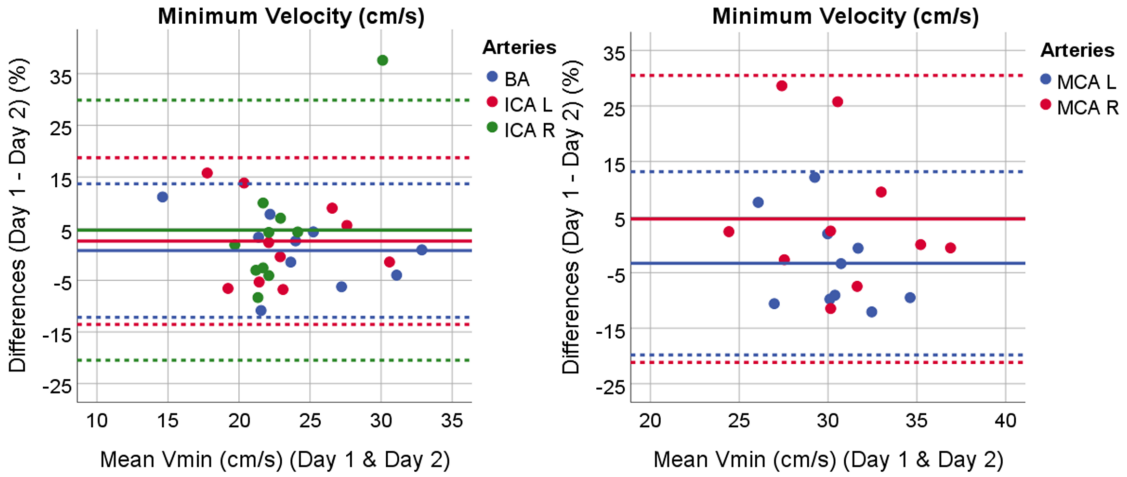

Figure 5.4: Bland-Altman plot for minimum velocity (cm/s) in the basilar artery and left and right internal carotid arteries (left) and left and right middle cerebral arteries (right). The relative difference between the measurements of the two days is plotted against the mean between the two measurements. The relative LoA are presented with dashed lines, and mean relative differences presented with continuous lines.

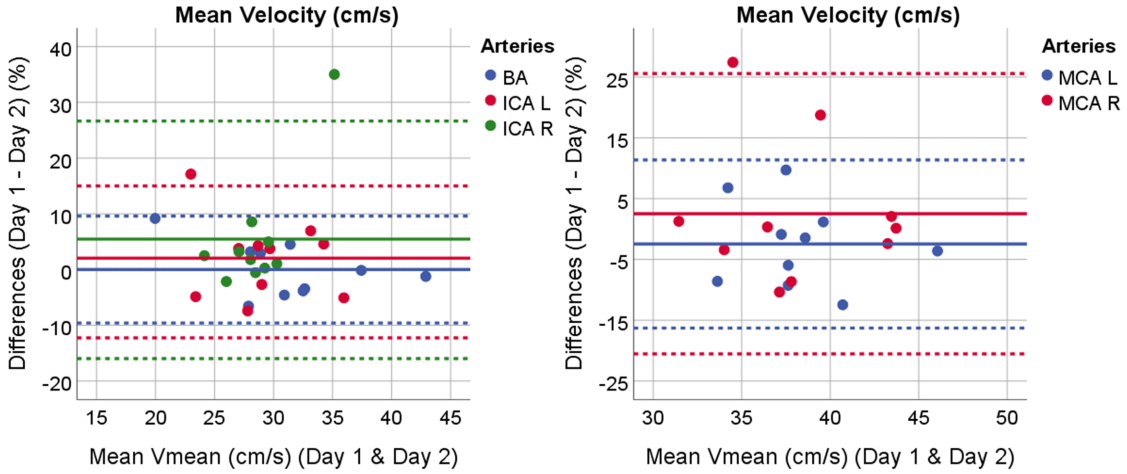

Figure 5.5: Bland-Altman plot for mean velocity (cm/s) in the basilar artery and left and right internal carotid arteries (left) and left and right middle cerebral arteries (right). The relative difference between the measurements of the two days is plotted against the mean between the two measurements. The relative LoA are presented with dashed lines, and mean relative differences presented with continuous lines.

It is possible to state that the results improved significantly, particularly for the area and velocity parameters. However, the mean relative difference for the FVP in the right ICA is 8.41%, which is higher than the maximum acceptable of 5%. As mentioned before, this value is due to a significant positive difference of 33% observed for one of the volunteers. Since the difference excluded was negative, the mean relative difference increased.

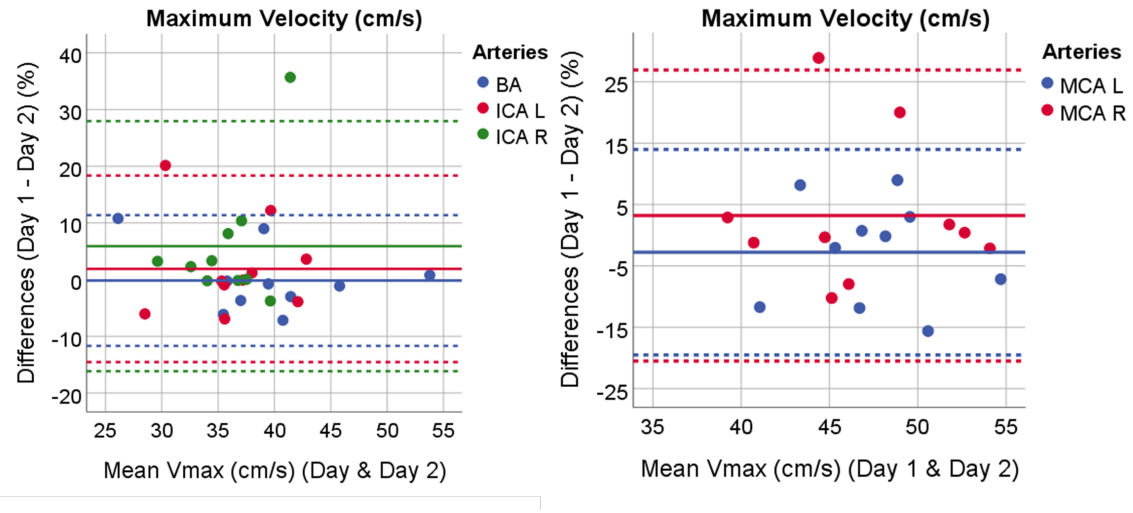

Figure 5.6: Bland-Altman plot for maximum velocity (cm/s) in the basilar artery and left and right internal carotid arteries (left) and left and right middle cerebral arteries (right). The relative difference between the measurements of the two days is plotted against the mean between the two measurements. The relative LoA are presented with dashed lines, and mean relative differences presented with continuous lines.

Table 5.14: Mean relative difference (MD (%)) and relative limits of agreement (LoA (%)) for the pulsatility index (PI), flow volume pulsatility (FVP) and cross-sectional area.

	PI		**FVP**		**Area**	
Vessel	MD (%)	LoA (%)	MD (%)	LoA (%)	MD (%)	LoA (%)
BA[1]	-0.76	21.91	0.25	21.19	0.05	8.72
ICA L[1]	-0.70	24.78	3.55	28.11	0.24	8.54
ICA R[1]	3.30	23.24	6.25	28.54	-3.35	18.18
MCA L[1]	0.95	19.44	0.32	24.34	1.58	17.34
MCA R[1]	-1.04	16.44	-2.01	37.88	-4.29	28.58

[1] **BA** = basilar artery; **ICA L** = left internal carotid artery; **ICA R** = right internal carotid artery; **MCA L** = left middle cerebral artery; **MCA R** = right middle cerebral artery.

After the exclusion of the measurements from these subjects, the better results from the area and velocity parameters in the right ICA when compared to the PI and FVP are even more noticeable. On the other hand, the right MCA presented narrow LoA for the PI when compared to the FVP and velocity parameters.

5.1.4 Pearson correlation analysis

To assess the correlation between measurements of the two days, a Pearson correlation analysis was held.

The PCC (r) results and respective p-values are shown in Tables 5.18 and 5.19. Additionally, correlation plots for all parameters analysed are presented in Figs. 5.7-5.12. As

stated in Chapter 4, an $r \geq 0.75$ and p-value ≤ 0.05 were set as goals to consider the results satisfactory.

Table 5.15: Mean relative difference (MD (%)) and relative limits of agreement (LoA (%)) for the minimum velocity (V_{min}), mean velocity (V_{mean}) and maximum velocity (V_{max})

	$\mathbf{V_{min}}$		$\mathbf{V_{mean}}$		$\mathbf{V_{max}}$	
Vessel	MD (%)	LoA (%)	MD (%)	LoA (%)	MD (%)	LoA (%)
BA[1]	0.76	12.93	0.00	9.59	-0.16	11.52
ICA L[1]	2.59	16.14	2.04	14.30	1.90	16.45
ICA R[1]	4.70	25.18	5.46	21.18	5.90	22.06
MCA L[1]	-3.32	16.49	-2.46	13.83	-2.77	16.75
MCA R[1]	4.66	25.83	2.51	23.06	3.21	23.72

[1] **BA** = basilar artery; **ICA L** = left internal carotid artery; **ICA R** = right internal carotid artery; **MCA L** = left middle cerebral artery; **MCA R** = right middle cerebral artery.

Table 5.16: Mean relative difference (MD (%)) and relative limits of agreement (LoA (%)) for the pulsatility index (PI), flow volume pulsatility (FVP) and cross-sectional area for the remaining 9 volunteers.

	PI		**FVP**		**Area**	
Vessel	MD (%)	LoA (%)	MD (%)	LoA (%)	MD (%)	LoA (%)
ICA R[1]	4.20	23.94	8.41	26.75	-0.50	4.67
MCA R[1]	-0.56	17.15	1.36	33.51	-0.15	13.33

[1] **ICA R** = right internal carotid artery; **MCA R** = right middle cerebral artery.

Table 5.17: Mean relative difference (MD (%)) and relative limits of agreement (LoA (%)) for the minimum velocity (V_{min}), mean velocity (V_{mean}) and maximum velocity (V_{max}) for the remaining 9 volunteers.

	$\mathbf{V_{min}}$		$\mathbf{V_{mean}}$		$\mathbf{V_{max}}$	
Vessel	MD (%)	LoA (%)	MD (%)	LoA (%)	MD (%)	LoA (%)
ICA R[1]	1.04	11.64	2.18	6.24	2.59	8.61
MCA R[1]	2.32	22.65	0.71	21.39	1.34	21.96

[1] **ICA R** = right internal carotid artery; **MCA R** = right middle cerebral artery.

After analyzing the results, it is possible to conclude that there is, in most cases, a significant correlation between the test and retest measurements.

For PI, only the left MCA did not present a significant correlation. The remaining arteries obtained good results ($r \geq 0.75$ and p-value ≤ 0.05).

All FVP measures were considered statistically significant, according to the attained p-value. However, for this thesis, an $r \geq 0.75$ was considered as the minimum acceptable correlation value. Therefore, the BA and right MCA did not fulfill those requirements.

Table 5.18: Results of the Pearson correlation analysis for pulsatility index (PI), flow volume pulsatility (FVP) and cross-sectional area. *r*, Pearson correlation coefficient.

	PI			**FVP**			**Area**		
	r	*p*	summary	*r*	*p*	summary	*r*	*p*	summary
BA[1]	0.75	0.013	*	0.69	0.026	*	0.95	0.000	**
ICA L[1]	0.75	0.012	*	0.85	0.002	**	0.99	0.000	**
ICA R[1]	0.78	0.007	**	0.78	0.008	**	0.86	0.001	**
MCA L[1]	0.52	0.120	ns	0.89	0.001	**	0.82	0.004	**
MCA R[1]	0.82	0.004	**	0.71	0.022	*	0.45	0.194	ns

ns, not significant.
* *p*-value ≤ 0.05; ** *p*-value ≤ 0.01.
[1] **BA** = basilar artery; **ICA L** = left internal carotid artery; **ICA R** = right internal carotid artery; **MCA L** = left middle cerebral artery; **MCA R** = right middle cerebral artery.

Table 5.19: Results of the Pearson correlation analysis for the minimum velocity (V_{min}), mean velocity (V_{mean}) and maximum velocity (V_{max}). *r*, Pearson correlation coefficient.

	$\mathbf{V_{min}}$			$\mathbf{V_{mean}}$			$\mathbf{V_{max}}$		
	r	*p*	summary	*r*	*p*	summary	*r*	*p*	summary
BA[1]	0.97	0.000	**	0.98	0.000	**	0.96	0.000	**
ICA L[1]	0.91	0.000	**	0.91	0.000	**	0.83	0.003	**
ICA R[1]	0.73	0.017	*	0.59	0.075	ns	0.41	0.236	ns
MCA L[1]	0.64	0.046	*	0.75	0.012	*	0.57	0.088	ns
MCA R[1]	0.59	0.076	ns	0.61	0.064	ns	0.53	0.116	ns

ns, not significant.
* *p*-value ≤ 0.05; ** *p*-value ≤ 0.01.
[1] **BA** = basilar artery; **ICA L** = left internal carotid artery; **ICA R** = right internal carotid artery; **MCA L** = left middle cerebral artery; **MCA R** = right middle cerebral artery.

Concerning the cross-sectional area, all arteries, except the right MCA, revealed good test-retest correlations, with simultaneous $r \geq 0.75$ and *p*-value ≤ 0.05. The minimum velocity presented similar results. However, although the right ICA and left MCA presented a *p*-value ≥ 0.05, the *r* exhibited in both cases is inferior to 0.75.

Regarding the mean velocity, the right ICA and right MCA demonstrated non significant correlation between the results. The remaining arteries revealed favorable results (both $r \geq 0.75$ and *p*-value ≤ 0.05). Concerning the maximum velocity, only the BA and left ICA presented significant results and *r* higher than 0.75.

Similarly to what was previously done for the ICC, mean values of *r* were calculated for each artery and parameter. The parameter with the highest *r* for each artery and the artery with the highest *r* for each parameter were also identified. The results are presented in Tables 5.20 and 5.21.

The BA exhibited an average *r* of 0.88, which indicates good correlation. Moreover, the mean velocity was the parameter, for the BA, that achieved the highest *r*, with an excellent correlation ($r = 0.98$).

Table 5.20: Mean Pearson correlation coefficient (r) for all arteries and the identification of the parameter with the highest r result and respective value for each vessel.

	BA[1]	**ICA L**[1]	**ICA R**[1]	**MCA L**[1]	**MCA R**[1]
Mean *r*	0.88	0.87	0.69	0.70	0.62
Best result	0.98	0.99	0.86	0.89	0.82
Best parameter	V_{mean}	Area	Area	FVP	PI

[1] **BA** = basilar artery; **ICA L** = left internal carotid artery; **ICA R** = right internal carotid artery; **MCA L** = left middle cerebral artery; **MCA R** = right middle cerebral artery.

Table 5.21: Mean Pearson correlation coefficient (r) for all parameters and the identification of the artery with the highest r result and respective value for each parameter.

	PI	**FVP**	**Area**	**V_{min}**	**V_{mean}**	**V_{max}**
Mean *r*	0.72	0.78	0.81	0.77	0.77	0.66
Best result	0.82	0.89	0.99	0.97	0.98	0.96
Best artery	MCA R[1]	MCA L[1]	ICA L[1]	BA[1]	BA[1]	BA[1]

[1] **BA** = basilar artery; **ICA L** = left internal carotid artery; **MCA L** = left middle cerebral artery; **MCA R** = right middle cerebral artery.

Regarding the left ICA, the mean r was 0.87, while the cross-sectional area showed the best r = 0.99. On the other hand, the right ICA presented a mean ICC = 0.69 and, similarly to the left ICA, the best result for this artery was found for the cross-sectional area (r = 0.86).

Concerning the left MCA, the average r was 0.70, whereas the best result on this vessel was obtained for the FVP (ICC = 0.89). Finally, the right MCA displayed the worst results, with an average ICC of 0.62 and the best ICC = 0.82 for the PI.

As far as the analysed parameters, the vessel cross-sectional area presented the highest mean r (0.81) and the best result of 0.99 for the left ICA. Moreover, the FVP exhibited an r = 0.78, while the best result was found for the left MCA (r = 0.89). Regarding the PI, the average ICC was 0.72, while the highest value was 0.82 for the right MCA.

The V_{min}, V_{mean} and V_{max} presented a mean r of 0.77, 0.77 and 0.66, respectively. The best velocity results were all found for the BA, with an ICC of 0.97 for the minimum velocity, 0.98 for the mean velocity and 0.96 for the maximum velocity.

Analogously to what was previously reported for the ICC and Wilcoxon test, the results from the volunteers that exhibited an abnormal difference in the measurements for the right ICA and right MCA were excluded. The Pearson correlation analysis was repeated for the remaining nine volunteers. The results from this analysis are presented in Tables 5.22 and 5.23. Additionally, the mean r values and the respective parameter and artery with the best result after the exclusion are represented in Tables 5.24 and 5.25.

After examining Tables 5.22 and 5.23, it is possible to verify that the Pearson correlation analysis results did not improve for the PI and FVP because, as mentioned before, there

were no significant differences for the two measurements of these parameters.

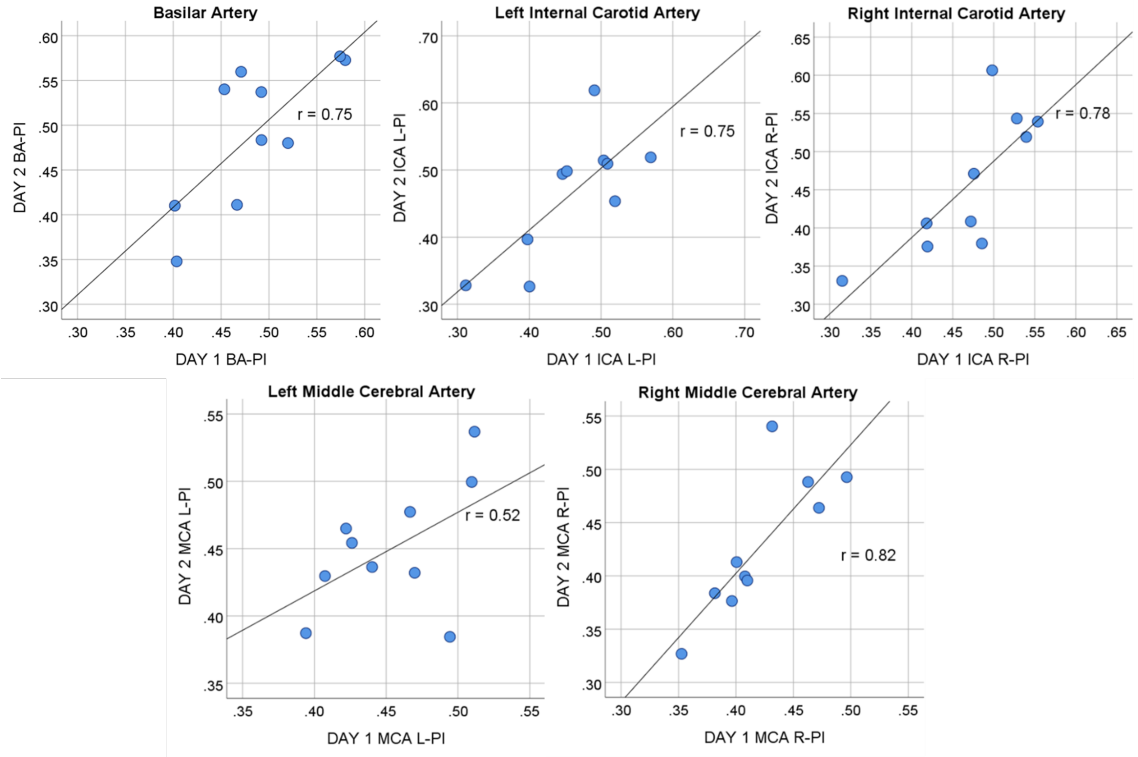

Figure 5.7: Correlation plot between the Day 1 and Day 2 measurements for the pulsatility index (PI). BA, basilar artery; ICA L, left internal carotid artery; ICA R, right internal carotid artery; MCA L, left middle cerebral artery; MCA R, right middle cerebral artery.

However, after excluding the previously mentioned cases, the results related to the cross-sectional area improved significantly. The right ICA presented an r of 0.99 and a p-value ≤ 0.01. The right MCA exhibited an r of 0.76 and p-value ≤ 0.05, which is considered a strong correlation.

Therefore, after this correction, the cross-sectional area results of all arteries presented significant correlation.

Although the r decreased for the minimum velocity in the case of the right ICA, the remaining velocities suffered a significant improvement. Both presented an r higher than 0.85 and p-value ≤ 0.001.

Concerning the right MCA, even after the exclusion of the volunteer measurements with the significant difference, the maximum velocity still did not present a significant correlation between measurements (p-value ≥ 0.05). The minimum and mean velocities revealed a p-value ≤ 0.05, however, the r for both cases is inferior to 0.75.

As shown in Table 5.24, after the exclusion of outliers, the mean general r result for the right ICA is 0.81, which is significantly closer to the value obtained for the left ICA (0.87). Similarly, after this process, the average ICC for the right MCA is 0.71, which is more consistent with the previously reported result for the left MCA of 0.70.

Additionally, as observed in Table 5.25, the cross-sectional area showed a mean r of

0.9, which is considered excellent.

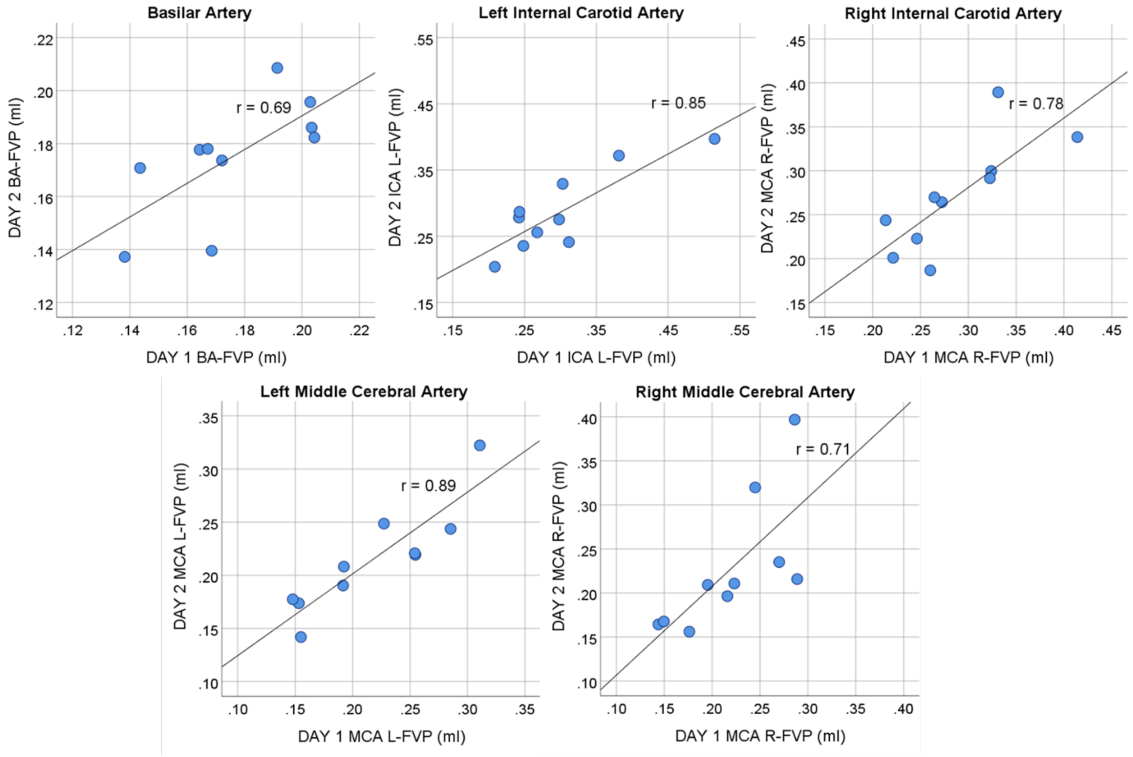

Figure 5.8: Correlation plot between the Day 1 and Day 2 measurements for the flow volume pulsatility (FVP). BA, basilar artery; ICA L, left internal carotid artery; ICA R, right internal carotid artery; MCA L, left middle cerebral artery; MCA R, right middle cerebral artery.

Table 5.22: Results of the Pearson correlation analysis for the pulsatility index (PI), flow volume pulsatility (FVP) and cross sectional area for the remaining 9 volunteers. *r*, Pearson correlation coefficient.

	PI			**FVP**			**Area**		
	r	*p*	summary	*r*	*p*	summary	*r*	*p*	summary
ICA R	0.73	0.026	*	0.79	0.011	*	0.99	0.000	**
MCA R	0.80	0.010	*	0.66	0.056	ns	0.76	0.017	*

ns, not significant.
* p-value ≤ 0.05; ** p-value ≤ 0.01.
ICA R = right internal carotid artery; **MCA R** = right middle cerebral artery.

The FVP, minimum, mean and maximum velocities presented a good average correlation ($r = 0.78$, 0.76, 0.85 and 0.77), which are higher than the proposed minimum goal of 0.75. The worst mean r (0.71) was once again observed for the PI.

Comparing the obtained values for maximum velocity (peak velocity) with a previously reported study [14], the values obtained for the left ICA where similar ($r = 0.83$ and p-value < 0.01 vs. $r = 0.86$ and p-value < 0.01). Regarding the right ICA, the results after

the exclusion of the outlier were also similar ($r = 0.90$ and p-value ≤ 0.01 vs $r = 0.87$ and p-value ≤ 0.01). However, the MCAs results from this research were considerably lower than the ones previously reported.

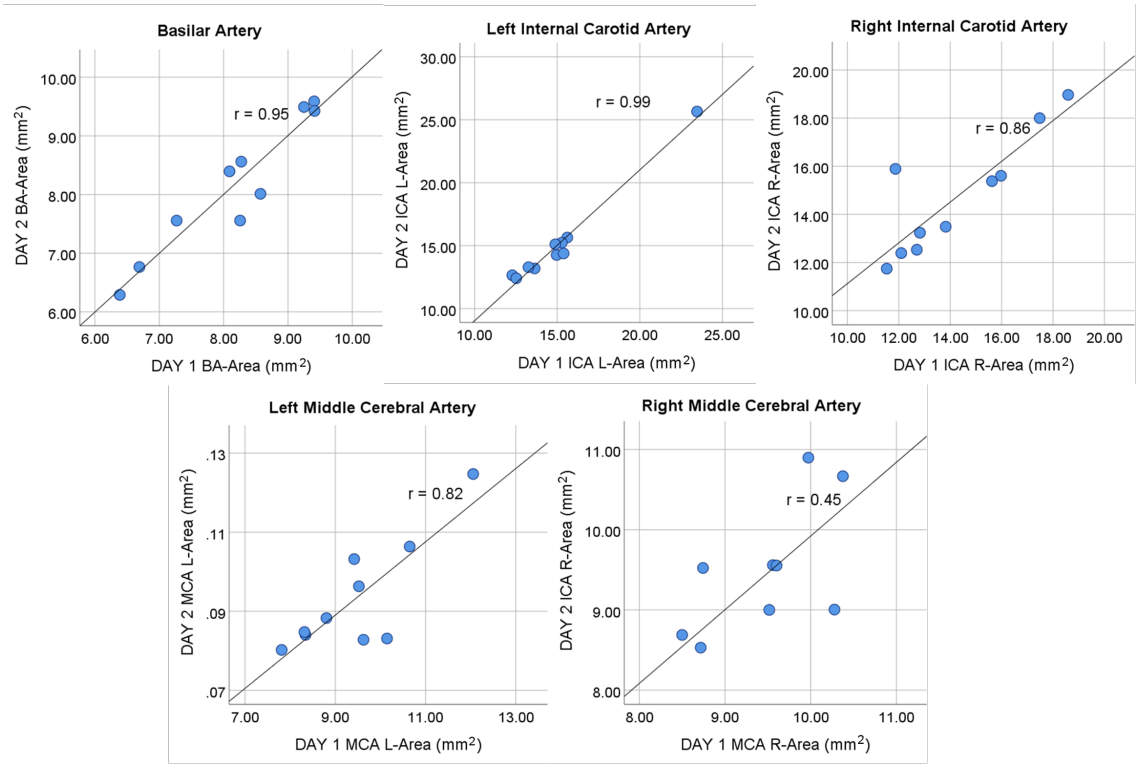

Figure 5.9: Correlation plot between the Day 1 and Day 2 measurements for the cross-sectional area. BA, basilar artery; ICA L, left internal carotid artery; ICA R, right internal carotid artery; MCA L, left middle cerebral artery; MCA R, right middle cerebral artery.

Table 5.23: Results of the Pearson correlation analysis for the minimum velocity (V_{min}), mean velocity (V_{mean}) and maximum velocity (V_{max}) for the remaining 9 volunteers. r, Pearson correlation coefficient.

	$\mathbf{V_{min}}$			$\mathbf{V_{mean}}$			$\mathbf{V_{max}}$		
	r	p	summary	r	p	summary	r	p	summary
ICA R	0.58	0.102	ns	0.90	0.001	**	0.87	0.003	**
MCA R	0.71	0.031	*	0.70	0.035	*	0.63	0.068	ns

ns, not significant.
* p-value ≤ 0.05; ** p-value ≤ 0.01.
ICA R = right internal carotid artery; **MCA R** = right middle cerebral artery.

Table 5.24: Mean Pearson correlation coefficient (r) for for the right internal carotid artery and middle cerebral artery and the identification of the parameter with the highest r and respective value for each vessel for the remaining 9 volunteers.

	ICA R[1]	**MCA R**[1]
Mean *r*	0.81	0.71
Best result	0.99	0.80
Best parameter	Area	PI

[1] **ICA R** = right internal carotid artery; **MCA R** = right middle cerebral artery.

Table 5.25: Mean Pearson correlation coefficient (r) for all parameters and the identification of the artery with the highest r result and respective value for each parameter, for the remaining 9 volunteers.

	PI	**FVP**	**Area**	$\mathbf{V_{min}}$	$\mathbf{V_{mean}}$	$\mathbf{V_{max}}$
Mean *r*	0.71	0.78	0.90	0.76	0.85	0.77
Best result	0.80	0.89	0.99	0.97	0.98	0.96
Best artery	MCA R[1]	MCA L[1]	ICA R[1]	BA[1]	BA[1]	BA[1]

[1] **BA** = basilar artery; **ICA R** = right internal carotid artery; **MCA L** = left middle cerebral artery; **MCA R** = right middle cerebral artery.

5.2 Evaluation of the relationship between the results and physiological alterations

In order to assess the relationship between PI, FVP and blood velocities with physiological variations of heart rate and arterial pressure, a correlation analysis was performed. This evaluation is of extreme importance to perceive whether the physiological alterations of HR and BP play a significant role in the measured parameter differences.

The HR used by GE's software for image reconstruction (present in the DICOM tags) was used for this analysis and was captured with the ECG utilized for synchronization during image capture. The arterial pressure was measured before and after MRI acquisitions. The values used for the analysis were considered a mean between the two acquisitions, assuming a linear progression of the values. Unfortunately, it was not possible to measure the arterial blood pressure during the scan.

The mean and standard deviation of the HR, mean blood pressure (MBP), diastolic blood pressure (DBP) and SBP over the two days are represented in table 5.26.

A p-value ≤ 0.05 was again considered significant. Additionally, for this correlation analysis, the results from both the left and right ICAs were combined, following the methodology presented in [42]. The same process was executed for the left and right MCAs. In order to achieve a clear presentation, the results were separated by parameter, where the correlations obtained are identified and presented in correlation plots.

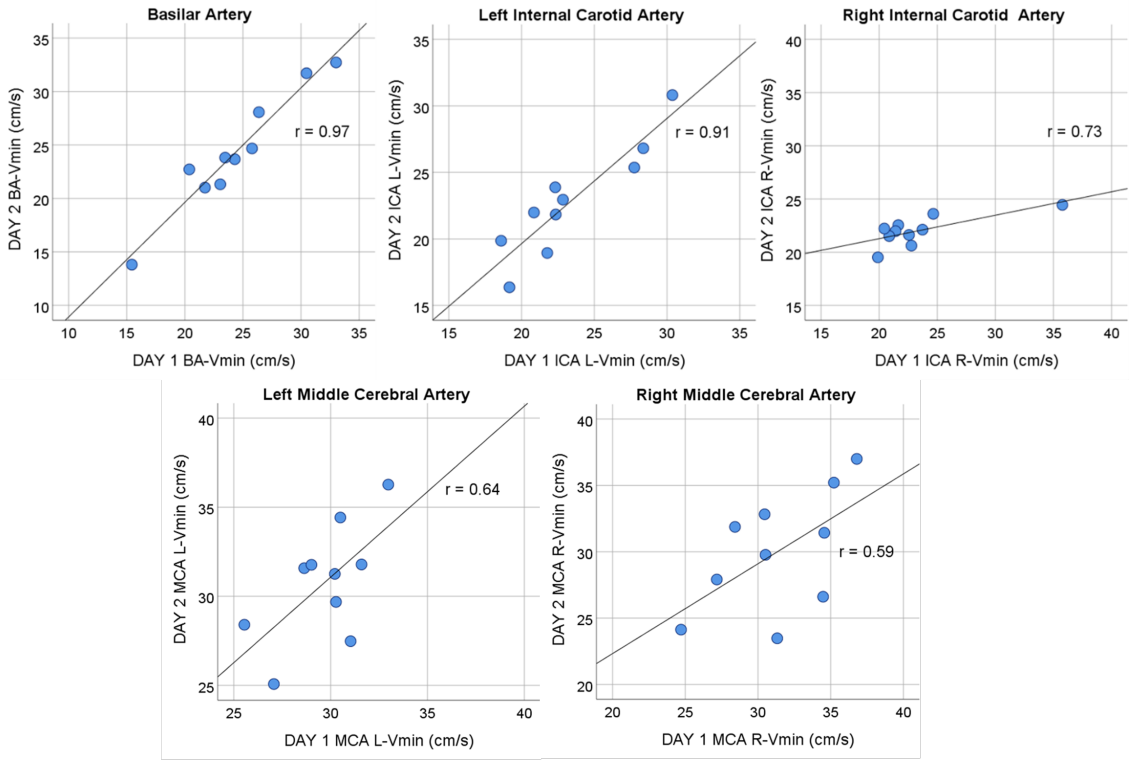

Figure 5.10: Correlation plot between the Day 1 and Day 2 measurements for the minimum velocity (Vmin). BA, basilar artery; ICA L, left internal carotid artery; ICA R, right internal carotid artery; MCA L, left middle cerebral artery; MCA R, right middle cerebral artery.

Table 5.26: Mean and standard deviation of the heart rate and mean, diastolic and systolic blood pressures measured on both days. HR, heart rate; MBP, mean blood pressure; DBP, diastolic blood pressure; SBP, systolic blood pressure.

	HR (BPM)	MBP (mmHg)	DBP (mmHg)	SBP (mmHg)
Day 1	74 ± 9	90 ± 12	72 ± 9	122 ± 14
Day 2	71 ± 7	86 ± 10	74 ± 8	122 ± 11

Pulsatility index

Regarding PI, no associations were found with HR and BP in any of the arteries analysed.

Flow volume pulsatility

Similarly to PI, no associations were found through correlation for the FVP.

Minimum velocity

The minimum flow velocity in the MCAs presented a significant linear correlation with HR, MBP and SBP ($r = -0.324$, p-value= 0.042, $r = -0.491$, p-value= 0.001, $r = -0.454$, p-value = 0.003, respectively), as illustrated in Figs. 5.13 and 5.14.

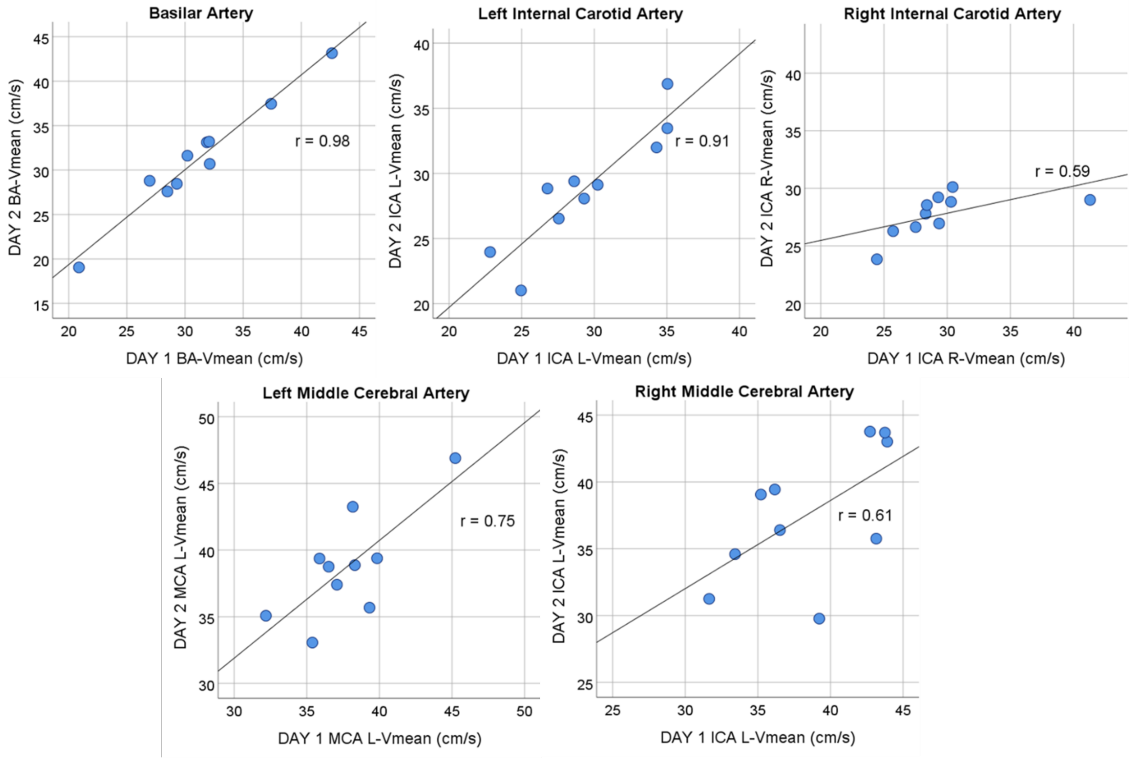

Figure 5.11: Correlation plot between the Day 1 and Day 2 measurements for the mean velocity (Vmean). BA, basilar artery; ICA L, left internal carotid artery; ICA R, right internal carotid artery; MCA L, left middle cerebral artery; MCA R, right middle cerebral artery.

Mean velocity

In the case of mean flow velocity, a significant Pearson correlation with HR was observed (Figure 5.15) for the BA ($r = -0.511$ and p-value = 0.021).

In relation to the mean velocity in the MCAs, significant Pearson correlations with HR ($r = -0.385$ and p-value =0.014), MBP ($r = -0.541$ and p-value =0.000), DBP ($r = -0.340$ and p-value =0.032) and SBP were verified ($r = -0.471$ and p-value =0.002). The plots of these correlations are represented in Figs. 5.16 and 5.17.

Maximum velocity

The maximum velocity in the BA was linearly correlated with HR ($r = -0.508$ and p-value = 0.006). The correlation plot is shown in Fig. 5.18.

Furthermore, the maximum velocity in the ICAs presented a significant correlation (Figure 5.19) with DBP ($r = -0.389$ and p-value =0.013).

Lastly, the maximum velocity in the MCAs presented significant correlations with HR ($r = -0.381$ and p-value = 0.015), MBP ($r = -0.533$ and p-value = 0.000), DBP ($r = -0.304$ and p-value = 0.030) and SBP ($r = -0.500$ and p-value = 0.001). The correlations are presented in Figs. 5.20 and 5.21.

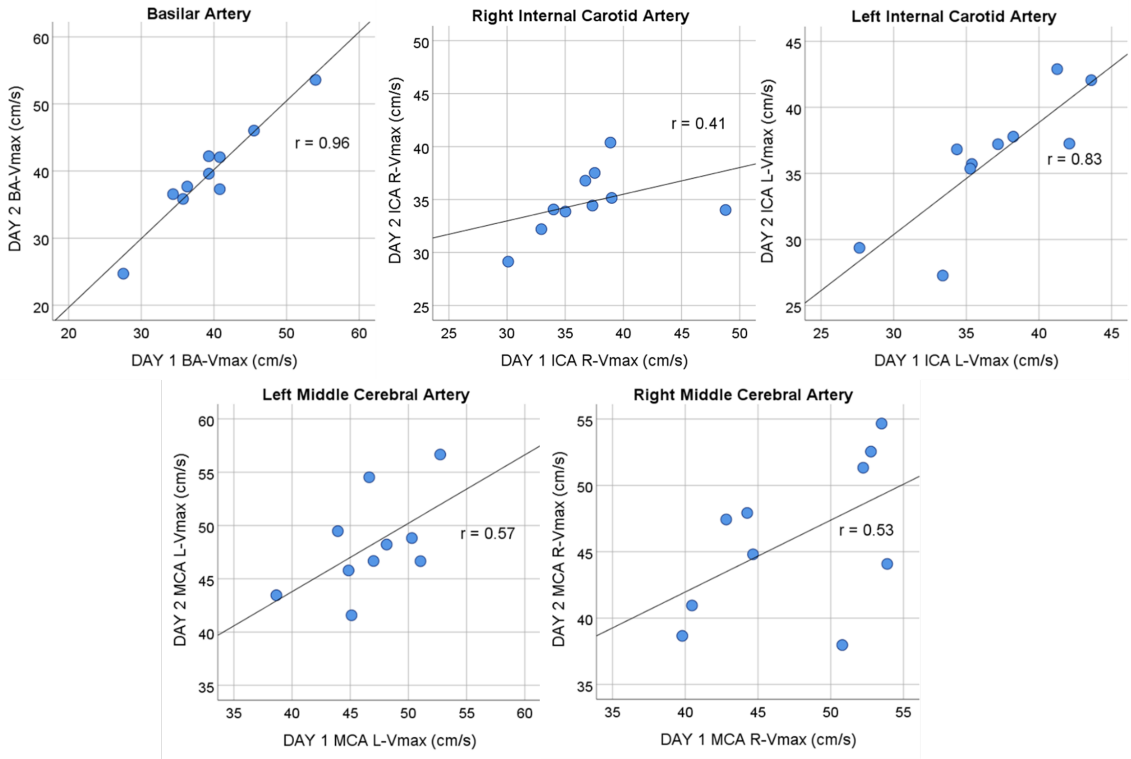

Figure 5.12: Correlation plot between the Day 1 and Day 2 measurements for the maximum velocity (Vmax). BA, basilar artery; ICA L, left internal carotid artery; ICA R, right internal carotid artery; MCA L, left middle cerebral artery; MCA R, right middle cerebral artery.

5.3 Comparison of the Results with other studies

In order to validate the results of this study and contribute to the normative basis of healthy volunteers, a comparison with other articles is necessary. Therefore, the results of the scan and re-scan were joined and the mean and standard deviation were calculated comprising the two measurements. The values obtained are presented in Tables 5.27 and 5.28.

In a similar manner to what was performed in Section 5.2, the results were separated by parameter, where the comparison with other studies is held for each of the arteries.

Pulsatility Index

Several studies [97]–[100] reported pulsatility indexes ranging from 0.8 to 1 in healthy young adults. The values obtained in the current research are, as observed in Table 5.27 significantly lower.

Flow volume pulsatility

Regarding the FVP, [17] compared 2D PC-MRI with 4D PC-MRI in healthy volunteers (age 29 to 53 years), and reported ΔV of 0.20 ± 0.08 ml for the BA, 0.35 ± 0.10 ml for ICA and 0.23 ± 0.05 ml for MCA. The results presented in this study are similar to those, with a slight higher difference for the ICA.

Higher FVP values were reported in other articles [19], [42]. However, participants

were older, suffered a transient ischemic attack, stroke or had carotid artery stenosis. Since these conditions can affect blood flow in the intracranial arteries, velocity and pulsatility are probably altered as well.

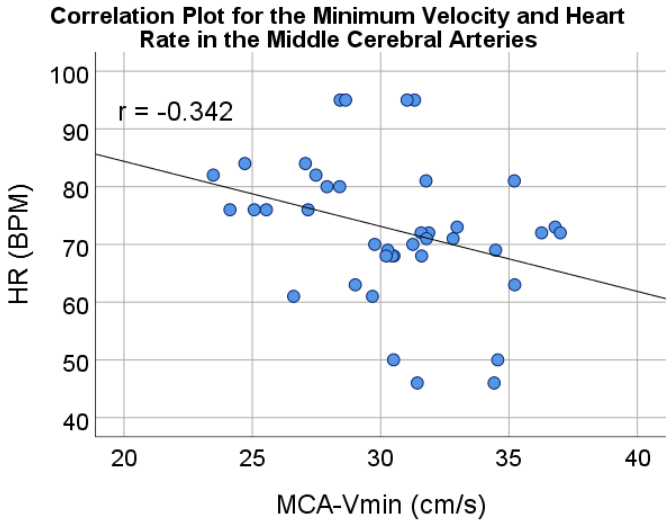

Figure 5.13: Correlation plot for minimum velocity and heart rate in the middle cerebral arteries. MCA, middle cerebral artery; Vmin, minimum velocity ; HR, heart rate.

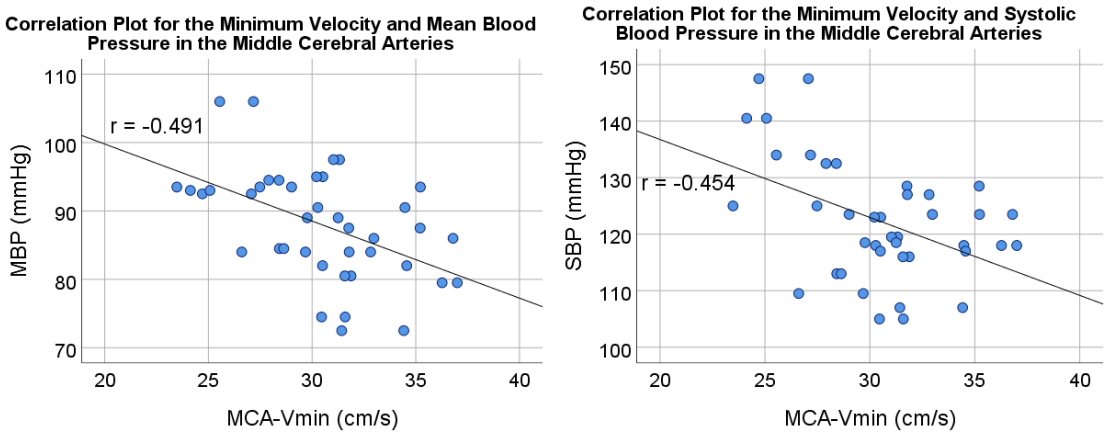

Figure 5.14: **Left**. Correlation plot for the minimum velocity and mean blood pressure in the middle cerebral arteries. **Right**. Correlation plot for the minimum velocity and systolic blood pressure in the middle cerebral arteries. MCA, middle cerebral artery; Vmin, minimum velocity; MBP, mean blood pressure; SBP, systolic blood pressure.

Cross-sectional area

In a recently published 4D flow study related to aging [100], aortic stiffness and cerebral arterial pulsatility, intracranial vessel diameters were reported for young healthy adults (age 18 to 35 years). ICA presented a mean diameter of 4.4 mm, MCA of 2.9 mm and BA of 3.2 mm. Assuming a circular shape, the cross-sectional area for the aforementioned vessels is 15.2 mm^2, 6.6 mm^2 and 8.04 mm^2, respectively. These results are very similar to

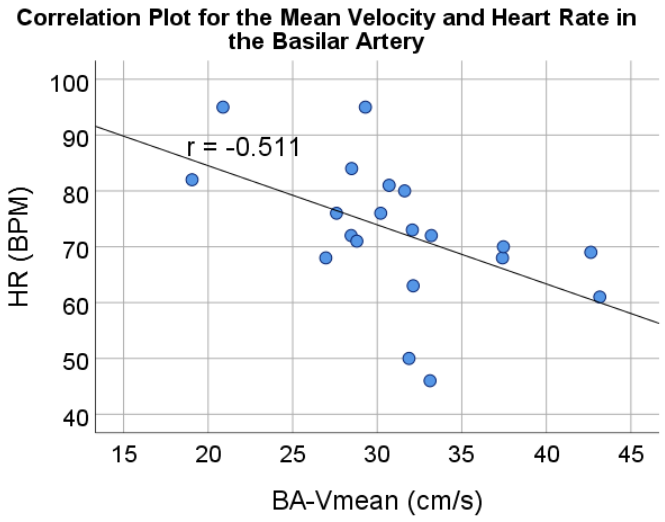

Figure 5.15: Correlation plot for mean velocity and heart rate in the basilar artery. BA, basilar artery; Vmin, minimum velocity; HR, heart rate.

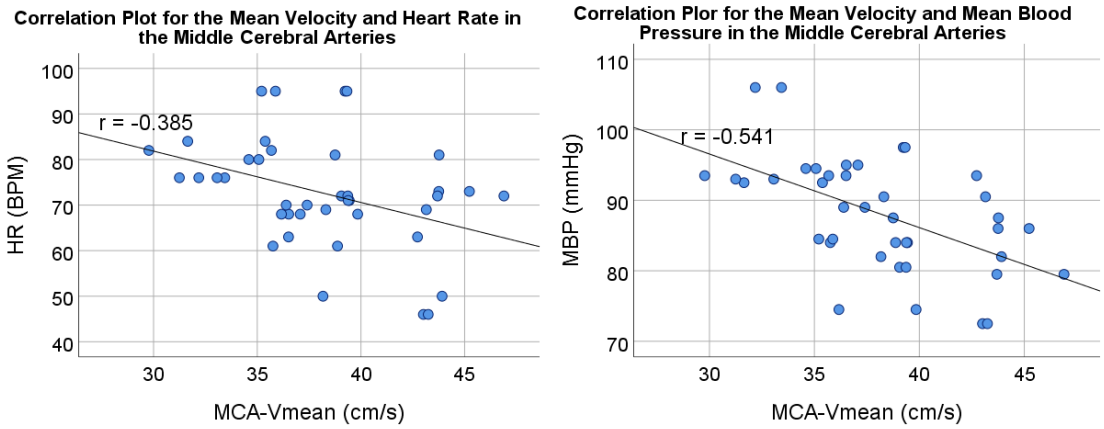

Figure 5.16: **Left**. Correlation plot for the mean velocity and heart rate in the middle cerebral arteries. **Right**. Correlation plot for the mean velocity and mean blood pressure in the middle cerebral arteries. MCA, middle cerebral artery; Vmean, mean velocity; HR, heart rate; MBP, mean blood pressure.

the ones found in this research, for ICA and BA. However, MCA presented a higher result with this study's methodology than the one reported in the referenced article.

In another study of 4D PC-MRI of intracranial vessels in Alzheimer's patients [8], the cross-sectional area of the MCA in the middle-age group was much closer to the result obtained in this project.

Additionally and regarding the ICAs, Tuijl et al. [101] presented lumen areas of 14.8 ± 4.48 mm^2 and 14.9 ± 4.38 mm^2 for the left and right arteries, respectively. Furthermore, the BA area was 7.2 ± 1.79 mm^2. Once again, the values are similar to the results of this research.

The results were also similar to the ones reported in [98].

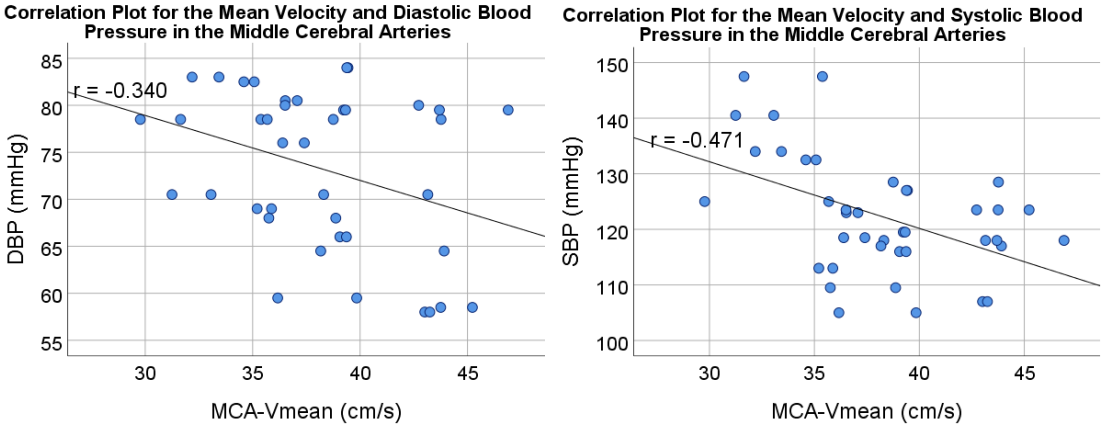

Figure 5.17: **Left**. Correlation plot for the mean velocity and diastolic blood pressure in the middle cerebral arteries. **Right**. Correlation plot for the mean velocity and systolic blood pressure in the middle cerebral arteries. MCA, middle cerebral artery; Vmean, minimum velocity ; DBP, diastolic blood pressure; SBP, systolic blood pressure.

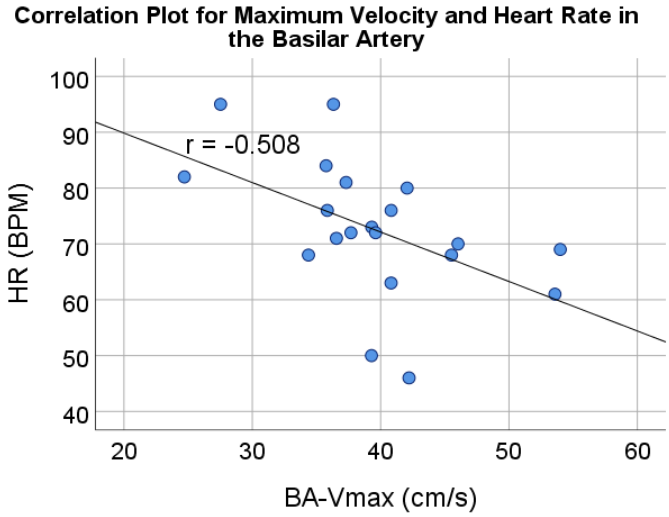

Figure 5.18: Correlation plot for maximum velocity and heart rate in the basilar artery. BA, basilar artery; Vmax, maximum velocity; HR, heart rate.

Minimum velocity

Regarding the minimum velocity, also known as the end diastolic velocity, a study [102] comparing different techniques for velocity assessment in intracranial arteries reported a value of 38 ± 8 cm/s for the M1 segment of the MCA. The results displayed in Table 5.27 are 30 ± 3 cm/s and 31 ± 4 cm/s for the left and right MCA, respectively. Therefore, a difference between these findings is observed, comprised of a velocity underestimation by the methodology proposed in this work. Additionally, the end-diastolic velocity reported for the ICA was 35 ± 6 cm/s, which is substantially higher than the ones obtained in this research (23 ± 4 for the left ICA and 23 ± 3 for the right ICA).

On another 4D flow study [103], comparing velocities in intracranial vessels with TCD,

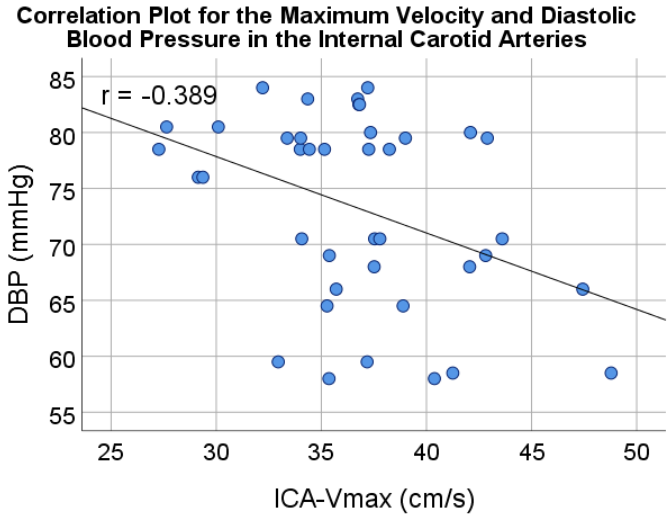

Figure 5.19: Correlation plot for the maximum velocity and diastolic blood pressure in the internal carotid arteries. ICA, internal carotid artery; Vmax, maximum velocity; DBP, diastolic blood pressure.

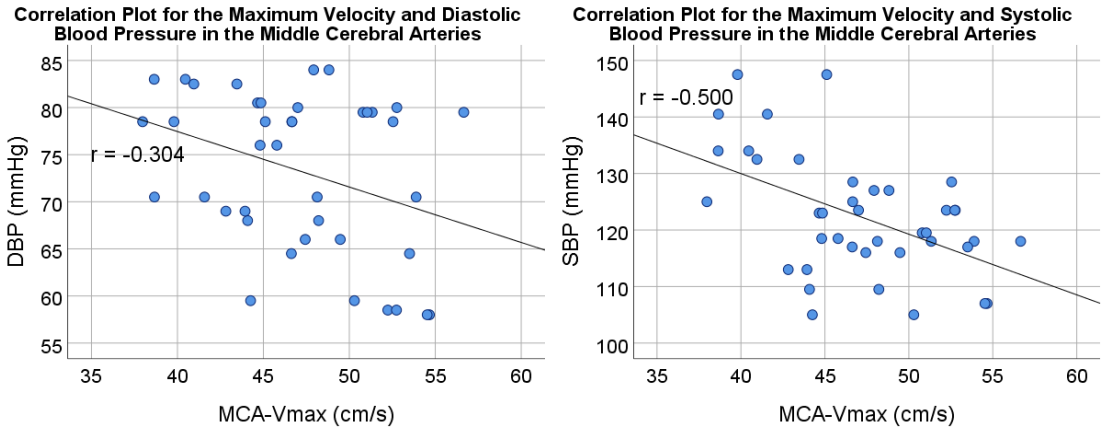

Figure 5.20: **Left**. Correlation plot for the maximum velocity and diastolic blood pressure in the middle cerebral arteries. **Right**. Correlation plot for the maximum velocity and systolic blood pressure in the middle cerebral arteries. MCA, middle cerebral artery; Vmax, maximum velocity ; DBP, diastolic blood pressure; SBP, systolic blood pressure.

the minimum velocity reported was even higher for the proximal segment of the M1 MCA (40.58 ± 8.75 cm/s). Regarding the BA, the average minimum velocity reported was 32.68 cm/s for the 4D flow and 26.86 cm/s for the TCD, which is closer to the velocity obtained in this study (24 ± 5 cm/s).

Mean velocity

Regarding the mean velocity comparisons, Tuijl et al. [101] reported 2D PC-MRI measurements of 25 ± 6.9 cm/s for the right ICA, 25 ± 7.7 cm/s for the left ICA and 32 ± 7.1 cm/s for the BA. No MCA mean velocity results were found.

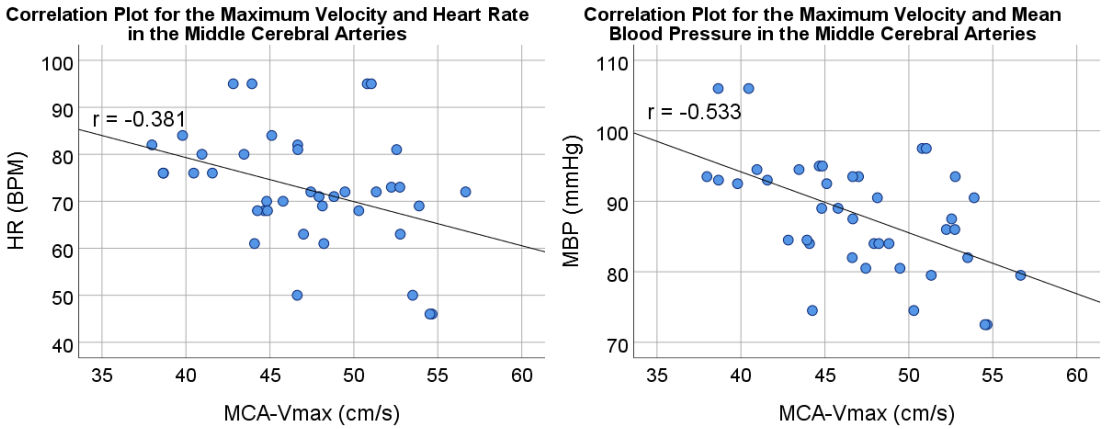

Figure 5.21: **Left**. Correlation plot for the mean velocity and heart rate in the middle cerebral arteries. **Right**. Correlation plot for the and mean blood pressure in the middle cerebral arteries. MCA, middle cerebral artery; Vmean, mean velocity; HR, heart rate; MBP, mean blood pressure.

Table 5.27: Mean and standard deviation for the pulsatility index (PI), flow volume pulsatility (FVP) and vessel cross-sectional area (Area) in all the arteries analysed.

Vessel	PI	FVP (ml)	Area (mm^2)
BA[1]	0.49 ± 0.07	0.18 ± 0.02	8 ± 1
ICA L[1]	0.46 ± 0.08	0.29 ± 0.07	15 ± 3
ICA R[1]	0.46 ± 0.08	0.28 ± 0.06	14 ± 2
MCA L[1]	0.45 ± 0.04	0.22 ± 0.05	9 ± 1
MCA R[1]	0.42 ± 0.05	0.22 ± 0.06	10 ± 1

[1] **BA** = basilar artery; **ICA L** = left internal carotid artery; **ICA R** = right internal carotid artery; **MCA L** = left middle cerebral artery; **MCA R** = right middle cerebral artery.

Comparing with the values obtained in this thesis, the mean velocity for the ICAs was similar, although the ones observed in this research were slightly higher. On the other hand, the BA values are much closer to the reported ones.

Maximum velocity

A 4D flow reproducibility study [14] with intra-site and inter-site comparisons reported maximum velocities for the ICAs and MCAs in ten healthy young volunteers (four females, age 22–33 years). The article did not present the mean value for all scans, only the mean value for each day and each site. However, the mean peak velocities (equivalent to the maximum velocities reported in this research) for the left ICA were between 39.5 cm/s and 40.6 cm/s, whereas in this study the mean result obtained was 37 ± 5 cm/s. Although the value is slightly inferior in the current research, it is still within an acceptable margin. Regarding the right ICA, the mean values ranged from 36.2 cm/s to 38.2. Since the mean value presented in this study is 36 ± 4, the results are very similar, further corroborating

the obtained findings.

Table 5.28: Mean and standard deviation for the minimum velocity (V_{min}), mean velocity (V_{mean}) and maximum velocity (V_{max}) in all the arteries analysed.

Vessel	V_{min} (cm/s)	V_{mean} (cm/s)	V_{max} (cm/s)
BA	24 ± 5	31 ± 6	40 ± 7
ICA L	23 ± 4	29 ± 4	37 ± 5
ICA R	23 ± 3	29 ± 4	36 ± 4
MCA L	30 ± 3	39 ± 4	48 ± 4
MCA R	31 ± 4	38 ± 5	47 ± 6

[1] **BA** = basilar artery; **ICA L** = left internal carotid artery; **ICA R** = right internal carotid artery; **MCA L** = left middle cerebral artery; **MCA R** = right middle cerebral artery.

Concerning the left MCA, the mean values reported in the mentioned research ranged from 48.7 cm/s to 50.4 cm/s, while the mean maximum velocity obtained in this study was 48 ± 4 cm/s. Finally, concerning the right MCA, the mean peak velocities obtained in [14] ranged from 48.8 cm/s to 50.7 cm/s, whereas the mean value exhibited in Table 5.28 is 47 ± 6 cm/s. Although in both MCAs the results were slightly inferior to the ones available in the referenced study, the values where considered similar, especially taking into account the small population used for both studies.

However, in several other studies [102], [103], the reported maximum velocities for the M1 segment of the MCA are 88 ± 13 cm/s and 82.57 cm/s, which are significantly higher that the exhibited velocities both in this study and in [14]. Similar findings where displayed for the BA, with maximum velocities of 78 ± 19 cm/s and 56.18 cm/s. Even in the two articles mentioned, the values presented significantly different results for the BA, unlike what happened for the MCAs.

6

Discussion

As mentioned in Section 1.2, the main goal of this research is the assessment of the test-retest reproducibility of the 4D PC-MRI technique and the software used for processing the scans. Furthermore, the examination of correlations between the results and physiological alterations of HR and blood pressure is of great importance. The results presented in this thesis will also contribute to the database of healthy subjects measurements of flow related parameters and cross-sectional area in intracranial vessels and, for this purpose, the comparison with measurements obtained in other studies is fundamental. In order to achieve a clearer discussion of the results, this chapter will be divided by sections for the analysis of each of the main goals.

6.1 Test-retest Reproducibility

In this section, each of the analysis developed for reproducibility assessement will be discussed, followed by the general insights taken from the test-retest accuracy results.

Intraclass Correlation Coefficient Analysis

In order to assess the reproducibility of the 4D flow technique and the post-processing software employed in this study, an ICC analysis was performed. As mentioned before, the ICC reflects not only the degree of correlation, but also the agreement between two variables. These concepts are distinct from one another, since correlation does not mean agreement.

The results of the ICC analysis revealed higher reproducibility for the vessel area, with an average ICC of 0.78, when considering all the measurements. These findings are expected, since the cross-sectional area is not as affected by physiological variations between measurements as the other parameters. Additionally, the segmentation process that leads to the estimation of the cross-sectional area is not as complex as that of velocity estimation, thus being less prone to errors. Other factors, such as motion artifacts, turbulent flows, or the lack of temporal resolution, do not affect the cross-section area estimations as significantly as those of velocity.

Considering that ICC values higher than 0.75 indicate good reliability, the only artery that exhibited no less than good results for all the parameters analysed was the left ICA. Although BA demonstrated better accuracy values for the velocities, it only displayed moderate reliability for the PI and FVP.

Before exclusion of the outliers, blood flow velocities presented worse reliability results than the other parameters, especially for the right ICA and the MCAs.

However, significant differences were found for one volunteer's right ICA and for another one's right MCA. These results were excluded, since the outliers responsible for the considerable differences were not only distinct from the measurement obtained in the scan for comparison, but also from the results of all the other volunteers, indicating a possible estimation error. Therefore, the ICC analysis was repeated after excluding the measurements of those subjects. As expected, the results improved for the cross-sectional area and blood flow velocities, since these were the parameters where the significant differences were observed. However, for PI, the ICC decreased, since there were no significant differences observed for this parameter in the subjects excluded. With such small sample sizes, of only ten volunteers, any minor alteration in the data can lead to significant changes in ICC. For example, the mean velocity in the right ICA suffered an impressive increase from ICC = 0.38 to ICC = 0.86, as a result of the exclusion of the measurements of a single volunteer.

After removing the outliers, the average ICC values for the left and right MCAs are more similar. The same observations were made for the ICC in the left and right ICAs. These results are more in accordance with the expectations, since the pairs of arteries have analogous anatomy and flow patterns in healthy patients, thus reproducibility in the measurements is expected to be similar.

In summary, after observing the results for the analysis with the remaining nine volunteers, it is possible to conclude that the PI only presents good reproducibility (ICC $\geq$ 0.75) in the left ICA and right MCA. On the other hand, FVP exhibited sufficient reproducibility in the ICAs and left MCA. The cross-sectional area ICC was higher than 0.75 in all arteries analysed, which indicates good reproducibility for all vessels. Despite the strong performance observed for the remaining arteries, velocity measurements in the MCAs did not present enough reproducibility.

In general, FVP exhibited higher ICC values than the PI, indicating that it can possibly be a more reliable biomarker for cerebrovascular diseases.

The worst ICC results were observed for the MCAs, especially for the velocity parameters. Since MCAs are smaller than ICAs and more tortuous than the BA, a poorer reproducibility should be expected, seeing as these properties negatively affect the vessel identification and velocity attainment by the post-processing software utilised in this research work.

The ICC results obtained were in line with previous reproducibility studies using 2D PC-MRI for FVP assessment in ICAs [94] and flow velocity measurements in MCAs [15]. However, the ICC values for the PI reported in this research are higher than the ones

exhibited in [15] for the MCAs.

Wilcoxon signed-rank test

In order to further test the agreement between measurements, a Wilcoxon signed-rank test was performed.

Since the initial intention was to apply a paired samples t-test, a Shapiro-Wilk test was performed to test the normality of the differences between the two measurements. In some cases, the normality hypothesis was rejected. Therefore, a non-parametric alternative to the paired samples t-test (the Wilcoxon signed-rank test) was applied instead.

According to the results, the differences were not significant, except for the mean velocity in the right ICA, since the p-value observed in that case was 0.037 (which is inferior to 0.05).

However, after excluding the aforementioned cases where significant differences occurred in the right MCA and ICA, all the p-values obtained were higher than 0.05, indicating that all median differences are statistically indistinct from zero, which suggests a good agreement between the two measurements.

However, this test evaluates not only if the median difference value is equal to zero, but also if the number of positive and negative differences are balanced. In the case of the mean velocity in the right ICA, although the median difference is 0.55 cm/s, there were 8 positive differences and 2 negative differences. Therefore, the Wilcoxon test result is low, despite the differences observed being close to 0, explaining why the median was almost 0. On the other hand, although the cross-sectional area in the right MCA presented an ICC of 0.31, which indicates poor reliability, it exhibited one of the best results for the Wilcoxon test (0.953). This is explained by the fact that the median difference in that case was close to 0 (-0.0009) and there were 4 negative differences, 5 positive differences and one tie. However, the correlation between the variables was low.

It is possible to conclude that the different tests and analyses, although applied to the same data, present different results, according to what is being tested. In the case of the Wilcoxon signed-rank test, in order to obtain a high p-value, not only the median differences need to be close to zero, but also present an almost symmetric distribution around zero. On the other hand, the ICC tests the correlation and the agreement simultaneously. Additionally, since the sample is small, the statistical analysis is very affected by minor differences, which also contributes to the large diversity of results.

However, since all the p-value results were higher than 0.05, except for the mean velocity in the right ICA, and after removing the outliers, even that result is improved, it is possible to conclude that the values obtained are in agreement, representing decent reproducibility. These findings are in conformity with the ICC results, further validating the reliability and test-retest accuracy of the 4D PC-MRI and post-processing techniques.

Bland-Altman plots and analysis

To assess the agreement between the values, the relative differences were confronted

against the mean vales of the measurements recorded for the two days in Bland-Altman plots. Additionally, the LoA were also calculated.

According to the proposed limits for acceptable reproducibility in Section 4.4, the PI presented simultaneously mean relative differences lower than 5% and LoA inferior to the limit proposed, indicating a good agreement between the measures.

However, for FVP, only the measurements in the BA and left MCA exhibited satisfactory results. Additionally, the right ICA displayed a mean difference of 6.25%, indicating a possible positive bias.

Concerning the cross-sectional area, only the right MCA presented LoA wider than the limit set as goal.

Lastly, all flow velocities also revealed wider LoA for the right ICA and right MCA.

After excluding the cases responsible for significant differences, as mentioned for the other analyses, the FVP results did not improve significantly and, therefore, the conclusions drawn earlier remain valid. However, the cross-sectional area exhibited satisfactory results for all arteries regarding the nine remaining volunteers, since the LoA value of the right MCA improved to 13.3%. On the other hand, although the velocity results for the right ICA are all within the limit proposed after the exclusion, that is not the case for the right MCA, where the LoA are wider than expected.

In general, narrower limits of agreement were found for the cross-sectional area. These findings are consistent with the results from the ICC analysis, indicating better test-retest reliability and less significant differences for the area measurements.

The flow velocity results were also better than PI and FVP, with narrower LoA. This is expected, since PI and FVP depend on other values to be calculated, leaving a lot more room for error.

Comparing the obtained results with previously mentioned mean relative differences and LoA for the maximum velocity, it is possible to state the values are in line with a previously mentioned 4D flow study [14] with similar methodology. However, the LoA are narrower than the ones presented in a 2D PC-MRI reproducibility study [15] for the maximum and minimum velocities, and for PI, which indicates better agreement results in this study. This result is expected due to the manual definition of the imaging planes in 2D PC-MRI that highly increases the operator dependence and, consequently, the possibility of error.

Pearson Correlation

To assess the correlation between day 1 and day 2 measurements, it was decided to calculate the correlation coefficient. Since PCC is frequently used for reproducibility analysis, it is possible to compare the values obtained with previous studies. The correlation was considered good for $r \geq 0.75$ and, similarly to the other tests, only p-values ≤ 0.05 were considered significant.

The results are similar to the ones found for the ICC, although slightly higher since the ICC analyses not only the correlation, but also the agreement.

Considering all the results obtained, PI revealed good correlation for the ICAs and right MCA, similarly to the observations obtained with ICC. Besides the r being lower than 0.75, the p-value found for the left MCA was not significant.

Regarding FVP, the results for all arteries were considered significant. However, the BA and right MCA presented a lower correlation than the acceptable threshold of 0.75.

Similarly to what was observed for ICC, only the right MCA's cross-sectional area measurements did not exhibit a correlation higher than the minimum acceptable value.

Regarding flow velocities, the BA and left ICA presented significant correlations and high r-values. However, that was not the case for the right ICA and the MCAs.

After exclusion of the aforementioned volunteers that presented significant differences for the right ICA and MCA, the results improved significantly, especially for the cross-sectional area and velocity parameters, as expected. However, the minimum velocity in the right ICA and all the velocity parameters in the right MCA still did not present correlations higher than 0.75, which indicates that the correlations for those cases were not strong enough to be considered successful results.

In summary, worst correlations were found for the MCAs, similarly to the results obtained by the remaining analyses, possibly explained by the size and anatomy factors presented before.

Once again, the left ICA was the only artery that obtained sufficient correlations for all parameters, corroborating the validity of 4D flow measurements for cerebrovascular disease assessment in this vessel.

When comparing the results obtained with the ones reported by Wen et al. [14], the values exhibited for the ICAs are in line with the ones mentioned. However, the MCAs correlations exhibited in this thesis are lower, suggesting that the software may have had more difficulties in the segmentation and velocity estimation processes, probably due to the reduced size of these arteries.

Reproducibility analysis summary

In this research, the test-retest reproducibility of 4D flow MRI PI, FVP, cross-sectional vessel area and velocity measures in intracranial arteries was assessed.

Throughout the analysis of the results, it is possible to state that the left ICA presented the most consistent reproducibility results across all the tests performed. The BA presented the best average reproducibility results and was the only artery were all the LoA were lower than the limits established. However, the results observed regarding this artery were considerably higher for the cross-sectional area and flow velocities, when compared to the PI and FVP.

Despite the inferior cross-sectional area of the BA when compared to the other arteries, it is less tortuous, causing the flow to present a more laminar pattern, which contributes to a better cross-sectional area and flow estimation by the post-processing tool, possibly explaining the good reliability results found. Additionally, as explained in the following section, it is hypothesized that the BA suffers less variability in blood flow related

measurements due to phyisiological alterations.

Slightly lower reproducibility was found for the right ICA, probably due to the small sample size, since the results should be similar to the contralateral artery. However, the worst test-retest reproducibility was observed for the MCAs, especially for the flow velocities. This can be explained by the correlations found between the flow velocities and physiological parameters, such as HR and BP, explored in detail in the next section. The tortuous shape of the MCAs leads to turbulent flow, which impairs the velocity estimation process.

In general, the best reproducibility was found for the cross-sectional area, since, as mentioned earlier, this parameter is not affected by physiological alterations. These results also validate the segmentation capabilities of the tool used for post-processing and the alterations applied in the software for the vessel separation from the background.

Additionally, the flow velocities also obtained a better test-retest accuracy than the PI and FVP, since, as aforementioned, the velocities are estimated directly from the images. Considering that the PI and FVP are calculated based on other measurements, the error possibility is much higher.

Similar or better results were observed in this study when compared to 2D flow measurements, which is expected since the 4D flow technique allows for whole brain coverage, removing the need for the operator to manually define the imaging plans. The automatic nature of the technique and post-processing software may reduce the variability introduced by the technician and interobserver, increasing reproducibility.

Despite the physiological related alterations, the 4D PC-MRI presents several limitations, such as limited spatial resolution when compared to intracranial vessel sizes [14], partial volume effects and the necessity of averaging over several cardiac cycles [101], resulting in inaccurate flow estimations.

Although volunteers were asked to abstain from activities that could potentially cause any alterations in the measurements, such as the consumption of caffeine, nicotine, or physical exercise, it is impossible to control all physiological factors that may provoke blood flow variability in the intracranial vessels.

6.2 Analysis of the relationship between the results and physiological alterations

Physiological alterations of blood pressure, heart rate and autoregulation are natural and must be taken into account when analyzing flow related parameters. In order to assess the existence of a relationship between the results obtained and physiological alterations of BP and HR, a correlation analysis between the variables was performed.

Only correlations with r higher than 0.3 or lower than -0.3 are considered significant, as recommended in [96].

In this research, no correlations were found between PI, HR and BP. Similarly, no associations between FVP and the physiological parameters analysed were observed. However, since this parameter was already based on a standardization of the R-R interval, these results were already expected.

A low negative correlation was found between the minimum velocity in the MCAs and HR, MBP and SBP, which means that an increase in HR, MBP or in SBP is associated with a decrease in minimum blood velocity in the MCAs. However, no correlations were found for DBP nor for the remaining arteries and the physiological measurements.

Furthermore, a moderate correlation was observed for the mean velocity in the BA and HR. Similar findings were verified for the mean velocity in the MCAs and MBP. On the other hand, a low negative correlation was found between the mean velocity in the MCAs and HR, DBP and SBP.

Similarly, a moderate negative correlation was detected for the maximum velocity and HR in the BA. However, the maximum velocity in the ICAs and DBP were also found to be negatively correlated. Lastly, the maximum velocity in the MCAs exhibited a negative correlation for all the comparisons. However, the correlation was low for the HR and DBP and moderate for the MBP and SBP.

Through these results, it is possible to conclude that the mean and maximum velocities in the BA present a negative correlation with only HR, but not with BP. As mentioned by [94], it is possible that the posterior circulation, of which the BA is a part of, may be less affected by physiological factors that result in blood flow variations, explaining the higher reproducibility obtained for this artery when compared to the other vessels, especially for the velocity parameters.

The MCAs were the vessels analysed that presented the strongest correlations with HR and BP, probably explaining the worst reproducibility results found in these arteries, especially for the velocities, since these are the parameters where the correlations were found.

Additionally, in the ICAs, only a relationship between the maximum velocity and DBP was observed, and it was considered a low correlation. Hence, it is possible to hypothesize that the measurements in the ICAs are less affected by physiological alterations of HR and BP, probably due to the fact that the ICAs have higher elasticity, dampening velocity variations.

Although significant correlations were found between the blood flow velocities and physiological parameters, such as HR and BP, it is important to emphasize that correlation does not imply causation. Hence, it is not possible to conclude that, for example, an increase in HR is responsible for a decrease in blood flow velocity, only that there is a correlation between these two parameters. Additionally, the correlations found were low to moderate, which indicates that even the linear relationships observed are not strong.

However, since the correlations were present it is possible to justify some of the differences verified between the test and retest, especially since most of the significant relationships happened in the MCAs, where these differences were more prominent.

Therefore, it is important to be aware of physiological parameters, such as HR and BP triggered, for example, by anxiety to enter the MRI scanner, or even day to day activities and habits, when executing blood flow related measurements in the intracranial arteries.

6.3 Analysis of the comparison with other studies

In order to validate the results obtained in this research, a comparison with other studies was performed.

Regarding the cross-sectional area, the values obtained were very similar to the ones exhibited in other studies, especially for the ICAs and BA. Larger differences were observed for the MCAs' values, however, a possible explanation might be the location chosen for the measurements. In this research the ROI was placed in the more proximal part of the M1 segment. In that location, the lumen area is bigger, since it is near the bifurcation of the ICA into the MCA and ACA.

Since the results are so consistent and accurate when compared to previous investigations, it is possible to validate the software used for analysis, namely the vessel segmentation and the improvement in the cross-section separation from the background, where a k-means cluster approach was replaced for a local thresholding technique suggested by [89]. Additionally, the sequence employed for scan acquisition is also adequate for identification of the intracranial vessels analysed in this study.

The minimum velocity results, on the other hand, were much lower than the ones reported in other studies for all arteries analysed, except for the BA, where the value observed was in line with TCD measurements. It is possible to conclude that the methodology used for this thesis is responsible for a minimum velocity underestimation when compared with other PC-MRI results.

On the other hand, the mean values exhibited in this research are in line with previously mentioned results, especially for the BA. However, the article found for comparison employed 2D PC-MRI, since no measurements of mean velocity with 4D PC-MRI were encountered. Additionally, that study only mentioned the ICAs and BA, preventing the investigation of similarities for the MCAs. Furthermore, the differences can be explained by the study population, since it consists of older volunteers (age range 20-70 years) and also subjects with pathologies (hypertension, ischemic stroke, etc.), which can affect velocity in the intracranial vessels.

Concerning the maximum velocity, the values obtained are very similar to the ones found in another study [14] with similar methodology. Hence, it is possible to again verify the accuracy of the post-processing software used in this thesis, seeing as a different commercial software with similar sequence presented equivalent results.

However, several other articles mentioned values significantly higher than those described in this thesis and, consequently, than the ones referred in [14].

This underestimation, also observed for the minimum velocity, is probably due to the sequence and sampling scheme used, since in [14] a kat-ARC with VDR sampling

sequence is also employed and no other article found used the same methodology. Some of the causes of the differences observed may be the limited and nonisotropic spatial resolution, when compared to the vessel size.

In other 4D flow studies [19], [42] the spatial resolution reported is $0.7 \times 0.7 \times 0.7$ mm^3, while the one in this methodology is $0.9 \times 0.9 \times 0.5$ mm^3. Since the spatial resolution is worse, partial volume effects are more likely to happen, interfering in velocity estimation.

Additionally, the sampling scheme mentioned in these articles is a vastly undersampled isotropic voxel radial projection imaging, which is different than the one utilized for this project and mentioned by Wen et al. [14]. This can also interfere with the sampling and image reconstruction and, consequently, the results obtained by the post-processing software.

As mentioned in Section 2.3, the PI is calculated as the difference between the maximum flow and minimum flow divided by the mean flow. Since the flow measurements are a result of the multiplication between the cross-sectional area and the velocity, a maximum velocity underestimation affects the peak blood flow value. Therefore, the PI results are lower than reported in other studies, similarly to the maximum velocity. Unfortunately, the article with a similar sequence did not report PI results for comparison.

On the other hand, the FVP is not as affected by underestimation of the velocities, therefore the values are in line with the ones found in other articles.

7

Conclusion

This thesis aimed to assess the test-retest reproducibility of 4D flow results in intracranial arteries, as well as to validate the post-processing software used for analysis. The results obtained in this project will contribute to the normative base of vascular function measurements in healthy volunteers, which is crucial for the diagnosis of cerebrovascular diseases.

To achieve this goal, PI, FVP, cross-sectional area, and minimum, mean and maximum blood flow velocities were measured in the ICAs, MCAs and BA in two occasions, 24 hours apart, on a population of 10 healthy volunteers.

7.1 Summary of findings

In order to evaluate the technique's accuracy, several statistic analyses were performed.

Considering all parameters analysed, it is possible to state that the most consistent results (average ICC of 0.9 and standard deviation lower than 10%) were found for the cross-sectional area, which was expected, because the vessel diameter is not as affected by physiological alterations, motion artifacts, temporal resolution or turbulent flow as the blood flow velocities estimations. Hence, this study validated the segmentation achieved by the post-processing software used for the analysis.

It is important to mention that the flow velocities also showed higher reproducibility than the PI and FVP, especially for the BA and ICAs. These findings are also in line with what was anticipated and reported in previous PC-MRI reproducibility studies, since PI and FVP are the result of calculations made upon other measurements, such as velocities. Hence, their values are affected by the propagation of individual errors present in each one of the composing measurements.

Regarding the arteries analysed, all vessel measurements presented moderate to good general reproducibility, especially after removing the outliers that affected particularly the right ICA and MCA. The BA and left ICA presented the best and most consistent results, especially for flow velocities and cross-sectional area. However, the BA was the only artery that presented LoA lower than the proposed acceptable limits for all parameters.

The right ICA also presented a high reproducibility, however the PI and mean velocity showed lower reliability. The accuracy differences observed between the right and left ICAs are probably due to the fact that this study was composed by a small population. In a larger cohort, the reliability between these arteries is expected to be similar.

As mentioned before, in general, the MCAs reproducibility was lower when compared with the other arteries analysed, especially for the flow velocities. Since the velocity measurements in these arteries showed significant correlations with HR and BP, it is possible that the differences observed between the test-retest were due to transient physiological alterations. Additionally, MCAs are smaller and more tortuous, thus being more prone to impose turbulent blood flow, which significantly affects the velocity estimation. It is possible that these arteries may be too small and tortuous for an accurate measurement of flow related parameters with this technique, without any type of normalisation.

When analysing the associations between the HR and BP and the results obtained, it is possible to conclude that the flow velocities in the MCAs presented several correlations with physiological measurements. Thus, these findings are in line with the reproducibility studies, since these vessels presented more significant differences between the scan-rescan measurements.

The ICAs and BA results did not show as many correlations with HR and BP, which again is consistent with the higher reproducibility results found for these arteries.

When comparing the obtained values, it was possible to conclude that the cross-sectional areas, FVP and mean velocities presented in this study are in line with the ones reported in other PC-MRI studies. However, the minimum and maximum velocities are underestimated, and, consequently, so is the PI. The spatial resolutions and the sampling scheme used for this project were distinct than the ones reported in the other studies, which possibly explains the differences observed. However, the results obtained are consistent with the ones mentioned in one other article [14] with similar methodology.

Although the BA and ICAs measurements demonstrated successful results, this project revealed that, in general, the vascular function measurements in the MCAs did not present enough reproducibility to be considered reliable for clinical applications. Hence, continuous measurements of HR and BP must be taken into account in future projects. Furthermore, if it is established that physiological changes can be described by a factor that is multiplied by the actual vascular function measurement, it is possible to normalise the values obtained. Since, theoretically, the physiological alterations are the same for both the right and left arteries, a normalization with the contralateral side can be performed, possibly obtaining a more reproducible result.

7.2 Limitations and future perspectives

This study presents several limitations. First, the small volunteer cohort severely conditions the power of the statistical analysis. Since the study population is reduced, outliers and minor differences highly affect the results. Additionally, since only one person was

responsible for the processing, some bias may be present, due to the reproducibility being highly dependent on the vessel location chosen for the analysis. For future investigations, it would be interesting to repeat the study with several independent observers, assessing the inter observer reproducibility.

As mentioned before, the nonisotropic and reduced spatial resolutions of the collected images, when compared to other studies, may also be a limiting factor, since increased spatial averaging and partial volume effects may be responsible for inaccurate maximum velocity and flow estimations.

A source of possible differences between the measurements is the location of the regions of interest, since it is not possible to guarantee that these are the same when evaluating the scan and rescan. However, the averaging of the results of six consecutive centerline points was used in an attempt to reduce the implications of this limitation.

The comparison between the presented results and the literature was also difficult due to the young age of the volunteers, since most studies present an older cohort or volunteers with pathologies, which are conditions that highly affect the cerebral blood flow.

The implementation of a similar study using also phantom measurements, would be of interest, since it would be possible to discard the differences generated by physiological alterations and assess the possible limitations of the technical aspects of the methodology employed in a controlled setting.

To achieve more reproducible results, it would be of interest to measure the heart rate and blood pressure throughout the acquisition, in order to be able to perform a normalization of the vascular function values measured. The other option would be to create categories of values in which normal values could vary. However, for this purpose, a larger population would be necessary. The proposed normalisation with contralateral arteries aforementioned is also a plausible possibility.

7.3 Study contribution

Overall, this thesis presented new functionalities and improvements to an already existing post-processing tool, as well as a 4D flow reproducibility study evaluating a more extensive variety of parameters in intracranial vessels, which will certainly contribute to more widespread implementation and validation of the technique. The results presented also contributed to the normative basis of healthy and young volunteers, useful for the comparison with pathological situations, which supports the early diagnosis of several neurovascular diseases, including CSVD. With the findings observed, it is possible to set ground for more research regarding the use of this technique for intracerebral applications.

Bibliography

[1] J. M. Lourenço, *The NOVAthesis LaTeX Template User's Manual*, NOVA University Lisbon, 2021. [Online]. Available: https://github.com/joaomlourenco/novathesis/raw/master/template.pdf.

[2] C. J. Kirkness, "Cerebral blood flow monitoring in clinical practice", *AACN Clinical Issues: Advanced Practice in Acute and Critical Care*, vol. 16, no. 4, pp. 476–487, 2005-10. DOI: 10.1097/00044067-200510000-00005.

[3] C. Björnfot, A. Garpebring, S. Qvarlander, J. Malm, A. Eklund, and A. Wåhlin, "Assessing cerebral arterial pulse wave velocity using 4d flow MRI", *Journal of Cerebral Blood Flow & Metabolism*, vol. 41, no. 10, pp. 2769–2777, 2021-04. DOI: 10.1177/0271678x211008744.

[4] A. Wåhlin, A. Eklund, and J. Malm, "4d flow MRI hemodynamic biomarkers for cerebrovascular diseases", *Journal of Internal Medicine*, vol. 291, no. 2, pp. 115–127, 2021-11. DOI: 10.1111/joim.13392.

[5] A. G. Morgan, M. J. Thrippleton, J. M. Wardlaw, and I. Marshall, "4d flow MRI for non-invasive measurement of blood flow in the brain: A systematic review", *Journal of Cerebral Blood Flow & Metabolism*, vol. 41, no. 2, pp. 206–218, 2020-09. DOI: 10.1177/0271678x20952014.

[6] D. S. Liebeskind, "Collateral circulation", *Stroke*, vol. 34, no. 9, pp. 2279–2284, 2003-09. DOI: 10.1161/01.str.0000086465.41263.06.

[7] P. Sachdev, R. Kalaria, J. O'Brien, *et al.*, "Diagnostic criteria for vascular cognitive disorders", *Alzheimer Disease & Associated Disorders*, vol. 28, no. 3, pp. 206–218, 2014-07. DOI: 10.1097/wad.0000000000000034.

[8] L. A. Rivera-Rivera, P. Turski, K. M. Johnson, *et al.*, "4d flow MRI for intracranial hemodynamics assessment in alzheimer's disease", *Journal of Cerebral Blood Flow & Metabolism*, vol. 36, no. 10, pp. 1718–1730, 2016-07. DOI: 10.1177/0271678x15617171.

[9] G. W. Blair, M. V. Hernandez, M. J. Thrippleton, F. N. Doubal, and J. M. Wardlaw, "Advanced neuroimaging of cerebral small vessel disease", *Current Treatment Options in Cardiovascular Medicine*, vol. 19, no. 7, 2017-06. DOI: 10.1007/s11936-017-0555-1.

[10] C. Moran, T. G. Phan, and V. K. Srikanth, "Cerebral small vessel disease: A review of clinical, radiological, and histopathological phenotypes", *International Journal of Stroke*, vol. 7, no. 1, pp. 36–46, 2011-11. DOI: 10.1111/j.1747-4949.2011.00725.x.

[11] O. Hamilton, S. Cox, L. Ballerini, *et al.*, "Associations between total MRI-visible small vessel disease burden and domain-specific cognitive abilities in a community-dwelling older-age cohort", *Neurobiology of Aging*, vol. 105, pp. 25–34, 2021-09. DOI: 10.1016/j.neurobiolaging.2021.04.007.

[12] J. M. Wardlaw, C. Smith, and M. Dichgans, "Small vessel disease: Mechanisms and clinical implications", *The Lancet Neurology*, vol. 18, no. 7, pp. 684–696, 2019-07. DOI: 10.1016/s1474-4422(19)30079-1.

[13] Z. Cai, C. Wang, W. He, *et al.*, "Cerebral small vessel disease and alzheimer's disease", *Clinical Interventions in Aging*, p. 1695, 2015-10. DOI: 10.2147/cia.s90871.

[14] B. Wen, S. Tian, J. Cheng, *et al.*, "Test–retest multisite reproducibility of neurovascular 4d flow MRI", *Journal of Magnetic Resonance Imaging*, vol. 49, no. 6, pp. 1543–1552, 2018-11. DOI: 10.1002/jmri.26564.

[15] M. C. de Verdier and J. Wikström, "Normal ranges and test-retest reproducibility of flow and velocity parameters in intracranial arteries measured with phase-contrast magnetic resonance imaging", *Neuroradiology*, vol. 58, no. 5, pp. 521–531, 2016-02. DOI: 10.1007/s00234-016-1661-6.

[16] V. M. Pereira, R. Ouared, O. Brina, *et al.*, "Quantification of internal carotid artery flow with digital subtraction angiography: Validation of an optical flow approach with doppler ultrasound", *American Journal of Neuroradiology*, vol. 35, no. 1, pp. 156–163, 2013-08. DOI: 10.3174/ajnr.a3662.

[17] A. Wåhlin, K. Ambarki, R. Birgander, *et al.*, "Measuring pulsatile flow in cerebral arteries using 4d phase-contrast MR imaging", *American Journal of Neuroradiology*, vol. 34, no. 9, pp. 1740–1745, 2013-03. DOI: 10.3174/ajnr.a3442.

[18] A. Harloff, F. Albrecht, J. Spreer, *et al.*, "3d blood flow characteristics in the carotid artery bifurcation assessed by flow-sensitive 4d MRI at 3t", *Magnetic Resonance in Medicine*, vol. 61, no. 1, pp. 65–74, 2008-12. DOI: 10.1002/mrm.21774.

[19] M. Holmgren, A. Wåhlin, T. Dunås, J. Malm, and A. Eklund, "Assessment of cerebral blood flow pulsatility and cerebral arterial compliance with 4d flow MRI", *Journal of Magnetic Resonance Imaging*, vol. 51, no. 5, pp. 1516–1525, 2019-11. DOI: 10.1002/jmri.26978.

[20] M. Markl, W. Wallis, and A. Harloff, "Reproducibility of flow and wall shear stress analysis using flow-sensitive four-dimensional MRI", *Journal of Magnetic Resonance Imaging*, vol. 33, no. 4, pp. 988–994, 2011-03. DOI: 10.1002/jmri.22519.

[21] S. Nordmeyer, E. Riesenkampff, G. Crelier, *et al.*, "Flow-sensitive four-dimensional cine magnetic resonance imaging for offline blood flow quantification in multiple vessels: A validation study", *Journal of Magnetic Resonance Imaging*, vol. 32, no. 3, pp. 677–683, 2010-08. DOI: 10.1002/jmri.22280.

[22] J. F. Feneis, E. Kyubwa, K. Atianzar, *et al.*, "4d flow MRI quantification of mitral and tricuspid regurgitation: Reproducibility and consistency relative to conventional MRI", *Journal of Magnetic Resonance Imaging*, vol. 48, no. 4, pp. 1147–1158, 2018-04. DOI: 10.1002/jmri.26040.

[23] Z. Stankovic, B. Jung, J. Collins, *et al.*, "Reproducibility study of four-dimensional flow MRI of arterial and portal venous liver hemodynamics: Influence of spatio-temporal resolution", *Magnetic Resonance in Medicine*, vol. 72, no. 2, pp. 477–484, 2013-09. DOI: 10.1002/mrm.24939.

[24] E. M. Schrauben, K. M. Johnson, J. Huston, *et al.*, "Reproducibility of cerebrospinal venous blood flow and vessel anatomy with the use of phase contrast-vastly under-sampled isotropic projection reconstruction and contrast-enhanced MRA", *American Journal of Neuroradiology*, vol. 35, no. 5, pp. 999–1006, 2013-11. DOI: 10.3174/ajnr.a3779.

[25] V. Baliyan, C. J. Das, R. Sharma, and A. K. Gupta, "Diffusion weighted imaging: Technique and applications", *World Journal of Radiology*, vol. 8, no. 9, p. 785, 2016. DOI: 10.4329/wjr.v8.i9.785.

[26] O. Wu, L. Østergaard, and A. G. Sorensen, "Technical aspects of perfusion-weighted imaging", *Neuroimaging Clinics of North America*, vol. 15, no. 3, pp. 623–637, 2005-08. DOI: 10.1016/j.nic.2005.08.009.

[27] S. Holdsworth and R. Bammer, "Magnetic resonance imaging techniques: fMRI, DWI, and PWI", *Seminars in Neurology*, vol. 28, no. 04, pp. 395–406, 2008-09. DOI: 10.1055/s-0028-1083697.

[28] M. P. Hartung, T. M. Grist, and C. J. François, "Magnetic resonance angiography: Current status and future directions", *Journal of Cardiovascular Magnetic Resonance*, vol. 13, no. 1, 2011-03. DOI: 10.1186/1532-429x-13-19.

[29] D. W. McRobbie, E. A. Moore, M. J. Graves, and M. R. Prince, *MRI from Picture to Proton*, 2nd ed. Cambridge University Press, 2006-09. DOI: 10.1017/cbo9780511545405.

[30] R. A. Pooley, "Fundamental physics of MR imaging", *RadioGraphics*, vol. 25, no. 4, pp. 1087–1099, 2005-07. DOI: 10.1148/rg.254055027.

[31] R. S. Balaban and D. C. Peters, *Basic Principles of Cardiovascular Magnetic Resonance*, 3rd ed. Philadelphia, PA: Elsevier, 2019, ch. 1, pp. 1–14. DOI: 10.1016/b978-0-323-41561-3.00001-x.

[32] A. J. Kiruluta and R. G. González, *Magnetic resonance angiography*. Elsevier, 2016-06, vol. 135, ch. 7, pp. 137–149. DOI: 10.1016/b978-0-444-53485-9.00007-6.

[33] S. J. Riederer, E. G. Stinson, and P. T. Weavers, "Technical aspects of contrast-enhanced MR angiography: Current status and new applications", *Magnetic Resonance in Medical Sciences*, vol. 17, no. 1, pp. 3–12, 2018. DOI: 10.2463/mrms.rev.2017-0053.

[34] A. H. Kuo, P. Nagpal, B. B. Ghoshhajra, and S. S. Hedgire, "Vascular magnetic resonance angiography techniques", *Cardiovascular Diagnosis and Therapy*, vol. 9, no. 1, pp. 28–36, 2019-08. DOI: 10.21037/cdt.2019.06.07.

[35] D. T. Wymer, K. P. Patel, W. F. Burke, and V. K. Bhatia, "Phase-contrast MRI: Physics, techniques, and clinical applications", *RadioGraphics*, vol. 40, no. 1, pp. 122–140, 2020-01. DOI: 10.1148/rg.2020190039.

[36] P. Turski, A. Scarano, E. Hartman, *et al.*, "Neurovascular 4dflow MRI (phase contrast MRA): Emerging clinical applications", *Neurovascular Imaging*, vol. 2, no. 1, 2016-04. DOI: 10.1186/s40809-016-0019-0.

[37] B. A. Jung and M. Weigel, "Spin echo magnetic resonance imaging", *Journal of Magnetic Resonance Imaging*, vol. 37, no. 4, pp. 805–817, 2013-03. DOI: 10.1002/jmri.24068.

[38] G. Soulat, P. McCarthy, and M. Markl, "4d flow with MRI", *Annual Review of Biomedical Engineering*, vol. 22, no. 1, pp. 103–126, 2020-06. DOI: 10.1146/annurev-bioeng-100219-110055.

[39] J. Lotz, C. Meier, A. Leppert, and M. Galanski, "Cardiovascular flow measurement with phase-contrast MR imaging: Basic facts and implementation", *RadioGraphics*, vol. 22, no. 3, pp. 651–671, 2002-05. DOI: 10.1148/radiographics.22.3.g02ma11651.

[40] K. S. Nayak, J.-F. Nielsen, M. A. Bernstein, *et al.*, "Cardiovascular magnetic resonance phase contrast imaging", *Journal of Cardiovascular Magnetic Resonance*, vol. 17, no. 1, 2015-08. DOI: 10.1186/s12968-015-0172-7.

[41] S. W. Youn and J. Lee, "From scp2d/scp to scp4d/scp phase-contrast scpMRI/scp in the neurovascular system: Will it be a quantum jump or a fancy decoration?", *Journal of Magnetic Resonance Imaging*, vol. 55, no. 2, pp. 347–372, 2020-11. DOI: 10.1002/jmri.27430.

[42] J. Birnefeld, A. Wåhlin, A. Eklund, and J. Malm, "Cerebral arterial pulsatility is associated with features of small vessel disease in patients with acute stroke and TIA: A 4d flow MRI study", *Journal of Neurology*, vol. 267, no. 3, pp. 721–730, 2019-11. DOI: 10.1007/s00415-019-09620-6.

[43] A. Vali, M. Aristova, P. Vakil, *et al.*, "Semi-automated analysis of 4d flow MRI to assess the hemodynamic impact of intracranial atherosclerotic disease", *Magnetic Resonance in Medicine*, vol. 82, no. 2, pp. 749–762, 2019-03. DOI: 10.1002/mrm.27747.

[44] L. Zarrinkoob, A. Wåhlin, K. Ambarki, R. Birgander, A. Eklund, and J. Malm, "Blood flow lateralization and collateral compensatory mechanisms in patients with carotid artery stenosis", *Stroke*, vol. 50, no. 5, pp. 1081–1088, 2019-05. DOI: 10.1161/strokeaha.119.024757.

[45] L. Zarrinkoob, A. Wåhlin, K. Ambarki, A. Eklund, and J. Malm, "Quantification and mapping of cerebral hemodynamics before and after carotid endarterectomy, using four-dimensional flow magnetic resonance imaging", *Journal of Vascular Surgery*, vol. 74, no. 3, pp. 910–920, 2021-09. DOI: 10.1016/j.jvs.2021.01.074.

[46] T. Vikner, L. Nyberg, M. Holmgren, J. Malm, A. Eklund, and A. Wåhlin, "Characterizing pulsatility in distal cerebral arteries using 4d flow MRI", *Journal of Cerebral Blood Flow & Metabolism*, vol. 40, no. 12, pp. 2429–2440, 2019-11. DOI: 10.1177/0271678x19886667.

[47] L. A. Rivera-Rivera, K. A. Cody, L. Eisenmenger, *et al.*, "Assessment of vascular stiffness in the internal carotid artery proximal to the carotid canal in alzheimer's disease using pulse wave velocity from low rank reconstructed 4d flow MRI", *Journal of Cerebral Blood Flow & Metabolism*, vol. 41, no. 2, pp. 298–311, 2020-03. DOI: 10.1177/0271678x20910302.

[48] L. Boussel, V. Rayz, A. Martin, *et al.*, "Phase-contrast magnetic resonance imaging measurements in intracranial aneurysms in vivo of flow patterns, velocity fields, and wall shear stress: Comparison with computational fluid dynamics", *Magnetic Resonance in Medicine*, vol. 61, no. 2, pp. 409–417, 2009-02. DOI: 10.1002/mrm.21861.

[49] S. Schnell, S. A. Ansari, P. Vakil, *et al.*, "Three-dimensional hemodynamics in intracranial aneurysms: Influence of size and morphology", *Journal of Magnetic Resonance Imaging*, vol. 39, no. 1, pp. 120–131, 2013-10. DOI: 10.1002/jmri.24110.

[50] C. Wu, S. Ansari, A. Honarmand, *et al.*, "Evaluation of 4d vascular flow and tissue perfusion in cerebral arteriovenous malformations: Influence of spetzler-martin grade, clinical presentation, and AVM risk factors", *American Journal of Neuroradiology*, vol. 36, no. 6, pp. 1142–1149, 2015-02. DOI: 10.3174/ajnr.a4259.

[51] L. A. Rivera-Rivera, T. Schubert, P. Turski, *et al.*, "Changes in intracranial venous blood flow and pulsatility in alzheimer's disease: A 4d flow MRI study", *Journal of Cerebral Blood Flow & Metabolism*, vol. 37, no. 6, pp. 2149–2158, 2016-08. DOI: 10.1177/0271678x16661340.

[52] F. F. Schuchardt, C. P. Kaller, C. Strecker, *et al.*, "Hemodynamics of cerebral veins analyzed by 2d and 4d flow mri and ultrasound in healthy volunteers and patients with multiple sclerosis", *Journal of Magnetic Resonance Imaging*, vol. 51, no. 1, pp. 205–217, 2019-05. DOI: 10.1002/jmri.26782.

[53] K. P. Pruessmann, M. Weiger, M. B. Scheidegger, and P. Boesiger, "SENSE: Sensitivity encoding for fast MRI", *Magnetic Resonance in Medicine*, vol. 42, no. 5, pp. 952–962, 1999-11. DOI: 10.1002/(sici)1522-2594(199911)42:5<952::aid-mrm16>3.0.co;2-s.

[54] M. A. Griswold, P. M. Jakob, R. M. Heidemann, *et al.*, "Generalized autocalibrating partially parallel acquisitions (GRAPPA)", *Magnetic Resonance in Medicine*, vol. 47, no. 6, pp. 1202–1210, 2002-06. DOI: 10.1002/mrm.10171.

[55] P. Lai, M. M. Fung, S. S. Vasanawala, and A. C. Brau, "Single breathhold three-dimensional cardiac cine MRI with whole ventricular coverage and retrospective cardiac gating using kat ARC", *Journal of Cardiovascular Magnetic Resonance*, vol. 14, no. 1, 2012-02. DOI: 10.1186/1532-429x-14-s1-w69.

[56] K. Palágyi, E. Balogh, A. Kuba, *et al.*, "A sequential 3d thinning algorithm and its medical applications", in *Lecture Notes in Computer Science*, Springer Berlin Heidelberg, 2001-06, pp. 409–415. DOI: 10.1007/3-540-45729-1_42.

[57] F. Huang, J. Akao, S. Vijayakumar, G. R. Duensing, and M. Limkeman, "K-t GRAPPA: Ak-space implementation for dynamic MRI with high reduction factor", *Magnetic Resonance in Medicine*, vol. 54, no. 5, pp. 1172–1184, 2005. DOI: 10.1002/mrm.20641.

[58] M. J. Cipolla, *The Cerebral Circulation* (Colloquium Series on Integrated Systems Physiology: From Molecule to Function to Disease), 2nd ed. Morgan & Claypool, 2016-07, ch. 2, pp. 3–14.

[59] S. Fantini, A. Sassaroli, K. T. Tgavalekos, and J. Kornbluth, "Cerebral blood flow and autoregulation: Current measurement techniques and prospects for noninvasive optical methods", *Neurophotonics*, vol. 3, no. 3, p. 031 411, 2016-06. DOI: 10.1117/1.nph.3.3.031411.

[60] D. N. Ku, "BLOOD FLOW IN ARTERIES", *Annual Review of Fluid Mechanics*, vol. 29, no. 1, pp. 399–434, 1997-01. DOI: 10.1146/annurev.fluid.29.1.399.

[61] *Laminar v turbulent - Questions and Answers in MRI*. [Online]. Available: https://www.mriquestions.com/laminar-v-turbulent.html (visited on 2022-05-30).

[62] J. E. Hall and A. C. Guyton, *Guyton and hall textbook of medical physiology*, 12th ed. London, England: Grune & Stratton, 2010-07, ch. 14, pp. 159–162.

[63] G. M. London and B. Pannier, "Arterial functions: How to interpret the complex physiology", *Nephrology Dialysis Transplantation*, vol. 25, no. 12, pp. 3815–3823, 2010-10. DOI: 10.1093/ndt/gfq614.

[64] M. F. O'Rourke and J. Hashimoto, "Mechanical factors in arterial aging", *Journal of the American College of Cardiology*, vol. 50, no. 1, pp. 1–13, 2007-07. DOI: 10.1016/j.jacc.2006.12.050.

[65] G. G. Belz, "Elastic properties and windkessel function of the human aorta", *Cardiovascular Drugs and Therapy*, vol. 9, no. 1, pp. 73–83, 1995-02. DOI: 10.1007/bf00877747.

[66] M. M. Poels, K. Zaccai, G. C. Verwoert, *et al.*, "Arterial stiffness and cerebral small vessel disease", *Stroke*, vol. 43, no. 10, pp. 2637–2642, 2012-10. DOI: 10.1161/strokeaha.111.642264.

[67] S.-Y. Chuang, H.-M. Cheng, C.-H. Bai, W.-T. Yeh, J.-R. Chen, and W.-H. Pan, "Blood pressure, carotid flow pulsatility, and the risk of stroke", *Stroke*, vol. 47, no. 9, pp. 2262–2268, 2016-09. DOI: 10.1161/strokeaha.116.013207.

[68] A. Scuteri, A. M. Brancati, W. Gianni, A. Assisi, and M. Volpe, "Arterial stiffness is an independent risk factor for cognitive impairment in the elderly: A pilot study", *Journal of Hypertension*, vol. 23, no. 6, pp. 1211–1216, DOI: 10.1097/01.hjh.0000170384.38708.b7.

[69] S. R. Waldstein, S. C. Rice, J. F. Thayer, S. S. Najjar, A. Scuteri, and A. B. Zonderman, "Pulse pressure and pulse wave velocity are related to cognitive decline in the baltimore longitudinal study of aging", *Hypertension*, vol. 51, no. 1, pp. 99–104, 2008-01. DOI: 10.1161/hypertensionaha.107.093674.

[70] M. Fukuhara, K. Matsumura, T. Ansai, *et al.*, "Prediction of cognitive function by arterial stiffness in the very elderly", *Circulation Journal*, vol. 70, no. 6, pp. 756–761, 2006. DOI: 10.1253/circj.70.756.

[71] A. N. Lyle and U. Raaz, "Killing me unsoftly", *Arteriosclerosis, Thrombosis, and Vascular Biology*, vol. 37, no. 2, 2017-02. DOI: 10.1161/atvbaha.116.308563.

[72] L. Pantoni, "Cerebral small vessel disease: From pathogenesis and clinical characteristics to therapeutic challenges", *The Lancet Neurology*, vol. 9, no. 7, pp. 689–701, 2010-07. DOI: 10.1016/s1474-4422(10)70104-6.

[73] J. M. Wardlaw, C. Smith, and M. Dichgans, "Mechanisms of sporadic cerebral small vessel disease: Insights from neuroimaging", *The Lancet Neurology*, vol. 12, no. 5, pp. 483–497, 2013-05. DOI: 10.1016/s1474-4422(13)70060-7.

[74] G. W. Petty, R. D. Brown, J. P. Whisnant, J. D. Sicks, W. M. O'Fallon, and D. O. Wiebers, "Ischemic stroke subtypes", *Stroke*, vol. 31, no. 5, pp. 1062–1068, 2000-05. DOI: 10.1161/01.str.31.5.1062.

[75] J. J. Zwanenburg and M. J. van Osch, "Targeting cerebral small vessel disease with MRI", *Stroke*, vol. 48, no. 11, pp. 3175–3182, 2017-11. DOI: 10.1161/strokeaha.117.016996.

[76] U. Khan, L. Porteous, A. Hassan, and H. S. Markus, "Risk factor profile of cerebral small vessel disease and its subtypes", *Journal of neurology, neurosurgery, and psychiatry*, vol. 78, no. 7, pp. 702–706, 2006-12. DOI: 10.1136/jnnp.2006.103549.

[77] R. G. Gosling and D. H. King, "Arterial assessment by doppler-shift ultrasound", en, *Proc. R. Soc. Med.*, vol. 67, no. 6, pp. 447–449, 1974-06.

[78] E. Michel and B. Zernikow, "Gosling's doppler pulsatility index revisited", en, *Ultrasound Med. Biol.*, vol. 24, no. 4, pp. 597–599, 1998-05.

[79] A. Stalder, M. Russe, A. Frydrychowicz, J. Bock, J. Hennig, and M. Markl, "Quantitative 2d and 3d phase contrast MRI: Optimized analysis of blood flow and vessel wall parameters", *Magnetic Resonance in Medicine*, vol. 60, no. 5, pp. 1218–1231, 2008-11. DOI: 10.1002/mrm.21778.

[80] Q. Li, Y. Yang, C. Reis, *et al.*, "Cerebral small vessel disease", *Cell Transplantation*, vol. 27, no. 12, pp. 1711–1722, 2018-09. DOI: 10.1177/0963689718795148.

[81] M. E. Gurol, G. J. Biessels, and J. R. Polimeni, "Advanced neuroimaging to unravel mechanisms of cerebral small vessel diseases", *Stroke*, vol. 51, no. 1, pp. 29–37, 2020-01. DOI: 10.1161/strokeaha.119.024149.

[82] T. Tarumi, M. A. Khan, J. Liu, *et al.*, "Cerebral hemodynamics in normal aging: Central artery stiffness, wave reflection, and pressure pulsatility", *Journal of Cerebral Blood Flow & Metabolism*, vol. 34, no. 6, pp. 971–978, 2014-03. DOI: 10.1038/jcbfm.2014.44.

[83] M. F. O'Rourke and M. E. Safar, "Relationship between aortic stiffening and microvascular disease in brain and kidney", *Hypertension*, vol. 46, no. 1, pp. 200–204, DOI: 10.1161/01.hyp.0000168052.00426.65.

[84] J. M. Wardlaw, E. E. Smith, G. J. Biessels, *et al.*, "Neuroimaging standards for research into small vessel disease and its contribution to ageing and neurodegeneration", *The Lancet Neurology*, vol. 12, no. 8, pp. 822–838, 2013-08. DOI: 10.1016/s1474-4422(13)70124-8.

[85] F. Fazekas, J. Chawluk, A. Alavi, H. Hurtig, and R. Zimmerman, "MR signal abnormalities at 1.5 t in alzheimer's dementia and normal aging", *American Journal of Roentgenology*, vol. 149, no. 2, pp. 351–356, 1987-08. DOI: 10.2214/ajr.149.2.351.

[86] M. A. Topcuoglu, "Transcranial doppler ultrasound in neurovascular diseases: Diagnostic and therapeutic aspects", *Journal of Neurochemistry*, vol. 123, pp. 39–51, 2012-10. DOI: 10.1111/j.1471-4159.2012.07942.x.

[87] Y. Shi, M. J. Thrippleton, I. Marshall, and J. M. Wardlaw, "Intracranial pulsatility in patients with cerebral small vessel disease: A systematic review", *Clinical Science*, vol. 132, no. 1, pp. 157–171, 2018-01. DOI: 10.1042/cs20171280.

[88] E. Schrauben, A. Wåhlin, K. Ambarki, *et al.*, "Fast 4d flow MRI intracranial segmentation and quantification in tortuous arteries", *Journal of Magnetic Resonance Imaging*, vol. 42, no. 5, pp. 1458–1464, 2015-04. DOI: 10.1002/jmri.24900.

[89] T. Dunås, M. Holmgren, A. Wåhlin, J. Malm, and A. Eklund, "Accuracy of blood flow assessment in cerebral arteries with 4d flow MRI: Evaluation with three segmentation methods", *Journal of Magnetic Resonance Imaging*, vol. 50, no. 2, pp. 511–518, 2019-01. DOI: 10.1002/jmri.26641.

[90] MATLAB, *version 9.12.0.2039608 (R2022a)*. Natick, Massachusetts: The MathWorks Inc., 2022.

[91] T. K. Koo and M. Y. Li, "A guideline of selecting and reporting intraclass correlation coefficients for reliability research", *Journal of Chiropractic Medicine*, vol. 15, no. 2, pp. 155–163, 2016-06. DOI: 10.1016/j.jcm.2016.02.012.

[92] A. Gupta, P. Mishra, C. Pandey, U. Singh, C. Sahu, and A. Keshri, "Descriptive statistics and normality tests for statistical data", *Annals of Cardiac Anaesthesia*, vol. 22, no. 1, p. 67, 2019. DOI: 10.4103/aca.aca_157_18.

[93] E. Whitley and J. Ball, *Critical Care*, vol. 6, no. 6, p. 509, 2002. DOI: 10.1186/cc1820.

[94] A. Wåhlin, K. Ambarki, J. Hauksson, R. Birgander, J. Malm, and A. Eklund, "Phase contrast MRI quantification of pulsatile volumes of brain arteries, veins, and cerebrospinal fluids compartments: Repeatability and physiological interactions", *Journal of Magnetic Resonance Imaging*, vol. 35, no. 5, pp. 1055–1062, 2011-12. DOI: 10.1002/jmri.23527.

[95] L. Portney, *Foundations of clinical research : Applications to practice*, 3rd ed. Philadelphia, PA: F.A. Davis Company, 2015-03, ch. 23, pp. 1–14.

[96] M. M. Mukaka, "Statistics corner: A guide to appropriate use of correlation coefficient in medical research", en, *Malawi Med. J.*, vol. 24, no. 3, pp. 69–71, 2012-09.

[97] L. Zarrinkoob, K. Ambarki, A. Wåhlin, *et al.*, "Aging alters the dampening of pulsatile blood flow in cerebral arteries", *Journal of Cerebral Blood Flow & Metabolism*, vol. 36, no. 9, pp. 1519–1527, 2016-07. DOI: 10.1177/0271678x16629486.

[98] J. M. Kellawan, J. W. Harrell, E. M. Schrauben, *et al.*, "Quantitative cerebrovascular 4d flow MRI at rest and during hypercapnia challenge", *Magnetic Resonance Imaging*, vol. 34, no. 4, pp. 422–428, 2016-05. DOI: 10.1016/j.mri.2015.12.016.

[99] M. R. Alwatban, S. E. Aaron, C. S. Kaufman, *et al.*, "Effects of age and sex on middle cerebral artery blood velocity and flow pulsatility index across the adult lifespan", *Journal of Applied Physiology*, vol. 130, no. 6, pp. 1675–1683, 2021-03. DOI: 10.1152/japplphysiol.00926.2020.

[100] B. G. Fico, K. B. Miller, L. A. Rivera-Rivera, *et al.*, "The impact of aging on the association between aortic stiffness and cerebral pulsatility index", *Frontiers in Cardiovascular Medicine*, vol. 9, 2022-02. DOI: 10.3389/fcvm.2022.821151.

[101] R. J. van Tuijl, Y. M. Ruigrok, B. K. Velthuis, I. C. van der Schaaf, G. J. E. Rinkel, and J. J. M. Zwanenburg, "Velocity pulsatility and arterial distensibility along the internal carotid artery", *Journal of the American Heart Association*, vol. 9, no. 16, 2020-08. DOI: 10.1161/jaha.120.016883.

[102] S. Meckel, L. Leitner, L. H. Bonati, *et al.*, "Intracranial artery velocity measurement using 4d PC MRI at 3 t: Comparison with transcranial ultrasound techniques and 2d PC MRI", *Neuroradiology*, vol. 55, no. 4, pp. 389–398, 2012-11. DOI: 10.1007/s00234-012-1103-z.

[103] S.-Y. Ha, Y. Kang, H.-J. Lee, M. Hwang, J. Baik, and S. Park, "Intracranial flow velocity quantification using non-contrast four-dimensional flow MRI: A prospective comparative study with transcranial doppler ultrasound", *Diagnostics*, vol. 12, no. 1, p. 23, 2021-12. DOI: 10.3390/diagnostics12010023.